

**UCSF**

**UC San Francisco Electronic Theses and Dissertations**

**Title**

Modeling the Impact of the Autonomic Nervous System on the Development of Human iPSC-Sinoatrial Nodal Cells

**Permalink**

<https://escholarship.org/uc/item/2j09v0xq>

**Author**

King, Jasmine

**Publication Date**

2023

**Supplemental Material**

<https://escholarship.org/uc/item/2j09v0xq#supplemental>

Peer reviewed|Thesis/dissertation

Modeling the Impact of the Autonomic Nervous System on the Development of Human iPSC-Sinoatrial Nodal Cells

by  
Jasmine King

DISSERTATION

Submitted in partial satisfaction of the requirements for degree of  
DOCTOR OF PHILOSOPHY

in

Bioengineering

in the

GRADUATE DIVISION

of the

UNIVERSITY OF CALIFORNIA, SAN FRANCISCO  
AND  
UNIVERSITY OF CALIFORNIA, BERKELEY

Approved:

DocuSigned by:

*Matthew Kutys*

7F11A9EBF99E49D...

Matthew Kutys

Chair

DocuSigned by:

*Vasanth Vedantham*

DocuSigned by:

**DAVID SCHAFFER**

7462D9FCC764410...

Vasanth Vedantham

DAVID SCHAFFER

Committee Members

Copyright 2023

by

Jasmine King

## DEDICATION

This body of work is dedicated to my family - my parents, Julia and Timothy King Sr., my brother, Timothy King Jr., and my late grandmothers, Lula Chatman and Melvin King - for their unconditional love, support and foundation. To my parents for constantly pushing me to be the greatest in everything that I do. To my brother for being one of my biggest supporters and motivators. To my late matriarchs (R.I.P.) for laying the foundation of love, education and perseverance. I wouldn't be the person I am today without them nor without the opportunities they provided me.

This work is also dedicated to all of my babies (present and future) - Amiren, Brayden, Kenzilyn, Makih, Phoenix, Elaina, Jace, etc. - this degree is a testament to you being able to achieve anything that you put your mind to! I'll never stop helping you reach for the stars.

I love you all! Y'all are my North Star! With y'all I know anything is possible!

## ACKNOWLEDGEMENTS

The amount of love and support that helped me through this tortuous journey is immeasurable and beyond the confines of this section.

I want to start off by thanking the UCSF Graduate Division for taking a chance on me as a novice scientist with only a year's worth of experience. I was an undergraduate trying to figure myself out, and you accepted my application for SRTP that catapulted me on a path of success to what has now manifested into a Ph.D. from UCSF and UC Berkeley's Bioengineering Program. I've had a team of supporters that have championed me through all my trials and tribulations. There's too many to name, but a special thank you is extended to Victoria Starrett for her countless help with keeping me on track and making sure I have been sufficiently supported by the program in every aspect, whether it be financial or non-monetarily.

Next, I have to thank my Gladstone Community for being everything that I needed in a science home. Drs. Deepak Srivastava and Bob Mahley, you truly made Gladstone a home away from home where I felt the most comfortable, even while walking the halls with Nobel Laureates and other intellectuals. You both set the tone for the supportive and fun-filled environment that I had the pleasure of calling home for the past 5 years. There are too many people in Gladstone alone that I'd like to shout-out for their instrumental part in my success thus far. Specifically for the submission of this dissertation, I would like to thank Dr. Kathryn Claiborn from Gladstone's Scientific Editing Department, Drs. Lana Zholudeva, and Jon Muncie for their help in providing ideas and revisions for this dissertation. I extend another special thanks to Tami Tolpa from Gladstone's Graphics

Department for formatting the graphical illustrations. I would also like to thank the Stem Cell Core (namely, Wendy Runyon) and the Flow Cytometry Core (namely, Drs. Jane Srivastava and Nandhini Raman). I learned so much from you all, but your services made my life so much easier. Thank you NIH S10 RR028962 and James B. Pendleton Charitable Trust for use of our FACSAria II and Fortessa X-20, DARPA for the use of our Fortessa X-20, and NIH P30 AI027763 for use of our FACSAria II. Another special thank you to Dr. Mike Lai for collecting and producing the Fluovolt data as well as being the core electrophysiologist this project needed. Last, but not least, I would like to thank Elevated Voices for providing a safe space to be heard in Gladstone, specifically: Zainab, Nicole and Linh.

To Dr. Todd McDevitt, my first PI for the first 4 years of my PhD, thank you for taking a chance on me and opening up your lab to an overly ambitious cardiac engineer. The McDevitt Lab helped raise me to be the analytical scientist that I am today. I'd like to thank the former McDevitt Lab for my formidable scientific upbringing, specifically: Drs. Ariel, Oriane, Serah, Ana, David, Ashley and Vaishaali. A special thank you to (Drs.) Nick and Emily (NEEB); thank you for all of your help with the molecular biology that went into creating the reporter line. Through navigating the chaos from a pandemic, you really helped take loads off of my back! And, another special thank you to Dr. Ivana Vasic (Muncie), you were everything to me during this PhD: first-friend turned best-friend (aka BioE PnC). Thank you for putting up with me and all of my shenanigans, all of you!

To Dr. Matt Kutys, thank you for adopting me into your lab for the last year of my PhD. It was quite a tumultuous journey after learning about Todd's planned departure. I was in a very tough place trying to find a new home within BioE as well as secure funding

for my next year, but you opened up your lab and resources to me and helped put me on the track that I needed to be on. You are the catalyst that this project needed. Thank you Kutys Lab ((Drs.) Kyle Jacobs, Lakyn Mayo, and Gretchen Ford) for taking me in as your own, and helping me get acclimated to the new environment. A special thank you to (Dr.) Tania for your help with getting me through the learning process of working with microfluidic devices.

To my thesis committee, Dr. Vasanth Vedantham and Dr. David Schaffer thank you for your guidance and expertise in all my projects and your support during the COVID-19 pandemic as well as my PI leaving. You challenged me and helped push me to the finish line.

To my collaborators that made this work possible, Drs. Stephanie Protze and Faranak Fattahi, thank you so much for the resources and knowledge that you gave. It was an actual dream come true to work with you both, the Queens of hPSC-sinoatrial nodal cells and hPSC-autonomic neurons, respectively. In the Fattahi Lab, I'd like to extend a special thank you to (Drs.) Jonathan Ramirez, Spencer Nyarady, and Ryan Samuel for their help in differentiating and supplying the neurons used in the work for this dissertation.

To my funding sources, NSF and Berkeley, you both honored a young scientist with the GRFP and Chancellor's Fellowship, respectively. I am forever grateful for such high honors from such prestigious institutions. You helped me believe in myself and helped make my first 5 years in grad school a breeze.

To my BE-STEM family, thank you for giving me the safe space and splash of color that I needed at UCSF. After choosing a UCSF lab, I got disconnected from BGESS at

Berkeley, but BE-STEM came around the corner, and didn't miss a beat! I'd like to give a special shout-out to Drs. Nadia and Muryam, (Drs.) Reuben, Jay'son, Jasmine, Ellery, Tianna, and Trace, to name a few. Y'all exemplify black excellence, and I'm honored to call y'all friends and colleagues! Zach, thank you for supporting us as our administrative rep and giving us the creative liberty in the safe space we built! And last, but certainly not least, Dr. D'anne Duncan, thank you for everything that you did for us as students of color. You were the voice and forceful hand that we needed! Your elevation is well-deserved, and I look forward to seeing how you continue to whip UCSF into shape.

To OCPD, thank you for your immense amount of support that you lent to me as a student and intern. The professional development that I underwent is invaluable, and I am forever grateful to you all, specifically: Drs. Linda Louie, Mike Matrone, and Rachel Care. Additionally, I'd like to thank Mike for leading the front in creating an ongoing paid-position in OCPD for BE-STEM officers through our partnership and Linda for helping me in making my dreams a reality by creating professional development events that were centered in blackness.

To my (Bay Area) hoop family, thank you for being everything I needed outside of lab: from teammates to competitors to party buddies. You all helped me keep my sanity and sense of self because I may be a scientist, but I'm forever a hooper. I'd like to give shout-outs to Stef, Kris, Paige, Rocky, Maddy, Mel, Deja, Holly, Jaz, Lex, Nicol, etc.

To my friends that turned into family, you made this PhD bearable with all the great memories and laughs! To Jadea, my longtime best-friend, from college teammates to soulmates, our long-distance relationship really helped keep me lifted and grounded all at the same time. Making me a god-daddy was one of the happiest days of my life and



has really helped keep me going through some of my darkest times. To Percy, haha thank you for always being the laugh and reality check that I need. You really push me to be great in everything that I do, on and off the court! To (Dr.) Kai, SRTP brought us together and life hasn't been the same since Summer '16! From colleagues to traveling around Iceland together, I can't wait to see what future adventures the world has to offer us. To Armanee', my high-school teammate/soul-sister, we made history together at Lafayette High. You always believed in me as your point guard and personal Bill Nye haha. To Desi, my brother from another mother, I appreciate our business brainstorming sessions and your bountiful support. To Saba, since you didn't believe I was a scientist haha, this one's for you; see, I did some stuff haha! But, I truly appreciate the endless amount of fun, laughs, and experiences that you've brought me over the past two years. To Adrienne, I didn't think God had another platonic soulmate in store for me so late in life, but you've been everything I needed from a best-friend out here in the Bay. I appreciate the wealth of knowledge, laughs and support that you've provided over just the past year. To Sasha, we also met at the tail end of my PhD journey, but you supported me in the times that I needed it the most in finishing this dissertation. Outside of my blood, y'all were some of my biggest supporters, and I love y'all forever! We're locked in for life, and this is just the beginning!

To (Dr.) Dina, thank you for impacting my life in a way that can't fully be conveyed here. SRTP brought us together, but fate kept us together. I honestly wouldn't be here without you and your editing skills that have been beyond your years. From applying to grad schools and fellowships together to getting into our dream schools and winning the

NSF together, I'm so proud of us, and that's just the tip of the iceberg. I look forward to what the future holds for us.

To my family! My parents and brother, I love y'all beyond words can explain. Mom and dad, y'all made the sacrifices that were necessary for me to get to this point and helped me build the confidence needed to take on this endeavor of being the first PhD in my family. Tim, having my brother alongside me these past three years have been instrumental for my mental health. Thank you, "Gordon Ramsey", for always opening up your kitchen to my hungry self. I'm so proud of the man that you're becoming and carving out your own path in Bioengineering. Shout-out to all of the Chatmans and Kings that have helped me along the way. Special shout-out to my cousins, Etosha and Maya, for being the mentors and role models that I needed as I navigated through various business ventures.

Last but certainly not least, to Dr. Jasmine Paulette King, you did it! You are the first of your kin. Through all of your self-doubt, trials and tribulations, a pandemic, switching labs after your PI left, losing your Granny, and getting your laptop stolen the week before your 28th (all while still chasing hoop dreams), you made it! I am so proud of you and let this be a testament to all that you can achieve! This is only the beginning!

# **MODELING THE IMPACT OF THE AUTONOMIC NERVOUS SYSTEM ON THE DEVELOPMENT OF HUMAN IPSC-SINOATRIAL NODAL CELLS**

**Jasmine King**

## **ABSTRACT**

The sinoatrial (SA) node initiates the heart's electrical impulse as the primary pacemaker. Since it leads the cardiac conduction system, its maturation at the tissue and cellular level are critical for proper cardiac function. Similar to cardiomyocytes (CMs), the maturing SA node is regulated by neuronal stimulation. Moreover, this tissue is more highly innervated than the working myocardium. Autonomic control is achieved through parasympathetic and sympathetic stimulation to slow down and speed up the heart rate, respectively. Previous studies have shown the importance of sympathetic neurons for the maturation of CMs by regulating cell size and cell cycle withdrawal. However, whether neuronal innervation similarly regulates the maturation of the SA node is not known. This dissertation seeks to bridge the gap between the shortage in knowledge of SA nodal development and innervation. Ultimately, we established a compartmentalized model system of the innervated SA node and myocardium.

Chapter 1 details the background about the SA node and respective innervation of the heart. There is also a discussion about tissue engineering strategies that go into modeling different cardiac systems *in vitro*. Chapter 2 includes various studies that screen for different combinations of small molecules to selectively differentiate SA nodal cells

(SANs) from hiPSCs. The culmination of studies supports previous reports that suggests Bmp4, RA, SB, and FGF $\alpha$  are the best cocktail for enriching SANs through transcriptional and functional assays. Due to the inefficiency of SAN differentiations compared to CMs, Chapter 3 describes our efforts to create a SHOX2:GFP reporter line for the identification and purification of SANs in heterogeneous differentiations. That chapter concludes with a study demonstrating the functionality of the reporter line through sorting and transcriptional analysis. Chapter 4 follows with functional analysis of SA nodal like pacemaker cells from the Protze Lab (SANLPCs). Different ratios of SANLPCs and CMs in aggregated microtissues demonstrate the importance of enriched SANLPC cultures for more applicable modeling of the SA node. Another study leverages the power of MEAs to assess the functional competency of SANLPCs to respond to neuronal signals prior to innervation. Chapter 5 conclusively describes the model system that was engineered to assess the differential innervation phenotypes and post-junctional changes between hiPSC-SANs (and SANLPCs) and hiPSC-CMs after co-culture with sympathetic neurons. Overall, this project suggests that SA nodal cells are preferentially targeted by autonomic neurons compared to cardiomyocytes, innervation induces cardiac maturation, and microfluidic systems can be a powerful tool to model and analyze complex heterotypic interactions.

## TABLE OF CONTENTS

<b>CHAPTER 1. INTRODUCTION</b> .....	<b>1</b>
<b>1.1. Overview</b> .....	<b>1</b>
<b>1.2. Cellular Complexity of the Native Human Heart</b> .....	<b>2</b>
<b>1.3. The SA Node</b> .....	<b>3</b>
1.3.1. Physiology of the SA node .....	3
1.3.2. Development of the SA node .....	5
1.3.3. Electrophysiology of SANs compared to CMs.....	6
1.3.4. Innervation of the SAN throughout development .....	8
<b>1.4. Tissue engineering strategies for cardiac modeling</b> .....	<b>10</b>
1.4.1. Small molecule directed differentiations .....	10
1.4.2. Considerations for tissue assembly .....	11
1.4.3. Characterization of <i>in vitro</i> cardiac systems .....	12
<b>1.5. Concluding Remarks</b> .....	<b>13</b>
<b>CHAPTER 2. PROTOCOL OPTIMIZATION FOR EFFICIENT SINOATRIAL NODAL CELL DIFFERENTIATION</b> .....	<b>1</b>
<b>2.1. Introduction</b> .....	<b>1</b>
<b>2.2. Materials &amp; Methods</b> .....	<b>3</b>
2.2.1. Pluripotent stem cell culture .....	3
2.2.2. vCM differentiation .....	4
2.2.3. Assessment of differentiation via gene expression .....	4
2.2.4. Optimization of SAN differentiation via molecular screen .....	5

2.2.5. Functional analysis via Pulse Contractility Assay .....	7
2.2.6. Phenotypic analysis via flow cytometry .....	7
2.2.7. Immunocytochemistry .....	8
2.2.8. Image acquisition & phenotypic assessment .....	8
<b>2.3. Results .....</b>	<b>8</b>
2.3.1. Wnt inhibition drives cardiac progenitor specification .....	8
2.3.2. The combination of RA and Bmp4 signaling with TGF- $\beta$ /Nodal/Activin inhibition promotes SAN development during early Wnt modulation .....	9
2.3.3. Timing of spatiotemporal inhibition of FGF pathway is critical for promoting optimal SAN enrichment .....	11
2.3.4. Statistics .....	13
<b>2.4. Discussion .....</b>	<b>14</b>
<b>2.5. Figures .....</b>	<b>17</b>
<b>CHAPTER 3. SHOX2 REPORTER LINE FOR IDENTIFICATION &amp; PURIFICATION OF HPSC-DERIVED SINOATRIAL NODAL CELLS .....</b>	<b>26</b>
<b>3.1. Introduction .....</b>	<b>26</b>
<b>3.2. Materials &amp; methods .....</b>	<b>27</b>
3.2.1. Molecular cloning .....	27
3.2.2. Transfection .....	28
3.2.3. Clonal expansion of edited cells .....	29
3.2.4. Quality control checkpoints .....	30
3.2.5. Functional testing of reporter line .....	31

<b>3.3. Results</b> .....	<b>33</b>
3.3.1. Generation of reporter line.....	33
3.3.2. Karyotyping for abnormalities .....	34
3.3.3. SHOX2:GFP signal is weak but detectable .....	35
3.3.4. SHOX2:GFP reporter supports RBS+ differentiation as the most optimal .....	36
<b>3.4. Discussion</b> .....	<b>38</b>
<b>3.5. Figures</b> .....	<b>40</b>
<b>CHAPTER 4. FUNCTIONAL CHARACTERIZATION OF CARDIAC CELLS</b> .....	<b>44</b>
<b>4.1. Introduction</b> .....	<b>44</b>
<b>4.2. Materials &amp; Methods</b> .....	<b>46</b>
4.2.1. Cardiac microtissue formation .....	46
4.2.2. GCaMP analysis of cardiac microtissues to understand the impact of SANLPCs .....	47
4.2.3. Voltage imaging .....	47
4.2.4. Chemical responsiveness assay of CMs and SANLPCs on MEAs .....	49
4.2.5. Statistics .....	51
<b>4.3. Results</b> .....	<b>51</b>
4.3.1. Visible phenotypic differences of cardiac microtissues .....	51
4.3.2. 10% or higher composition of SANLPCs shift the calcium handling properties of cardiac microtissues .....	52

4.3.3. RBS+ treatment shifts the bulk electrophysiology to a more SAN-like phenotype.....	54
4.3.4. SANLPCs are responsive to adrenergic and cholinergic stimulants.....	54
<b>4.4. Discussion.....</b>	<b>57</b>
<b>4.5. Figures.....</b>	<b>61</b>
<b>CHAPTER 5. IN VITRO INNERVATED CARDIAC SYSTEM.....</b>	<b>71</b>
<b>5.1. Introduction.....</b>	<b>71</b>
<b>5.2. Materials &amp; Methods.....</b>	<b>73</b>
5.2.1. Pluripotent stem cell culture.....	73
5.2.2. Cardiomyocyte differentiation.....	73
5.2.3. Derivation of stem cells into sympathetic neurons.....	74
5.2.4. Fabrication & preparation of microfluidic devices.....	74
5.2.5. Loading of microfluidic devices.....	75
5.2.6. Immunocytochemistry.....	76
5.2.7. Image acquisition & phenotypic assessment.....	76
<b>5.3. Results.....</b>	<b>77</b>
5.3.1. Microfluidics model innervated cardiac tissue.....	77
5.3.2. More abundant axiogenesis in SANLPC devices.....	77
5.3.3. More cytosolic L-type calcium channel in cardiac cells with sympathetic innervation.....	78
<b>5.4. Discussion.....</b>	<b>79</b>
<b>5.5. Future Directions.....</b>	<b>79</b>



<b>5.6. Figures .....</b>	<b>82</b>
<b><i>REFERENCES</i> .....</b>	<b>85</b>

## LIST OF FIGURES

<b>Figure 2.1. Timing of cardiac markers early in a ventricular differentiation. ....</b>	<b>18</b>
<b>Figure 2.2. Differentiation and phenotypic characterization of SAN-like cells from hiPSCs. ....</b>	<b>20</b>
<b>Figure 2.3. Optimal timing and concentration of FGFi is essential in SANLC differentiations.....</b>	<b>22</b>
<b>Figure S2.2. Characterizing FGFi treatment groups for enrichment of SANLCs and upregulation of functional transcripts.....</b>	<b>25</b>
<b>Figure 3.1: Creating a SHOX2:GFP reporter line.....</b>	<b>41</b>
<b>Figure 3.2: SHOX2:GFP signal is weak but detectable. ....</b>	<b>43</b>
<b>Figure S3.1. Live SHOX2:GFP sorting is comparable to fixed sorting.....</b>	<b>43</b>
<b>Figure 4.1: 10% or great SANLPCs are needed to shift the calcium handling properties of cardiac microtissues. ....</b>	<b>62</b>
<b>Figure 4.2: Electrophysiological analysis demonstrates an enrichment of SANLCs in RBS+ differentiations. ....</b>	<b>64</b>
<b>Figure 4.3: MEAs elucidate heterogeneity in SANLPCs and responsiveness of cardiac cell types to cholinergic and adrenergic stimulants. ....</b>	<b>66</b>
<b>Figure S4.1. GCaMP analysis of heterotypic microtissues. ....</b>	<b>68</b>

**Figure S4.2. MEAs additionally elucidate a poor dose-response of cardiac cell types to drugs, a fatty acid-induced maturation of cardiomyocytes, and a regression of maturation in SANLPCs and CMs with a lapse in cholinergic and adrenergic stimulation..... 70**

**Figure 5.1. An innervated cardiac platform models the myocardium and SA node. .... 82**

**Figure 5.2. Differential innervation and functional phenotypes in SANLPCs and CMs cultured with SNs. .... 83**

**Figure S5.1. SANLCs differentiated with RBS+ protocol demonstrate less axiogenesis. .... 84**

## LIST OF ABBREVIATIONS

**Bmp4** – *bone morphogenic protein-4*

**BME** –  *$\beta$ -mercaptoethanol*

**bpm** – *beats per minute*

**CRISPR** – *clustered regularly interspaced short palindromic repeats*

**CMs** – *cardiomyocytes*

**diff** – *differentiation*

**ECM** – *extracellular matrix*

**FACS** – *fluorescence-activated cell sorting*

**FGFi** – *fibroblast growth factor inhibitor*

**fps** – *frames per second*

**GiWi** – *GSK inhibitor WNT inhibitor protocol*

**hiPSC** – *human induced pluripotent stem cell*

**hiPSC-SANs** – *hiPSC-derived sinoatrial nodal cells*

**hPSC** – *human pluripotent stem cell*

**MEA** – *multielectrode array*

**PSNs** – *parasympathetic neurons*

**PCR** – *polymerase chain reaction*

**qPCR** – *quantitative polymerase chain reaction*

**RA** – *retinoic acid*

**RI** – *rock inhibitor*

**ROI** – *region of interest*

**SANs** – *sinoatrial nodal cells*

**SANLCs – sinoatrial nodal-like cells (hiPSC-SANs)**

**SANLPCs – sinoatrial nodal-like pacemaker cells from Protze lab**

**SB – SB-431542 (Activin/Nodal/TGF- $\beta$  signaling inhibitor)**

**SNs – sympathetic neurons**

**WT – wild type**

## **CHAPTER 1. INTRODUCTION**

### **1.1. Overview**

The sinoatrial (SA) node is the primary pacemaker of the heart, and by leading the cardiac conduction system, this complex tissue (comprised of SA nodal cells) is more highly innervated for proper function than the working myocardium (mostly comprised of cardiomyocytes)<sup>1-4</sup>. The autonomic nervous system innervates the heart through primarily the parasympathetic and sympathetic nervous system, and they work together to regulate heart rate. Parasympathetic neurons are the inhibitory stimulus, and sympathetic neurons are the excitatory stimulus. In various mammalian systems, innervation specifically by sympathetic neurons has been shown to cause phenotypic changes in cardiomyocytes (CMs) like hypertrophy that correspond to maturation<sup>5,6</sup>. Conversely, the role of innervation in SA node maturation is relatively unknown. Though there are discrepancies among the studies that assess the maturation of CMs versus SA nodal cells (SANs), van Eif et al. reported there is an upregulation of important ion channels in SANs that correspond to the timing of innervation<sup>7</sup>. More studies are needed to conclusively determine the impact of innervation on the maturation of SANs.

There are transitional stages in cardiac innervation that are observed throughout mammalian development<sup>8</sup>. In infancy, the sympathetic neural supply dominates the cardiac conduction system which correlates to the fetal rapid heart rate<sup>8</sup>. There is a shift to a co-dominant system in adulthood, and with age, denervation occurs. However, denervation has also been linked to pathologies like heart failure, diabetes mellitus, myocardial ischemia and infarction, hibernating myocardium, and Parkinson's disease<sup>9,10</sup>. Autonomic disorders (AKA dysautonomias) are heterogeneous and primarily treated with

palliative medications, which have known systemic side effects. A more complete understanding of the implications of innervation of SA node development might be key to developing new therapeutic targets and drug discovery assays for dysautonomias. This thesis focuses on advancing toward that goal by developing an *in vitro* model of the innervated SA node using human induced pluripotent stem cell (hiPSC) derived cells.

## **1.2. Cellular Complexity of the Native Human Heart**

The heart is the first organ to form and develop in the embryo, reflecting the heart's overall importance in bodily function and development<sup>4</sup>. The heart is a complex organ that is composed of various cell types to support its intricate function. The heterotypic interactions between various cardiac cell types promote stable tissue structure, function and development<sup>11-13</sup>. Some of the most abundant cell types include cardiac muscle cells, stromal, and endothelial cells. CMs and pacemaker cells are the two major cardiac muscle cell types that make up about 70-80% of the heart cellular volume<sup>14</sup>. Within that portion, pacemaker cells only make up about 1% of the cellular volume<sup>15</sup>. The small fraction of pacemaker cells constitutes the cardiac conduction system that initiates and propagates the action potential throughout the heart. Within this subset of cells, there is an even more specialized group of pacemaker cells called SANs that reside in the SA node. In humans, the center of the SA node is considered to contain the leading pacemaker cells or "typical SANs" that are roughly spindle-shaped<sup>16,17</sup>. In general, SANs are small in comparison to CMs; specifically in humans, central SANs are 5-10 $\mu$ m in diameter and 25-30 $\mu$ m in length. By comparison, atrial CMs are 15-20 $\mu$ m in diameter and ~100 $\mu$ m in length<sup>16</sup>.

### **1.3. The SA Node**

The SA node plays an integral role in the cardiac conduction system by being the primary pacemaker of the heart. This nodal tissue is buried in the myocardial junction of the right atrium and the superior vena cava. The intricate function of the SA node demands and engenders complexity in its structure.

#### **1.3.1. Physiology of the SA node**

The SA node is composed of a number of supporting cell types and various types of SANs that represent a gradient from nodal cells at the center to atrial-like cells on the periphery<sup>18,19</sup>. Specifically, at the center of the node, leading SANs are in an “empty state” characterized by few randomly organized myofilaments, mitochondria, and little sarcoplasmic reticulum. As one moves outward toward the atria, SANs express “transitional states” characterized by increasing numbers of myofilaments and mitochondria, until they resemble an atrial-like phenotype<sup>16,19</sup>. Additionally, the cells transition from being poorly organized and interwoven to a more organized and bricklike pattern that exists in the myocardium. SANs are weakly coupled as a result of the differential expression of gap junctions that contain low conductance connexins (Connexin45)<sup>16,20</sup>. The differential expression of ion channels is also a factor in the unique electrical phenotype of SANs which manifests into distinct action potential profiles. A number of distinct factors contribute to the pacemaker electrophysiology, and the unique electro-anatomical feature of the SA node maintains the essential “source-sink



relationship” for proper SA nodal function in the surrounding hyperpolarizing myocardium<sup>17,19</sup>.

The SA node generally has an elongated structure that is detailed as comma-shaped in most adult mammals with a head and tail region<sup>21</sup>. The head and tail have separate regulatory domains that express distinct genetic programs<sup>22</sup>. The head is characterized as *SHOX2*<sup>+</sup> *TBX18*<sup>+</sup> *TBX3*<sup>+</sup> *NKX2.5*<sup>-</sup>, and the tail is delineated as *SHOX2*<sup>+</sup> *TBX18*<sup>-</sup> *TBX3*<sup>+</sup> *NKX2.5*<sup>+</sup>. Interestingly, previous reports have shown that the tail can maintain pacemaker function in the absence of the head in *TBX18* mutants. Conversely, SA nodes lacking a tail in *Shox2* mutant mice exhibit severe dysfunction, regardless of the presence of a normal SA node head<sup>23</sup>. These findings indicate that the tail SANs are necessary for normal pacemaking function. Tail SANs are synonymous with the transitional cells that have electrophysiological properties that are a hybrid between atrial and SA nodal head cells<sup>24</sup>.

SANs have the unique capacity to spontaneously fire an action potential. However, they are regulated by electrical stimuli from the autonomic nervous system. Sympathetic and parasympathetic neurons are the two main subtypes of autonomic neurons that work together to control heart rate. Consequently, the SA node is highly innervated in comparison to the working myocardium. Evaluation of the dense innervation in the SA node has revealed that parasympathetic neurons outnumber sympathetic neurons in the mature tissue<sup>3</sup>. There are a number of physiological and developmental changes that the SA node undergoes that correlate with the development of cardiac innervation and interstitial fibrosis<sup>7,19</sup>. These age-related changes contribute to SA node dysfunction which manifests as irregular rhythmicity in the heart. There is a major need in the field for

a holistic understanding of the development and electro-anatomy of the SA node for advancements of therapeutics for SA node dysfunction and dysautonomias.

### **1.3.2. Development of the SA node**

The linear heart tube becomes an erratic functional unit that contracts spontaneously and irregularly starting as early as embryonic day 8 (E8.0) in mice<sup>25</sup>. The heart beat becomes regular and organized in the heart tube with a caudal to cranial directionality by E9.0, and this regularity coincides with the development of the SA node in the sinus venosus located in the caudal region of the heart tube<sup>26,27</sup>. Prior to the development of the SA node, immature CMs are responsible for the erratic heartbeat with their expression of *HCN4*, a specific marker for the pacemaker that encodes the hyperpolarization-gated cyclic nucleotide cation-activated channel<sup>25</sup>. *HCN4* is expressed in the cardiac crescent as early as E7.5 before it becomes restricted to the SA node by E12.5. SANs are transcriptionally distinct from CMs and other pacemaker cells in the mature heart, and this unique genetic program is conserved in mice and humans<sup>7,28</sup>. *Shox2* is the transcription factor (TF) that is considered to lead the SA node transcriptional profile by being one of the first TFs expressed (E8.5) and driving a downstream genetic cascade primarily via the repression of *NKX2.5*, an early cardiac TF<sup>25</sup>. *SHOX2* expression is integral for the differentiation of SANs and the expression of other SA nodal genes like *ISL1*, *TBX3*, and *TBX18*. SANs differentially express various genes including TFs and ion channels that are important for their functional phenotype. Around E11.5 in mice (or day 35 of human gestation) the SA node matures as it organizes into its distinguishable structure present in the mature heart<sup>4,25</sup>. This event corresponds with maturity in cardiac

function as the normal embryonic heart rate becomes detectable at 90-110 bpm around the fifth-sixth gestational week<sup>29</sup>.

### **1.3.3. Electrophysiology of SANs compared to CMs**

Different cardiac cell types have unique electrophysiology that is dependent on their function and phenotype. CMs have a need for fast conduction velocities due to their role as the contractile cells of the high energy-demanding working myocardium. Consequently, Connexin 43 (Cx43) and Cx40 are abundantly expressed in the myocardium for their large conduction gap junction channels and greater capacity for speed to support synchronous beating<sup>30</sup>. Conversely, SANs and other pacemaker cells early in the cardiac conduction system have slower conduction velocities to allow sufficient timing for ventricular filling. Therefore, the poorly electrically coupled center SANs express Cx45, which forms smaller gap junctions<sup>29</sup>. As you move to the periphery of the SA node, SANs start to express Cx43 and Cx40 to improve electrical coupling and therefore insulate the SA node from the hyperpolarizing atrial muscle. To support this insulation, the SA node is also surrounded by fatty tissue.

Another key difference between SANs and CMs are their action potentials due to the automaticity that is retained by SANs. A hallmark of this automaticity is the diastolic depolarization (or “pacemaker potential”) that enables them to initiate the cardiac electrical impulse. HCN ion channels and spontaneous release of calcium from the sarcoplasmic reticulum are the primary components that facilitate the spontaneity in pacemaker cells. As mentioned previously, CMs lose expression of HCN4; therefore, CMs’ rapid depolarization is heavily reliant on sodium and calcium channels. The slower

upstroke is brought about by the L-type calcium current, while T-type calcium currents help mediate the spontaneous depolarization that is specific to SANs<sup>7,17</sup>. In contrast, L-type calcium channels are less abundant in CMs, but they still contribute to the influx of calcium, trigger calcium release from the sarcoplasmic reticulum, and cause a distinctive plateau phase. SANs are also unique for their lack of a resting membrane potential which is a consequence of their lack of the inward rectifier K<sup>+</sup> channel<sup>31</sup>. Their relatively depolarized natural state permits their excitation with a less negative membrane potential, which is important for their function as the primary pacemaker.

Studies have shown that the electrophysiology of SANs changes with age in correlation with the upregulation of essential ion channels<sup>7</sup>. SANs exhibit increasing automaticity throughout development up until adulthood with a decrease in cycle length and an increase in diastolic depolarization rate and upstroke velocity. This coincides with an increase in *Hcn4*, *Cacnb2* (L-type Ca<sup>2+</sup> channel), *Cacna1g* (T-type Ca<sup>2+</sup> channel), and potassium channel transcripts. In addition to the age-related changes of SANs, their resting membrane potential becomes more negative; their action potential amplitude increases; and their upstroke velocity increases to support their function with age-related stressors. Furthermore, the same studies that track phenotypic changes of SANs in development suggest that these transcriptional and electrophysiological changes correlate with the timing of innervation. Targeted studies are needed to conclusively determine if innervation induces these changes or if they are intrinsic to pacemaker development.

#### **1.3.4. Innervation of the SAN throughout development**

The autonomic nervous system innervates the heart via parasympathetic and sympathetic fibers, preferentially innervating the subepicardium and the SA node<sup>8,32</sup>. These neurons have a common neural crest origin. Cardiac neural crest cells migrate to the base of the atrium and form the cardiac (parasympathetic) ganglia; while trunk neural crest cells migrate to the stellate ganglion and form the sympathetic ganglia, respectively<sup>33</sup>. These regions are where the neurons extend from to form their postganglionic synaptic connections in the various parts of the heart. PSNs preferentially colonize the atria, and in turn the SA node; there, they secrete acetylcholine as their primary neurotransmitter in order to slow down the increasing automaticity of the pacemaking SANs. Acetylcholine signaling is mediated by two types of receptors: muscarinic and nicotinic. These receptors are functionally distinct; muscarinic receptors are G-protein coupled receptors that facilitate a slow-metabolic response via cascades, while nicotinic receptors are ligand-gated ion channels that facilitate a fast-synaptic transmission of acetylcholine<sup>18,32</sup>. Sympathetic neurons secrete norepinephrine to speed up heart rate via adrenergic receptors.

Cardiac innervation is slow to develop and occurs in waves of neuronal dominance, and synaptic formation is consequently a delayed process. However, prior to formation of functional synapses, immature PSNs are known to secrete acetylcholine. The timing of initial PSN innervation coincides with slower heart rate (90-110 bpm) that is seen in the fifth gestational week in comparison to the faster heart beats (140-170 bpm) throughout the rest of the pregnancy<sup>34</sup>. This corresponds to the initial sympathetic dominance that is observed in the fetal stage after innervation is established.

Subsequently, there is an increase in PSNs that contribute to the gradual transition to the sympathetic and parasympathetic co-dominance that is observed in adolescence and adulthood<sup>35</sup>. This is also consistent with the relatively slow and more stable heart rate (60-100bpm) observed in adulthood. In the same data set that showed an upregulation of pacemaker and functional genes via bulk sequencing, CHRN4 - cholinergic receptor nicotinic beta 4 – was significantly expressed in more mature samples, which may be representative of the acetylcholine signaling. This correlates with studies that show a higher abundance of nicotinic transcripts compared to muscarinic in humans and porcine<sup>3</sup>.

With the age-related denervation of the heart, dysautonomias arise, along with other comorbidities like heart failure, diabetes mellitus, myocardial ischemia and infarction, hibernating myocardium, and Parkinson's disease<sup>9,10</sup>. There are over 70 million people living with dysautonomias, but there is no cure for it. Dysautonomias sometimes get better with treatment of underlying diseases. However, they often can worsen with time, and patients are then primarily treated to address symptoms of co-morbidities.

To my knowledge, there have been no correlative studies done to assess the requirement for innervation for SA node development. Conversely, there are *in vitro* and clinical observations that suggest innervation induces post-junctional changes in the membrane characteristics of CMs, but whether these also occur in SANs is unknown<sup>36,37</sup>. Therefore, the following study will establish a platform to assess the correlation of innervation to the development of SANs as well as create a system that helps advance treatment for cardiac pathologies that involve dysautonomias.

#### **1.4. Tissue engineering strategies for cardiac modeling**

There have been significant advancements in the field of cellular and tissue engineering that enable innovative strategies for cardiac modeling. One major advancement was the development of hiPSCs and their use in engineered systems due to their unique self-renewing ability<sup>38,39</sup>. They also make great sources for various physiological model systems because of their ability to differentiate into cell types from all germ layers. Specifically, there are robust protocols to differentiate various cardiac cell types as well as autonomic neurons<sup>40–43</sup>.

There are many variables that go into engineering tissues for cardiac modeling beyond the composition of different cell types. Another key factor is the assembly of cells for the different tissue systems of interest<sup>44</sup>. Functional tissues in the body are heterogeneous with complex interactions between the ECM and other cell types. Modeling these complexities *in vitro* is often difficult, but simple and/or 2D systems are often not good at predicting *in vivo* phenomena, similar to some animal models. Ultimately, tissue engineers seek to recapitulate unique characteristics of target tissues to be able to ask and answer questions about physiology and disease.

##### **1.4.1. Small molecule directed differentiations**

The vast potential of hiPSCs has provided ample protocols for the differentiation of various cardiac and neural cell types<sup>40–43,45–47</sup>. Many methods including directed differentiations and cellular reprogramming have been shown to be successful for the differentiation of these various cell types with defined chemical cocktails of small molecules and the overexpression of transcription factors, respectively<sup>48–51</sup>. Each method

has its own limitations, but directed differentiations with the modulation of Wnt signaling have shown to be the most efficient for the differentiation of cardiomyocytes (GiWi = GSK inhibitor Wnt inhibitor protocol)<sup>40</sup>. Similarly, small molecules that activate the Wnt and FGF pathways have been demonstrated in screens to robustly and efficiently derive autonomic neurons from hPSCs<sup>46</sup>.

However, at the time of this study, the further specification of cells within the general lineages of cardiac muscle cells and autonomic neurons were proven to be less efficient and poorly reproducible. For instance, available protocols for the generation of pacemaker cells produced populations that were ~35% or less SA nodal-like cells (SANLCs) without a reporter line to help purify the cultures, and there was no specific protocol for the differentiation of parasympathetic neurons<sup>42</sup>. The “Protze protocol” uses Bmp4, RA, FGF, and Nodal pathways to differentiate SANLPCs and leverages the power of FACS to purify them with a negative selection NKX2-5:GFP reporter line. Although sorting enriches cultures for SANLPCs (+70% CTNT+/NKX2-5-), this approach limits the overall SA nodal phenotype and potential applications for cells generated using this methodology. To date, the SAN factors from the “Protze protocol” have demonstrated to be the best at directly differentiating SANLCs, and differentiation factors for the specification of sympathetic and parasympathetic neurons have been identified for the optimization of these protocols<sup>47,52,53</sup>.

#### **1.4.2. Considerations for tissue assembly**

There are numerous tissue systems that are at play in the heart: heterotypic myocardium and SA node, vascular system, etc. In addition, there are a variety of ways



one can model the heart in attempts to recapitulate physiological characteristics. Previous studies have shown self-assembled microtissues can recapitulate myocardial phenomena with 3D heterotypic interactions<sup>11,54</sup>. Alternatively microfluidic devices have been used to mimic blood flow and the innervating system of the heart<sup>47,55,56</sup>. The SA node is primarily innervated by the right atrial ganglionated plexus (RAGP). The RAGP is diversely composed of SNs and PSNs, but it is densely populated with PSNs to exhibit a cholinergic phenotype<sup>3</sup>. The compartmentalized platform of a microfluidic chip allows the construction of physiologically relevant chambers similar to the RAGP, SA node and/or myocardium that is central to tissue development and disease<sup>55,57</sup>. This approach additionally allows the individual assessment of different cell types and mechanisms (i.e. juxtacrine vs paracrine signaling) that mimic a complex physiological system.

#### **1.4.3. Characterization of *in vitro* cardiac systems**

Characterization methods are crucial for understanding the physiological relevance of a system. Furthermore, special electrophysiological and functional assays are important in the modeling of the SA node due to its unique function as the primary pacemaker. Patch clamp has notoriously been the electrophysiological assay used to distinguish between different cardiac cell types (i.e. ventricular-like vs atrial-like vs nodal-like). There is also an abundance of fluorescent dyes (i.e. FluoVolt) and genetically encoded voltage indicators (i.e. VSP1) that are used to analyze a cell's action potential. Moreover, dynamic calcium measurements are also important in understanding cardiac muscle cell physiology, pathology, and therapeutic potential. Similarly, calcium indicators (i.e. Fluo-4), genetically encoded calcium sensors (GCaMP), and MatLab algorithms (i.e.

CalTrack) have transformed the way calcium transients are analyzed<sup>58</sup>. Additionally, cardiac muscle cells are notoriously dosed with agonists and antagonists to assess their responsiveness to physiologically relevant drugs.

In parallel with the unique transcriptional profiles for different cardiac cell types, there are also divergent functional phenotypes that are reflected in the transcriptional and proteomic phenotype of each cell<sup>7,28,42,59</sup>. Quantitative proteomics, single-cell and bulk-RNA sequencing have elucidated the foundation of cardiac pacemaking throughout development. Nonetheless, previous studies have demonstrated that qPCR, immunofluorescence, and cytometric analyses are sufficient screening methods for assessing the phenotype of different protocols for the generation of various cell types.

### **1.5. Concluding Remarks**

This dissertation applies a combination of bioengineering principles to establish an innervated SA node *in vitro* for the assessment of how autonomic neurons impact the development of hiPSC-SANs in comparison to hiPSC-CMs. Understanding cardiac development and the interplay of the nervous system is crucial for the future of *ex-vivo* modeling and the development of cellular therapies for the treatment of SA node and autonomic dysfunctions. Historically, animal studies have been at the forefront of medical research and drug discovery, but over the past decade, data has pointed to animal studies being poor predictive models for human diseases<sup>47,60</sup>. With the establishment of this model system, there is a great potential for not only understanding cardiac development but also using diseased-patient lines (i.e. from Parkinson's patients) to create hiPSCs and test how the disease affects the functional phenotype of this model system.

## CHAPTER 2. PROTOCOL OPTIMIZATION FOR EFFICIENT SINOATRIAL NODAL CELL DIFFERENTIATION

### *2.1. Introduction*

Scientific advances in the recent decades have led to the thorough understanding of cardiogenesis and robust protocols for generating cardiomyocytes (CMs) from human induced pluripotent stem cells (hiPSCs) by administering developmental cues crucial for proper differentiation<sup>40,42,61,62</sup>. hiPSCs are commonly used based on their limitless supply, unique human applications, and robust differentiation capacity. One of the most widely used protocols for monolayer differentiation utilizes temporal Wnt signaling (GiWi = Gsk3 inhibitor, Wnt inhibitor) to direct differentiation to primarily ventricular CMs (vCMs) from hPSCs (hPSC-vCMs) due to its simplicity, scalability, and cost-effectiveness<sup>40,61</sup>. However, GiWi, along with the majority of other robust protocols, was not designed to derive specific cardiac cells in the cardiac conduction system, like sinoatrial nodal cells (SANs). Nonetheless, the GiWi protocol also derives atrial and SAN-like cells (SANLCs) based on previously published papers and in-house characterization<sup>52,63</sup>. Protocols for the specification of both atrial and SANLCs have been optimized by enriching for these cardiac subtypes with specific molecules like retinoic acid (RA) in addition to ventricular-biased differentiation protocols<sup>41,63</sup>.

One of the first protocols to effectively differentiate hPSC-SANs used molecular pathways that are known to be involved with their development<sup>61</sup>. Protze et al. reported that RA, bone morphogenic protein (BMP), inhibition of fibroblast growth factor (FGF), and inhibition of nodal/TGF- $\beta$  signaling pathways is important for specification of SAN-like pacemaker cells (SANLPCs = specifically from Protze lab). Altogether, Protze et al.

found that their SANLPCs have a gene-expression and functional profile that is similar to that of fetal SAN tissue. Following this study, Liu et al. also supported the significance of BMP, FGF, and RA signaling at the cardiac mesodermal stage for the enrichment of SAN-like cells (SANLCs)<sup>52</sup>. Additionally, Yechikov et al. reported Nodal inhibition promotes the differentiation of SANLCs by using SB-431542 (Activin/Nodal/TGF- $\beta$  signaling inhibitor; Stemgent), and Ren et al. showed that a second Wnt activation with CHIR99021 in the cardiac mesodermal stage can also enrich the differentiation for SANLCs<sup>64,65</sup>. Based on this knowledge, we optimized a protocol for differentiating hPSC-SANs in parallel to hPSC-vCMs using the GiWi protocol. SANLPCs shipped from the Protze lab were used as a positive control in this optimization. The following optimization used a characterization pipeline that started with gene expression analysis (qPCR), followed by functional assessment via Pulse Contractility Software, and phenotypic analysis via flow cytometry and/or immunofluorescence.

The functional properties of SANs are distinct from vCMs due to their unique electrophysiology and critical role in the cardiac conduction system as the primary pacemaker<sup>7,66</sup>. SANs have a faster beat rate, spontaneous depolarization, and slower upstroke velocity. Historically, patch clamp was the only tool used to characterize the electrophysiology of CMs. However, due to its complexity, patch clamp is very low throughput and dependent on an electrophysiologist to perform analysis. Consequently, labs have made attempts at creating alternatives for this method such as contractility motion analysis, micro-electrode arrays (MEAs), and voltage sensitive dyes<sup>67-69</sup>. In the following study, the Pulse platform was used as a screening tool for different treatment groups to understand their sufficiency in promoting an SAN phenotype based on a faster

beat rate that is comparable to the human fetal heart (120-160 beats per minute)<sup>34,40</sup>. Pulse uses video microscopy and image-analysis algorithms to capture motion and quantify the beating patterns of CMs. It is important to note that Pulse cannot altogether replace electrophysiology or other methods like MEAs or voltage-sensitive dyes. MEA systems are high-throughput solutions that assess the changes in electrophysiology of electrically active cells by measuring their extracellular field potentials<sup>67</sup>. Alternatively, voltage-sensitive dyes are a high-throughput solution for measuring changes in membrane potential for the analysis of action potentials and cellular subtypes. Technology continues to advance tools created for the efficient development and characterization of CMs and SANLCs.

## **2.2. Materials & Methods**

### **2.2.1. Pluripotent stem cell culture**

Wild type C2A (CVCL\_D081) and WTC11 hiPSCs were generously donated by Dr. Olaia Vila and Dr. Bruce Conklin, respectively, and cultured in mTeSR medium (Stem Cell Technologies) on plates coated with 80µg/mL Matrigel (Corning)<sup>70</sup>. Cells were grown to 70% confluence and passaged using Accutase (Innovative Cell Technologies) and PBS (Corning). Cells were then seeded at a density of  $1.3 \times 10^4$  cells/cm<sup>2</sup> in tissue culture flasks in mTeSR medium with 10µM Rock Inhibitor (RI, Y27632, SelleckChem) for the first 24 hours. hiPSCs were passaged roughly every 3 days, and media was refreshed every day with mTeSR.

### **2.2.2. vCM differentiation**

vCMs were differentiated from C2A and WTC11 hiPSCs using the chemically-defined, serum-free GiWi protocol<sup>40,61</sup>. Cells were plated onto matrigel-coated 12-well tissue culture plates (12WPs) at  $3.9 \times 10^4$  cells/cm<sup>2</sup> in mTeSR medium with 10 $\mu$ M RI for the first 24 hours. Once the cells reached 80-90% confluency, 12 $\mu$ M CHIR (Gsk3 inhibitor, SelleckChem) was added into RPMI 1640 medium (Thermo Fisher) supplemented with B27 minus insulin (RPMI/B27-; Life Technologies) on differentiation day 0 (D0). The Wnt pathway was deactivated by removing CHIR exactly 24 hours later by replacing medium with fresh RPMI/B27- on D1. On D3, the Wnt pathway was inhibited with 5 $\mu$ M IWP2 (Wnt inhibitor, Tocris) spiked into RPMI/B27- and then removed after 48 hours by refreshing the medium with RPMI/B27- on D5. On D7, medium was switched to RPMI 1640 medium supplemented with B27 with insulin (RPMI/B27+; Life Technologies) and fed every 3 days thereafter until harvest (D20  $\pm$  15).

### **2.2.3. Assessment of differentiation via gene expression**

hPSC differentiations are known to be variable across different cell lines. Though the GiWi protocol is well-defined and our lab has widely used WTC11 cells for these cardiac differentiations, C2A cells were collected at D0, D3, D4 and D5 of differentiations to assess the gene expression profiles and efficiency of cardiac specification in comparison to WTC11 cells. The gene expression profiles that arise during cardiogenesis driven by specific molecules are well characterized and are dependent on the cardiac fate after mesodermal commitment<sup>42,71</sup>. Cells were collected at each time point by dissociating 1 well with 0.25% trypsin for 15-20 minutes at 37°C. Trypsin was quenched with

RPMI/B27- supplemented with 10 $\mu$ M RI and 15% fetal bovine serum (FBS). Cells were spun down at 84g x 5 minutes, resuspended in RPMI/B27- with RI and counted with Countess Cell Counter (Thermo Fischer Scientific). 1x10<sup>6</sup> cells were collected and spun down to remove media. Cell pellets were lysed with 700 $\mu$ L of RLT Buffer (Qiagen) with 1:100  $\beta$ -mercaptoethanol (BME; Sigma-Aldrich) and stored at -80°C until all samples were collected. Time points were collected in triplicates using biological replicates (sequential differentiations).

RNA was extracted from lysates with the RNeasy Mini Kit (Qiagen). RNA was reverse-transcribed to cDNA using the iScript cDNA Synthesis Kit (Bio-Rad). Forward and reverse primers (Table 2.1) were designed with the NCBI Primer-BLAST. qPCR reactions were subsequently performed with the SYBR green PCR mix with samples analyzed with 3 technical replicates. *18S* was used for normalization in analysis using the  $\Delta\Delta$ Ct to calculate fold change in comparison to D0 values.

#### **2.2.4. Optimization of SAN differentiation via molecular screen**

SANs were differentiated from hiPSCs by using a modified GiWi protocol and adding molecules that were identified in the Protze protocol (and supported by Liu et al., Yechikov et al., Hou et al.) and Ren protocol as enriching factors for SANLPCs in heterogeneous cardiac differentiations<sup>40,45,52,64,65</sup>. Reproducibly, RA, Bmp4, FGF $\beta$ , and SB can improve differentiation efficiency for SANLCs (per initial reports from Protze et al.). However, the timing and concentration of molecules varies between protocols, and these variables were optimized in-house. Furthermore, re-activation of Wnt signaling with a second dose of CHIR (2xCHIR) after Wnt inhibition has also been demonstrated to be

sufficient for promoting the differentiation of SANLCs (per Ren et al.). Gene expression analysis via qPCR was used to assess the necessary molecules for yielding the best protocol for differentiating SANLCs based on upregulation of pacemaker genes after adding RA alone (0.25 $\mu$ M), Bmp4 alone (3ng/mL), SB alone (10mM), Bmp4 + SB, RA + Bmp4 + SB (RBS), and 2xCHIR (6 $\mu$ M) . After the initial round of testing, the timing (D3 and D4) and concentration (100-1000mM) of FGFi (RBS + FGFi = RBS+) were also optimized. Concentrations for these assays were taken from the Protze (for RA, Bmp4, SB and FGFi) and Ren (for CHIR) protocols<sup>40,65</sup>. The concentration of FGFi was the only molecule that was modulated due to the specificity of FGFi in different cell lines and the significance of FGFi in decreasing the percentage of CMs and enriching for SANLCs. Additionally, the results from the assessment of differentiation timing via gene expression in C2As (Figure 2.1) was used to time the administration of molecules. Samples were collected at D20  $\pm$ 15 and subsequently processed and analyzed as reported in the previous section detailing the qPCR protocol. 18S was used for normalization in analysis using the  $\Delta\Delta$ Ct to calculate fold change of genes in comparison to the GiWi protocol. Treatment groups had at least three biological replicates\*.

\*Only 1 biological replicate was run for each treatment group before passing to subsequent characterization assays. Other biological replicates were run after evidence of SANLC enrichment from other characterization assays. i.e. 2xCHIR didn't have more than three replicates because of its low beat rate (in Section 2.2.5) in comparison to RBS



### **2.2.5. Functional analysis via Pulse Contractility Assay**

GiWi and other treatment groups were performed in 12-well plates. Samples were recorded in a temperature/gas-controlled Oko chamber (Okolab) using a Zeiss Axio Observer Z1 inverted microscope equipped with a Hamamatsu ORCA-Flash 4.0 camera at intervals of 10ms (100 fps). 3-6 fields of view were captured at 10x and uploaded to the Pulse website for subsequent contractility analysis.

### **2.2.6. Phenotypic analysis via flow cytometry**

Cardiac cells (D20  $\pm$ 15) were dissociated with 0.25% trypsin for 30 minutes before trituration and quenching with 1mL of RPMI/B27+, 15% FBS, and 10 $\mu$ M RI (cardiac quench media). Cells were then collected and spun down at 80 – 190g x 5 minutes, resuspended in RPMI/B27+ with 10 $\mu$ M RI, and counted. 1x10<sup>6</sup> cells were collected from groups in microfuge tubes and fixed with 4% paraformaldehyde for 15-20 minutes at RT. Cells were subsequently spun down at 400g x 3 minutes in a tabletop centrifuge and subsequently washed 2x with PBS. Cells were then separated for different controls in a v-bottom 96-well plate (Costar). Cardiac cells were stained for cardiac troponin-T (cTnT) and Nkx2.5 (Table 2.2 for antibody information and concentrations) overnight using FACS buffer (PBS, 5% BSA, 5mM EDTA, 0.25% triton-X). Subsequently, cells were washed, and Alexa Fluor 488 and 647 were added for 1-2 hours at RT. Samples were analyzed on a Fortessa X-20 and the resulting data was analyzed using FlowJo software (v.11).

### **2.2.7. Immunocytochemistry**

Cardiac cells were dissociated as detailed in Section 2.2.6 and replated on matrigel-coated, plasma-treated glass multi-well plates at  $1 \times 10^4$  cells/cm<sup>2</sup> for immunofluorescent analysis. Cells were allowed 3-5 days to recover before being fixed with 4% paraformaldehyde for 15-20 minutes at RT and stained with cTnT, Shox2, and Nkx2.5 overnight at 4°C. Alexa Fluor 488, 555, 647, and Hoechst were added for 1-2 hours at RT (Table 2.2 for antibody information and concentrations). Stained cardiac cells were imaged on the Zeiss Axio Observer Z1 inverted microscope and then analyzed on Fiji (v.2.3) with a macro to quantify the percentage of Shox2+ cells (SANLCs).

### **2.2.8. Image acquisition & phenotypic assessment**

Minimally, 5 fields of view were imaged for each treatment group on the Zeiss Axio Observer Z1 inverted microscope. At least 10,000 cells were analyzed with a macro on Fiji (v.2.3) to obtain the percentage of Shox2+ cells (SANLCs) in the total cell population (DAPI+).

## **2.3. Results**

### **2.3.1. Wnt inhibition drives cardiac progenitor specification**

CMs and SANLCs undergo differentiation through multiple stages of cell-fate determination that is reflected by the expression of specific marker genes (Figure 2.1A). Zhao et al. have shown the expression of pluripotency (i.e. OCT4 and SOX2) and emergence of mesodermal (i.e. MESP1 and KDR), cardiac progenitor (i.e. NKX2.5, HAND1), and cardiomyocyte (TNNT2) markers from hPSCs<sup>71</sup>. We assessed fluctuations

in gene expression of important cardiac genes between D3-5 during a GiWi differentiation, compared to expression levels at D0 (Figure 2.1B). Genes typically upregulated during cardiac mesoderm specification (i.e. *NKX2.5*) increased around D3 in C2As similarly to WTC11s. Other early and late cardiac progenitor markers like *TBX5*, *ISL1*, and *SHOX2* were unchanged at D3. Increased expression of *TBX5* was observed at D4 and D5 (relative to D0), while *ISL1* and *SHOX2* gene expression was upregulated at D5 (compared to D0). This study confirmed the similar timing of cardiac specification in C2As and WTC11s after Wnt inhibition.

### **2.3.2. The combination of RA and Bmp4 signaling with TGF- $\beta$ /Nodal/Activin inhibition promotes SAN development during early Wnt modulation**

RA, Bmp4, and SB have been shown to be crucial for enhancing differentiation of pacemaker cells during cardiac differentiations<sup>42</sup>. A second (additional) dose of CHIR after Wnt inhibition has also been demonstrated to improve differentiation to SANLCs<sup>65</sup>. Therefore, we tested the hypothesis that Bmp4, RA, FGF and Nodal signaling with Wnt modulation would enrich SANLCs in comparison to the differentiation efficiency of the GiWi protocol. Cardiac cells were collected and initially analyzed for cardiac markers using qPCR every 5 days up to D20 (Figure S2.1). For overall cardiac differentiation assessment, *TNNT2* transcript levels were analyzed over time, and the consistent elevation of *TNNT2* transcripts in the RBS group suggested an improved cardiac differentiation with all three molecules compared to other groups.

By D20, RBS-treated cells typically expressed the highest levels of cardiac markers (*TNNT2*, *SHOX2*, *HCN4*, and *TBX18*) excluding *NKX2.5*, *ISL1*, and *TBX3*, which

were mostly upregulated in the BS (Bmp4 and SB) group. Notably, *NKX2.5* was most highly expressed by D10 in RBS, but it was downregulated by at least 3-fold over the next 5-10 days. This downregulation corresponded to the gradual significant increase of *SHOX2* in RBS-treated cells. *TBX3* and *ISL1* demonstrated similar expression profiles in the RBS group that remained upregulated by about 2-fold in comparison to cells in the GiWi protocol. On D5, *TBX18* expression was upregulated by over 3 to 100-fold in the RBS group compared to GiWi and other groups; however, this gene was downregulated with time, similar to what has been reported with high expression of *TBX18* observed only in early development<sup>22,42,64</sup>.

Previous studies have reported pacemaker-specific transcription factor expressions to be downregulated after D15<sup>22,64</sup>. We similarly found that all cardiac transcripts assayed (except *SHOX2*) either decreased on D15 or D20. After RBS, the RA alone and BS conditions resulted in the most efficient induction of the SANLC phenotype with upregulation of SA node markers and downregulation of *NKX2.5*. However, after his initial subtractive screen RA was chosen to move forward in subsequent analyses with 2xCHIR due to its role in upregulating *SHOX2*, an essential gene for pacemaker differentiation (Figure 2.2A)<sup>25</sup>.

The double dose of CHIR showed potential by sustaining increased *TBX18* levels similar to RBS by D20 of the differentiation (Figure 2.2B). Ultimately, the RBS group demonstrated the highest efficiency for generating a SANLC phenotype via transcriptional analysis of pacemaking and cardiac gene expression. Thus, we advanced cells treated with GiWi, RA, RBS, and 2xCHIR protocols to assessment with Pulse software for contractility analysis (Figure 2.2C). The addition of RA alone, RBS combination, and

additional CHIR significantly increased the beat rate of cardiac tissue in comparison to ventricular-like tissue produced by the GiWi protocol (~32bpm). RA alone increased the beat rate to ~53bpm; RBS increased the rate to ~100bpm; and 2xCHIR increased the rate to ~76bpm. Additionally, the long contraction time of ~0.41s in GiWi cells was significantly decreased to 0.14 - 0.15s. with the addition of the small molecules. This secondary screen prioritized the RBS protocol for the subsequent cytometric assay.

D10 differentiated cells using GiWi and RBS protocols were dissociated, fixed and stained with cTnT and Nkx2.5 for cytometric analysis. Both the GiWi and RBS groups had ~70% cTnT<sup>+</sup> cells, confirming the presence of CMs in both treatment groups (Figure 2.2D-E). To assess the differentiation efficiency of SANLCs (Nkx2.5<sup>-</sup>/cTnT<sup>+</sup>), Nkx2.5 expression was quantified, as previously reported in Protze et al. GiWi notably generated ~13% Nkx2.5<sup>-</sup>/cTnT<sup>+</sup> cells, and RBS improved the differentiation to ~20% Nkx2.5<sup>-</sup>/cTnT<sup>+</sup> cells. There was poor separation of both positive and negative cTnT and Nkx2.5 populations due to the early (D8) collection and analysis of differentiated cells as a result of the untimely COVID-19 shutdowns. However, four definitive populations were still identified. These findings indicate that the RBS protocol recapitulates the phenotype of developing SANs and suggests that later time points may be critical to isolate more defined and committed cell types.

### **2.3.3. Timing of spatiotemporal inhibition of FGF pathway is critical for promoting optimal SAN enrichment**

When we were permitted to resume wet lab work, we attempted to further improve the differentiation with the addition of FGF<sub>i</sub> in the RBS protocol. We tested different

concentrations (100nM, 300nM, 1000nM) and timing (D3 and D4) of FGF $\alpha$  similar to what has been published (Figure 2.3A)<sup>42</sup>. SANLPCs from the Protze lab were used as a positive control for the direct comparison of differentiation phenotype and efficiency. In the primary screen on D20, qPCR suggested 100nM and 300nM on D4 were the best groups for enrichment of SANLCs based on expression of important SAN genes (Figure 2.3B). *TNNT2*, *SHOX2*, and *TBX18* were notably upregulated in D4-300nM in comparison to GiWi, while *TNNT2* and *ISL1* were the upregulated in D4-100nM group. However, *NKX2.5* was also the most upregulated in these two groups. Intriguingly, the positive control SANLPCs only had upregulation of *TNNT2*, *NKX2.5*, and *TBX18* in comparison to in-house cells differentiated with the *GiWi* protocol.

Due to our knowledge of transcript levels being poor predictors of proteomics and phenotypes, flow cytometry was used to assess all seven groups and their expression of Nkx2.5. D20 cells were collected in this analysis, fixed and stained for cTnT. As observed previously, separation of cTnT<sup>+</sup> and cTnT<sup>-</sup> cells was best in the GiWi group where ~67% of the cells were cardiomyocytes (Figure S2.2a). Overall, there was reduced segregation of cTnT<sup>+</sup> and cTnT<sup>-</sup> populations with the addition of FGF $\alpha$ , but it was far less in D3 groups due to the presence of more transitional cells with longer exposure to FGF $\alpha$ . Treatment with 300nM FGF $\alpha$  on D3 appeared to generate the highest percentage of cardiomyocytes with 71% cTnT<sup>+</sup> cells. However, there were significantly more cells in groups treated with lower concentrations (100nM and 300nM) of FGF $\alpha$  and less exposure time (D4). Furthermore, there was still exceptionally poor separation between Nkx2.5<sup>+</sup> and Nkx2.5<sup>-</sup> populations. Therefore, Nkx2.5 expression was specifically assessed in the cTnT<sup>+</sup> population for more definitive analysis. Previous functional analysis of the GiWi

differentiation has shown  $\sim 5\% \pm 2\%$  of SANLCs are generated from this protocol. Therefore, we conservatively gated  $\sim 3\%$  Nkx2.5<sup>-</sup>/cTnT<sup>+</sup> cells in GiWi for downstream analysis of Nkx2.5 expression for all six RBS + FGFi groups (Figure 2.3c and S2.2). This elucidated 100nM on D3 and 300nM on D4 as the best two groups with  $\sim 40\%$  and  $\sim 35\%$  cTnT<sup>+</sup>/Nkx2.5<sup>-</sup> cells, respectively (Figure 2.3c).

The cytometry data was used to inform subsequent immunofluorescent analyses of Shox2 and Nkx2.5 expression in these two treatment groups in comparison to GiWi. When stained, Shox2<sup>+</sup> cells visibly increased with the addition of FGFi (Figure 2.3d); moreover, the percentage of Shox2<sup>+</sup> cells when stained with the antibody increase from 3% in GiWi to  $\sim 5\%$  and  $\sim 25\%$  in D4-300nM and D3-100nM groups, respectively (Figure 2.3e). To provide more confidence in analysis, Shox2<sup>+</sup> cells in SANLPCs were also quantified after fixing and staining.  $\sim 75\%$  Shox2<sup>+</sup> cells were detected in shipped SANLPC cultures which is comparable to the numbers of Nkx2.5<sup>-</sup>/cTnT<sup>+</sup> (78%) from cytometric analysis using the Nkx2.5:GFP expression from the reporter line (Figure 2.2c and e). Additionally, Nkx2.5 staining qualitatively showed the shift in SANLC enrichment with the stark decrease in Nkx2.5 expression compared to GiWi and supported the claim that D3-100nM induces the SANLC phenotype (Figure 2.3f). Therefore, 100nM on D3 was selected as the chosen “RBS+” protocol for future differentiations of SANLCs. These results demonstrate that the differentiation towards an SANLC fate is temporal- and dose-dependent.

#### **2.3.4. Statistics**

The mean +/- standard deviation was calculated from at least 3 biological replicates for all data unless otherwise noted. One-way analysis of variance (ANOVA)

followed by Tukey's post hoc analysis was performed to compare three or more groups. For all comparisons, statistical significance was determined at  $p < 0.05$ . The range of statistical significance is shown by an asterisk within the figure panels: ns = not significant, \* =  $p < 0.05$ , \*\* =  $p < 0.01$ , \*\*\* =  $p < 0.001$ , \*\*\*\* =  $p < 0.0001$ . All statistical analysis was performed using GraphPad Prism 9.0 software

## **2.4. Discussion**

Studies have shown that Wnt signaling induces stage-dependent changes in cardiac differentiations similar to what has been observed in development, and the timing can vary between cell lines. Understanding this timing is important for modifying and optimizing differentiations for specific cell types like SANs. We did this optimization by analyzing transcript levels of cells collected early in the heterotypic ventricular differentiation protocol (GiWi). The first heart field marker, *TBX5*, and cardiac progenitor marker, *NKX2.5*, were upregulated at similar levels to one another on D4 after 24 hours of Wnt inhibition<sup>72</sup>. *TBX5* and *NKX2.5* expression continued to increase at D5 after the full 48 hours of Wnt inhibition. *ISL1* (a second heart field marker) and *SHOX2* (a SAN marker) were not upregulated until D5. Figure S2.1 supports the hypothesis that pacemaker cells derive from a population in which *NKX2.5* is upregulated early in differentiation, followed by downregulation upon the rise of *SHOX2* (a known repressor of *NKX2.5*)<sup>25,73</sup>. Contrary to the lack of *ISL1* transcripts that we observed at D3, Zhao et al. showed that *ISL1* expression is significantly upregulated during D2 and D3 of the GiWi



protocol<sup>71</sup>. The delayed expression of *ISL1* and *SHOX2* aligns with what is expected of cells that are derived from the second heart field.

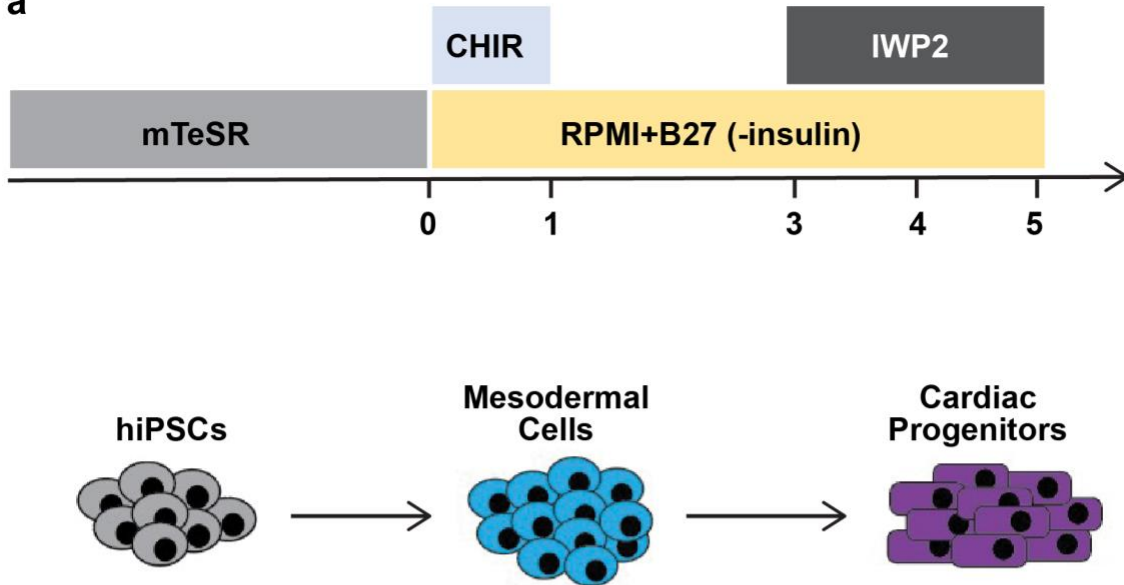
The RBS group consistently expressed some of the highest levels of pro-pacemaking transcripts. Although D15 or later SANLCs have historically exhibited lower levels of pacemaking transcription factors *in vitro*, in our hands, the transcripts seem to equilibrate and become reflective of respective cardiac phenotype by D20. Therefore, for purposes of the following study, D20 or later were time points mostly used for collection of a more differentiated batch of cells. The combination of RA, Bmp4, Nodal/TGF- $\beta$ /Activin, and FGF signaling was demonstrated to be important in SAN development for their specification from vCMs. The ventricular differentiation notably generated between 3% - 13% SANLCs (Nkx2.5<sup>-</sup>cTnT<sup>+</sup>Shox2<sup>+</sup>) per cytometric analysis. The addition of RA, Bmp4, and SB slightly improved the SANLC differentiation by increasing Nkx2.5<sup>-</sup>cTnT<sup>+</sup> numbers to about 20%. The addition of 100nM FGF<sub>i</sub> on D3 - D5 significantly increased SANLCs cells to 25% - 40% per cytometric and immunofluorescent analysis of Nkx2.5 and Shox2, respectively.

This study also demonstrated the importance of protein-level analysis for characterization of SAN differentiations because transcript levels are not always great predictors of phenotype. qPCR analysis suggested that 100nM of FGF<sub>i</sub> on D3 was one of the least successful protocols for inducing SA node differentiation; however, cytometry and immunocytochemistry showed the contrary. Additionally, Pulse contractility analysis helped predict the cardiac phenotype as a primary screening tool. The increase in beat rate and slowed contractility time was the best predictor of SANLC enrichment. The RBS group had rates up to 120bpm and contraction time as low as 0.1s. Ultimately, the series

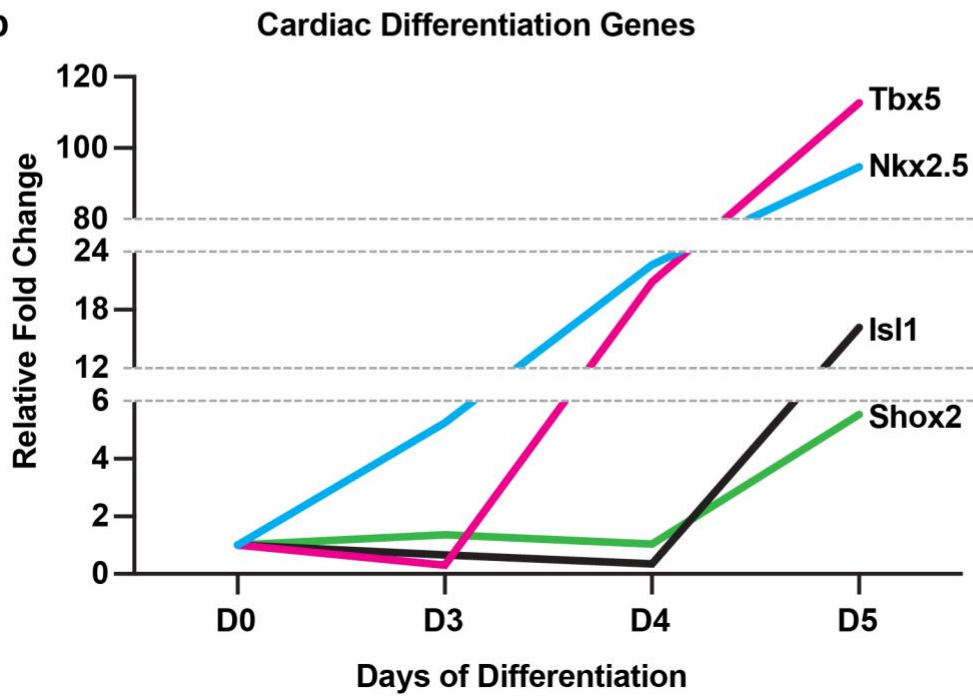
of screening methods led to RBS+ being chosen as the protocol for differentiation of SANLCs. However, the enrichment of SANLCs from RBS+ alone was inadequate (~25% Shox2+ cells) compared to Protze protocol used for SANLPCs (~75% Shox2+ cells). They used negative selection with a NKX2.5:GFP reporter line to enrich for Nkx2.5<sup>-</sup>cTnT<sup>+</sup> cells. Due to the expression of Nkx2.5 in the tail of the SAN, this reporter line has limitations for differentiating all types of SANs. We hypothesize that a SHOX2:GFP reporter line would alleviate these limitations by providing a more holistic approach to sorting SANLCs.

## 2.5. Figures

a

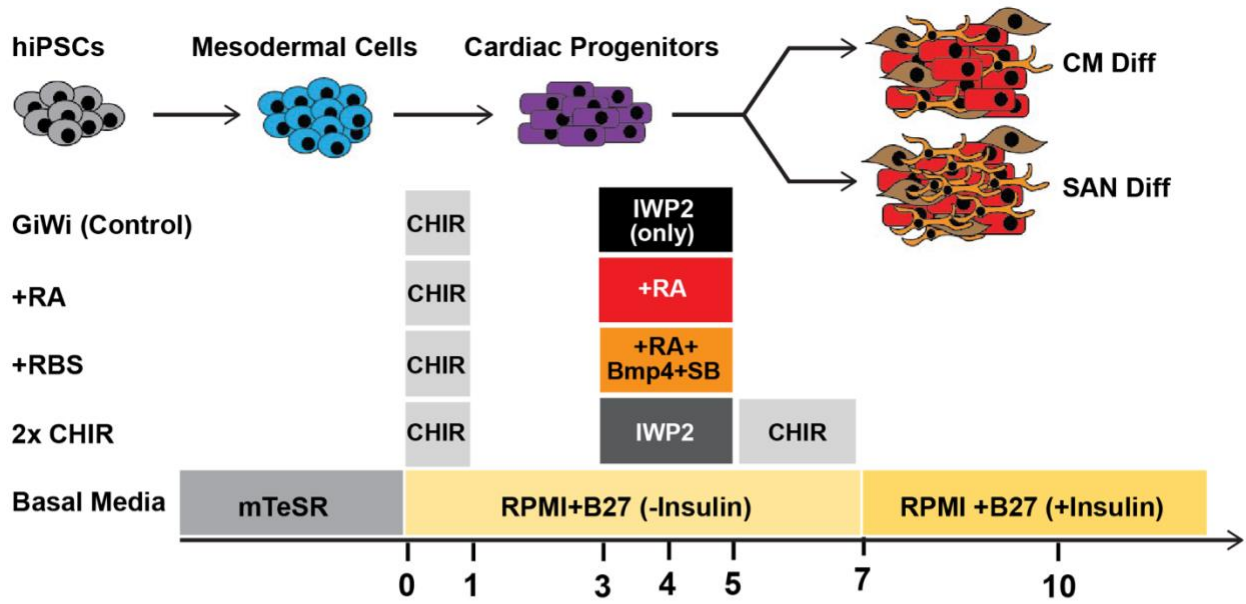


b

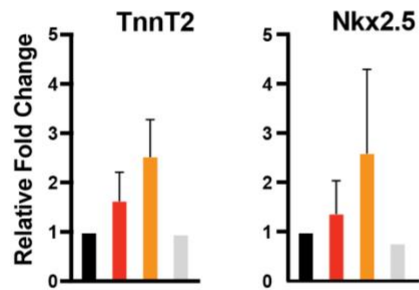
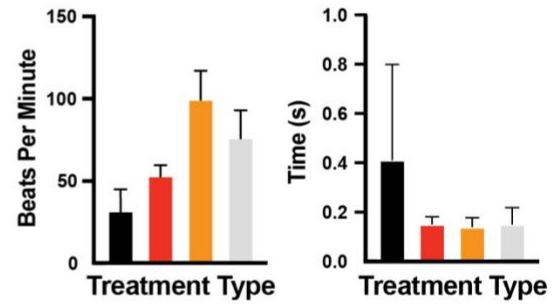
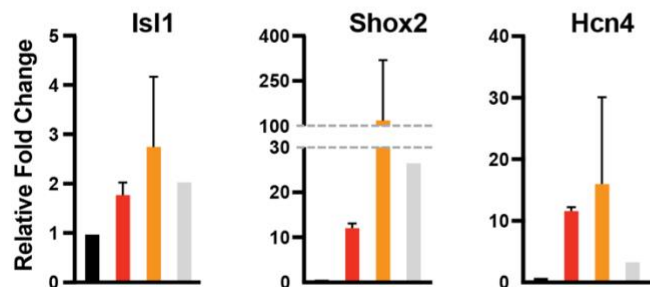
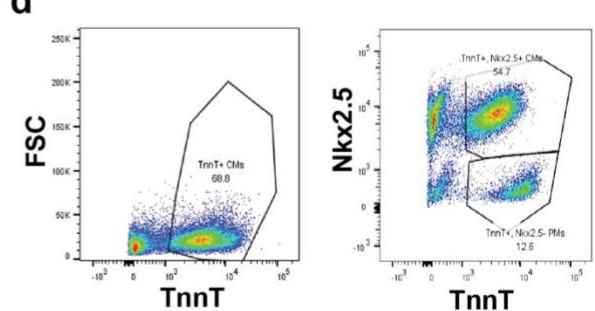
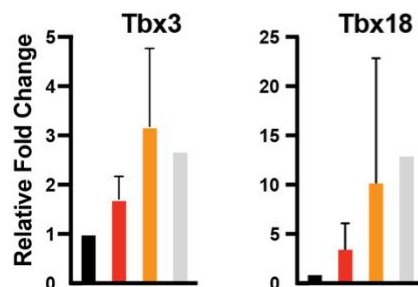
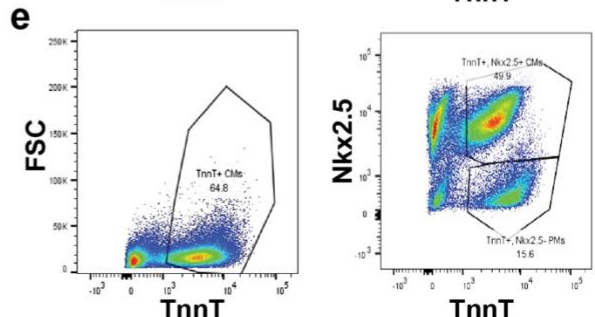


**Figure 2.1. Timing of cardiac markers early in a ventricular differentiation.**

(a) A schematic of the experimental set up of a ventricular (GiWi) differentiation up until day 5 (collection day) with corresponding stage-dependent cell types. (b) Expression levels of important cardiac transcripts on corresponding days of the differentiation.

**a****b**

■ GiWi  
 ■ +RA  
 ■ +R/B/S  
 ■ 2xCHIR

**c****d****e****f****g**

**Figure 2.2. Differentiation and phenotypic characterization of SAN-like cells from hiPSCs.**

(a) Layout of (part 1) differentiation protocols for the specification of cardiac cells: ventricular-like and SAN-like. (b) Transcriptional profiles of pacemaker and cardiomyocyte markers for different treatment groups: GiWi (black), +RA (red), +RBS (orange), and +2xCHIR (grey). Error bars depict standard deviation. (c) Quantification of spontaneous beat rate and contraction times for each respective treatment group using Pulse software (n = 15). (d) Representative flow cytometric analysis of the percentage of cardiac cells (TnnT+) and SANLCs (TnnT+/Nkx2-5-) for GiWi and (E) +RBS.

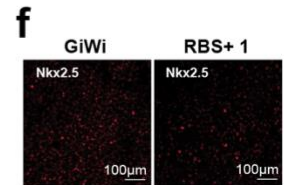
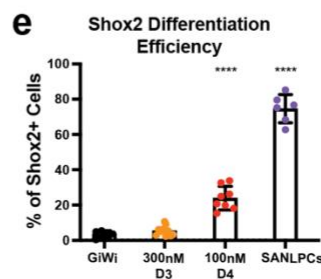
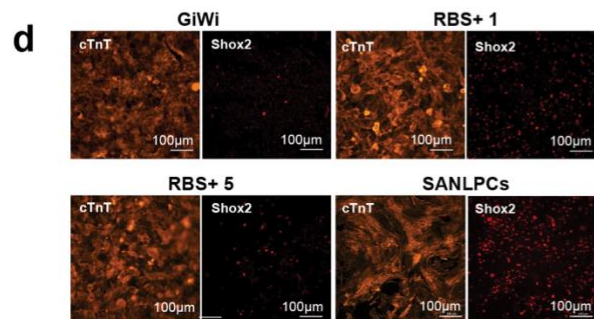
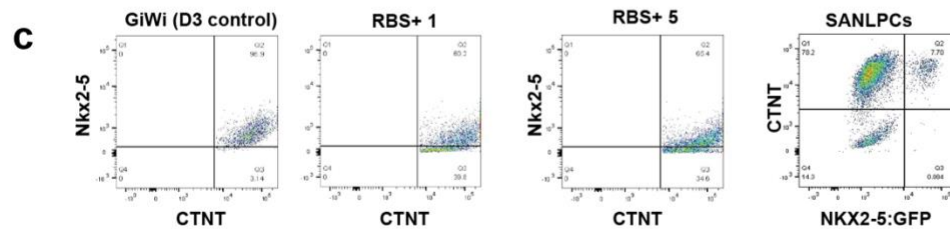
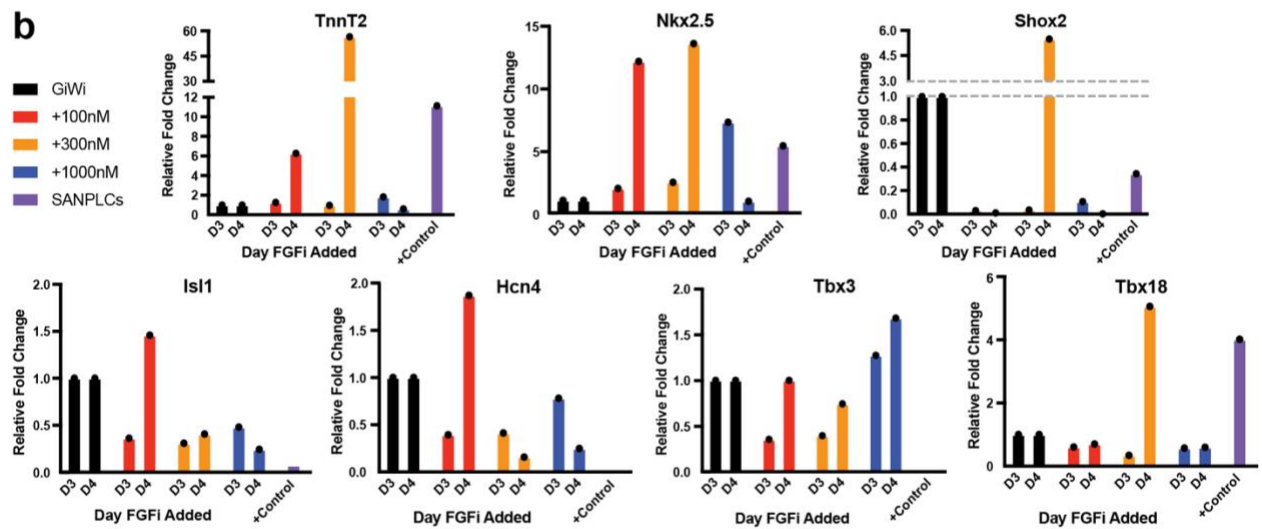
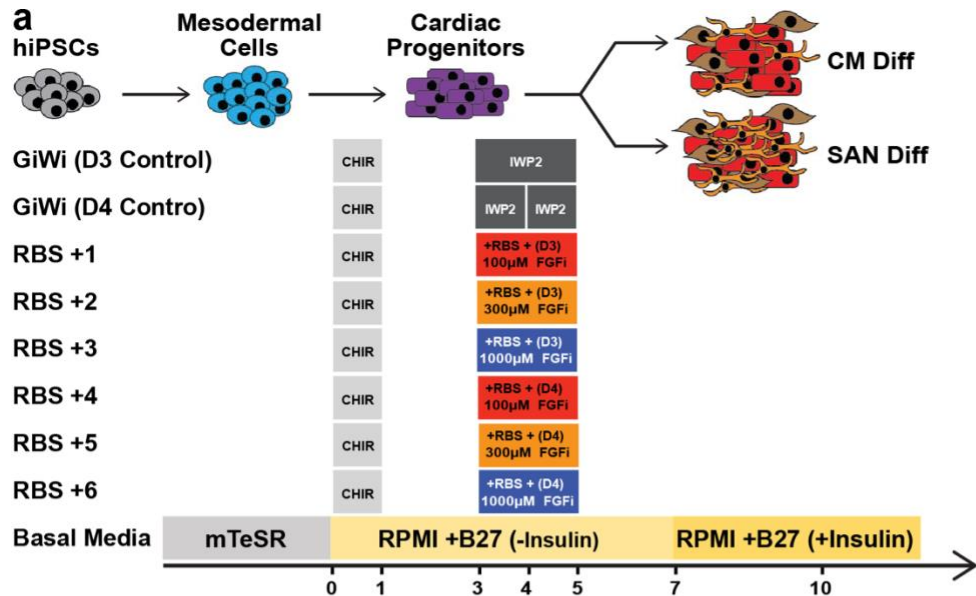


**Figure 2.3. Optimal timing and concentration of FGFi is essential in SANLC differentiations.**

(a) Layout of (part 2) differentiation protocols that vary the timing (D3 vs D4) and concentration (100 $\mu$ M, 300 $\mu$ M, and 1000 $\mu$ M) of FGFi for the specification of cardiac cells: ventricular-like and SAN-like. (b) Transcriptional profiling of pacemaker and cardiomyocyte markers in respective treatment groups (GiWi ,6 FGFi groups, and SANLPCs) relative to GiWi. (c) Representative flow cytometric analysis of immunofluorescent NKX2.5 expression of GiWi and the best FGFi treatment groups (RBS+ 1 and RBS+ 5), in addition to SANLPCs using endogenous NKX2-5:GFP signal. (d) Immunofluorescent imaging of GiWi, the chosen FGFi treatments and SANLPCs stained with *CTNT* and *SHOX2*. (e) Quantification of SANLPCs (*SHOX2*+ cells) via immunofluorescence (n = 6). (f) Representative immunofluorescent imaging of NKX2-5 for GiWi and RBS+ 1

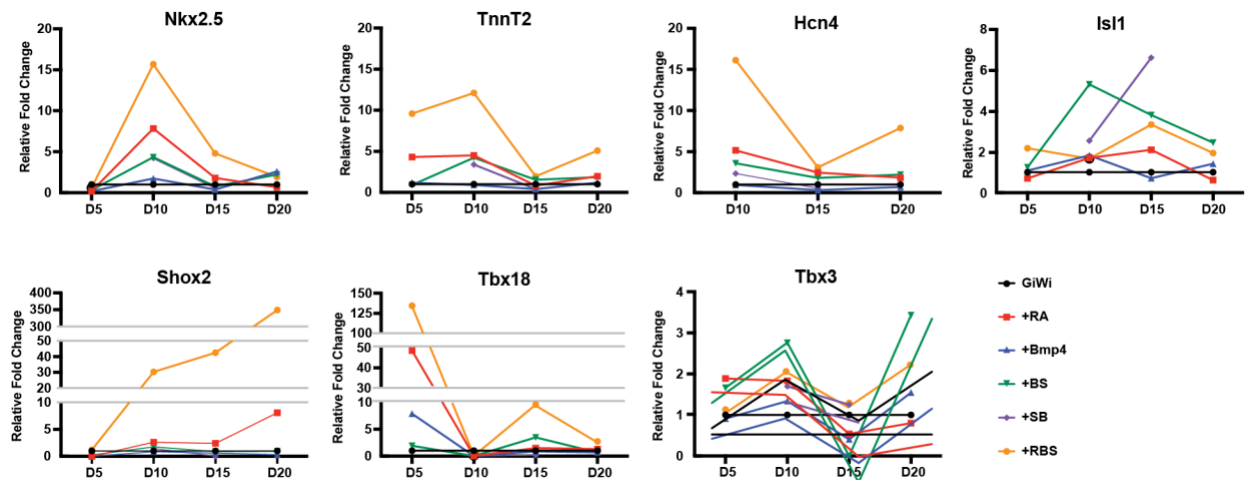




**Figure S2.1. Temporal expression of cardiac markers throughout hiPSC differentiation supports RBS as the best group for generation of a SANLC phenotype.**

Transcriptional analysis of cardiac and pacemaker genes throughout a 20-day differentiation for a molecular screen of the optimal cocktail needed for SANLC enrichment

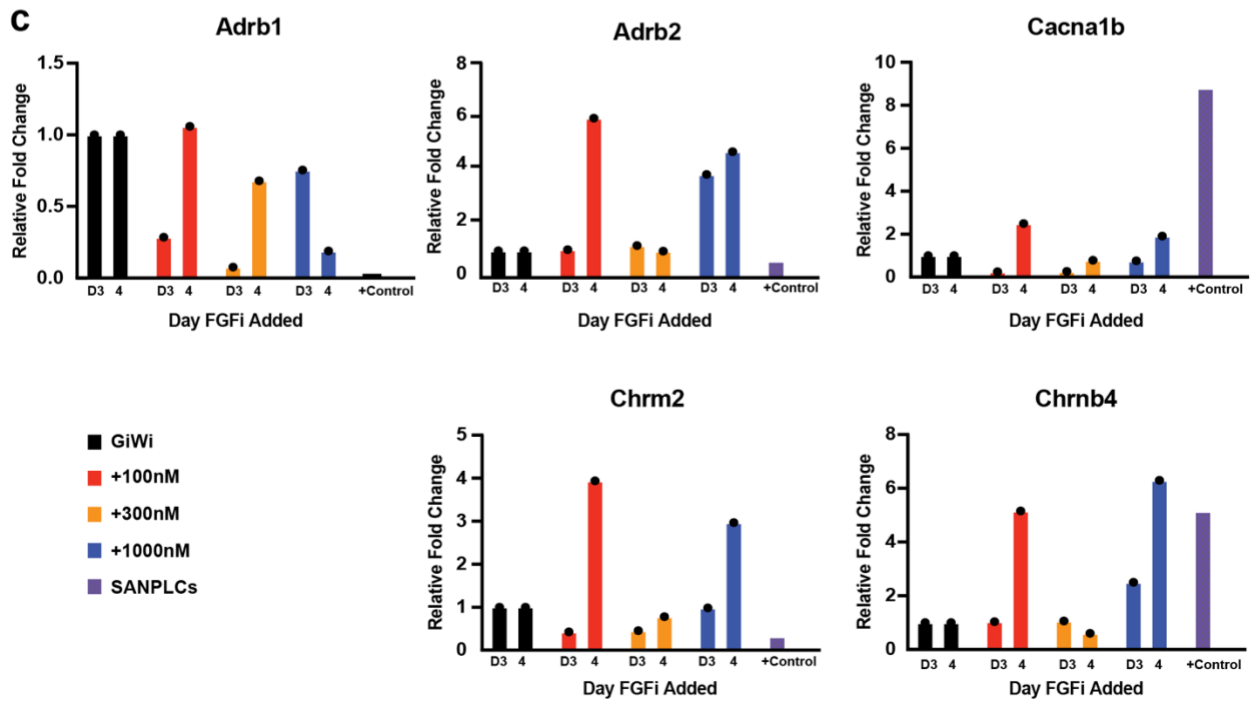
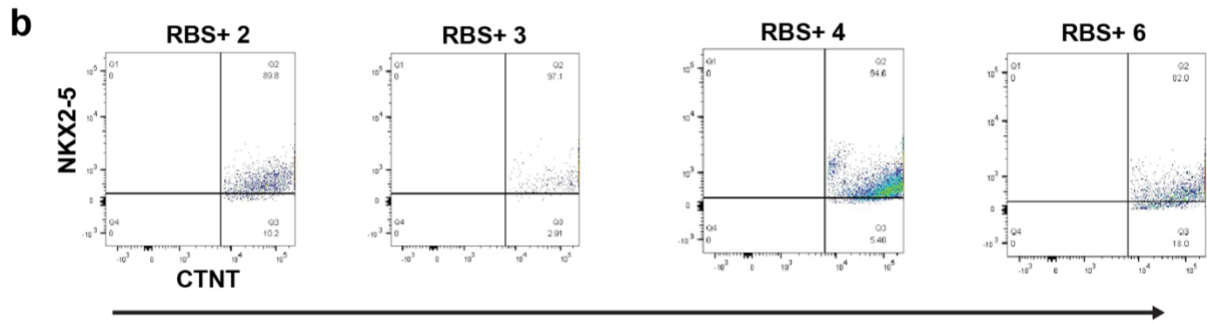
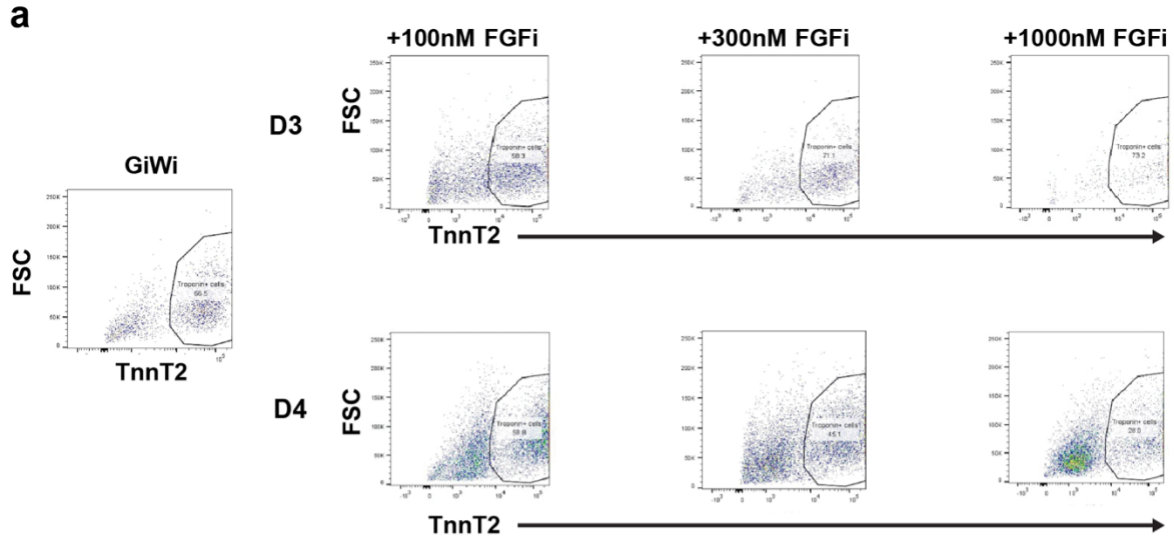


**Figure S2.2. Characterizing FGF*i* treatment groups for enrichment of SANLCs and upregulation of functional transcripts.**

(a) Cytometric analysis of cardiomyocyte differentiation efficiency from different FGF*i* treatment groups based on percentage of CTNT+ cells (b) Representative flow cytometric analysis of NKX2.5 expression of the additional FGF*i* treatment groups (RBS+ 2, RBS+ 3, RBS+ 4, and RBS+ 6) (c) Transcriptional analysis of receptors and ion channels critical for electrophysiological function of pacemakers and cardiomyocytes.

## CHAPTER 3. SHOX2 REPORTER LINE FOR IDENTIFICATION & PURIFICATION OF HPSC-DERIVED SINOATRIAL NODAL CELLS

### 3.1. Introduction

Reporter lines have conventionally been leveraged to identify cells of interest in various complex systems. Furthermore, labs have created reporter lines to help purify and quantify the purity of heterogeneous differentiations. Due to the inefficiency of *in vitro* differentiations of sinoatrial nodal cells (SANs), Protze et al. created a pluripotent Nkx2.5<sup>gfp/w</sup> reporter line to help identify pathways that regulate the development of Nkx2.5:GFP<sup>-</sup> SANs<sup>42</sup>. Due to the complexity of the SA node, this Nkx2.5<sup>gfp/w</sup> reporter line has technical limitations. Nkx2.5 is a key transcription factor in cardiac morphogenesis and a canonical marker of working cardiomyocytes<sup>74</sup>. Though Nkx2.5:GFP<sup>-</sup> cardiac cells are typically identified as pacemaker cells, not all SANs are Nkx2.5:GFP<sup>-</sup>.

The SA node is structurally heterogenous and is largely separated into head and tail regions<sup>22,75</sup>. The head of the SA node does not express NKX2.5, but the tail of the SA node does have a subset of cells that express this cardiomyocyte marker<sup>76</sup>. The head of the SA node is characterized largely by Shox2<sup>+</sup>, Tbx18<sup>+</sup>, Tbx3<sup>+</sup>, and Nkx2.5<sup>-</sup> expression; whereas, the tail is characterized by Shox2<sup>+</sup>, Tbx18<sup>-</sup>, Tbx3<sup>+</sup>, and Nkx2.5<sup>+</sup> expression<sup>22</sup>. Shox2 and Tbx3 are the only known transcription factors to be expressed in the entire SA node, but Tbx3 is a well-known marker for all pacemaker cells in the cardiac conduction system<sup>25,77</sup>. Consequently, Shox2 is one of the only known markers that distinctly labels SANs from cardiomyocytes (CMs) and other pacemaker cells. Additionally, Shox2 expression is one of the key upstream regulators in the SAN being found as early as E8.5 in the sinus venosus, a structure within the developing heart that gives rise to the primitive

pacemaker region<sup>25,76</sup>. To date, there has only been one study that has created and used a SHOX2:GFP reporter line to quantify and purify SA nodal-like cells (SANLCs)<sup>78</sup>. However, at the time of our study, that manuscript wasn't published yet, and the main purification approaches in hPSC systems used overexpression of SAN-specific transcription factors or a Nkx2.5 negative selection approach with a directed differentiation<sup>48,78,79</sup>. Here, we detail the steps that went into creating a pluripotent SHOX2:GFP reporter line, validating the phenotype, and leveraging it in some experiments.

## **3.2. Materials & methods**

### **3.2.1. Molecular cloning**

The SHOX2:GFP reporter line was generated utilizing CRISPR technology to insert the GFP cassette directly upstream of the *SHOX2* stop codon. The first steps involved designing a single guide RNA (sgRNA) from Synthego that targeted a specific region that was closest to 5' end of the *Shox2* stop codon using the Broad Institute GPP Web Portal (with guidance from Beeke Wienert, a former Gladstone postdoc; sequence in Table S3). Subsequently, ~800bp homology arms (5' and 3') were cloned from the genomic DNA of the WTC line via a 2-step PCR and specific primers targeting regions around the *Shox2* stop codon (cloning primer sequences in Table S3). The sequence of the homology arms was cleaned up in the second PCR step with a different set of primers and was validated using electrophoresis and Sanger sequencing. Subsequently, homology arms were ligated into Allen Institute's p05 backbone plasmid that contained the P2A-NLS-mEGFP cassette using a HiFi Gibson assembly (Figure 3.1a). Additionally,

this plasmid contained a TiaL1 selection cassette that contained a constitutively active mCherry directly downstream of mEGFP for validation and selection of transfected cells. Subsequently, the final plasmid was validated via electrophoresis and Sanger sequencing. Plasmids were transformed into NEB HiFi competent cells (New England BioLabs), colony picked, minipreped, and sequenced for the final stages of plasmid selection and construction of the SHOX2:GFP plasmid. Ultimately, a single clone (#8) was chosen as the best candidate and expanded for use in all Shox2 reporter experiments.

### **3.2.2. Transfection**

Lipofection was used to deliver the sgRNA, HiFi Cas9, and SHOX2:GFP plasmid. Our in-house wild-type (WT) C2A line (CVCL\_D081) was chosen for expansion of this SHOX2:GFP pluripotent stem cell line;  $1 \times 10^5$  cells/well were passaged and plated in a 6-well plate. Cells were fed with mTeSR daily and cultured until they reached about 50-60% confluency on the day of transfection. Invitrogen's transfection protocol was used to lipofect the cells. The five reagents used for this lipofection included OptiMEM, lipofectamine, sgRNA, HiFi Cas9, and the SHOX2:GFP plasmid. Each lipofection requires 50 $\mu$ L/well, and a GFP control was transfected in parallel to the replicate wells for the SHOX2:GFP transfection. For two reactions, 100 $\mu$ L of OptiMEM and 4 $\mu$ L Lipofectamine were added together and mixed in one tube; while 100 $\mu$ L OptiMEM, ~50ng (0.5 $\mu$ L) of sgRNA and HiFi Cas9, and 2 $\mu$ L of plasmid were added together and mixed in a second tube. Tube 2 was added to tube 1 and mixed well; subsequently, the tube was incubated at room temperature for 10 minutes. After incubation, 50 $\mu$ L were added to each well with a fresh 1mL of mTeSR media and incubated at 37°C overnight.

### 3.2.3. Clonal expansion of edited cells

Newly transfected cells were assessed for constitutive mCherry expression from successful transfection. Cells were cultured and maintained in mTeSR for an additional two days with daily media changes. Cells were subsequently passaged and split into two 10cm dishes at very low densities ( $1 \times 10^4$  cells/plate) per line and stocks of transfected cells were frozen down. Cells were plated sparsely for optimal clonal expansion and cultured with RI for 3-5 days after plating to allow for colony expansion. Cells were cultured in mTeSR with daily media changes, and colonies were picked in a sterile hood using an EVOS FL Cell Imaging System (Thermo Fisher Scientific) based on homogenous mCherry expression and re-plated in wells of a 48-well plate. Clones were cultured for an additional 3-5 days for expansion, but they were split before colonies became overgrown. Subsequently, cells were passaged into T25 flasks (Corning) for expansion. After a quality check and expansion, the  $1 \times 10^5$  cells expanded from the selected clone were passaged into a 6-well plate for a secondary transfection and removal of the Tial1 selection cassette. Invitrogen's transfection protocol was used again except with the Tial1 sgRNA for the directed cut of Cas9 and homologous recombination. The same expansion protocol was used as previously described except mCherry<sup>-</sup> cells were selected for in this secondary process (Figure 3.1c). Finally, clones were selected and characterized for quality of gene editing and final selection of the clonal pluripotent stem cell reporter line (C2A-SHOX2:GFP).

### 3.2.4. Quality control checkpoints

Quality control was performed before and after each transformation and transfection as a checkpoint. Electrophoresis, sanger sequencing, and karyotyping were the three main characterization methods used for quality control. Electrophoresis was the primary checkpoint used for validation of ligation or insertion with proper band size prior to sending samples to Quintara Biosciences for sequencing. Finally, karyotyping was utilized for a final quality control check before proceeding with functional tests with the reporter line to assess the functionality of Shox2-P2A-GFP cassette for downstream experiments.

Linearized plasmids were run on a 1.5% agarose gel to confirm plasmid sizes via electrophoresis. Samples were subsequently sent out for genotyping to validate sequences and alignment. For best assessment, primers approximately 100bp upstream of the junction or locus of interest were designed in-house and used in combination with primers designed by Quintara. For instance, the designed N-eGFP reverse primer and Quintara's free M13 reverse primer were used for validating the in-frame ligation of the homology arms. The sequences for all primers used for generating the donor plasmids are listed in Table S3.

Following clonal expansion,  $2.5 \times 10^5$  cells were collected and lysed with Lucigen's DNA Extraction Solution (Lucigen). *SHOX2* PCR primers were designed to target noncoding regions of the genomic *SHOX2* DNA that was upstream and downstream the 5' and 3' arm, respectively, while working around the high GC content of the *SHOX2* locus. The 3' end of the *SHOX2* locus was amplified with PCR using the KOD Hot Start kit (Sigma-Aldrich) with a 25 $\mu$ L reaction. The cycling conditions were as follows: 95°C x



2min, 95°C x 20s, 60°C x 10s, 70°C x 6min and repeated for 30 cycles. Samples were subsequently run on a 1.5% gel to validate insertion compared to a control WT non-transfected line (Figure 3.1b). Samples were once again validated by sequencing before transfecting with Tial1 gRNA and removal of the selection cassette. Validation was repeated after the second round of transfection (Figure 3.1c). The chosen clonal line was subsequently assessed for chromosomal abnormalities via quantitative fluorescence-PCR (QF-PCR) and shipped to Cell Line Genetics for karyotyping (Figure 3.1d-e).

### 3.2.5. Functional testing of reporter line

A functional test of the fluorescent tag is needed due to C2A-SHOX2:GFP being a hiPSC line and *SHOX2* only being expressed in differentiated cell types. For dual application, the best modified protocol to differentiate SAN-like cells (per Chapter 2) was used to test the functionality of the reporter line and assess *SHOX2:GFP*<sup>+</sup> cells versus *SHOX2:GFP*<sup>-</sup> cells. As detailed previously, published protocols such as those from Protze et al. and Birket et al. demonstrated that Bmp4, retinoic acid (RA), Activin/Nodal/TGFβ signaling inhibitor SB-431542 (SB), and FGF inhibitor PD173074 (FGFi) are important factors in the differentiation of SANs. To efficiently utilize these differentiations with the reporter line, a control GiWi (ventricular) protocol was differentiated in parallel to the RBS+ protocol with 100μM of FGFi on D3, as described in Chapter 2. Using these two protocols along with the newly constructed reporter cell line, I was able to assess the enrichment of SANs in our differentiations.

On D20-30, hiPSC-cardiac cells from both GiWi and SAN differentiations were collected and analyzed via flow cytometry to assess the expression of the *SHOX2:GFP*

tag (Figure 3.1b). 3 wells from a 12-well plate were initially dissociated using 0.5mL of 0.25% trypsin for 30 minutes before trituration and quenching with 1mL of RPMI/B27+ with 15% FBS and 10 $\mu$ M RI (quench media). Cells were then collected and spun down at 84g x 5 minutes, resuspended in cardiac maintenance media with RI, and counted with Countess Cell Counter (Thermo Fisher Scientific). 1x10<sup>6</sup> cells were collected from both groups and separated for both live and fixed cytometry. Cells were also replated on matrigel-coated, plasma-treated glass multi-well plates at about 1x10<sup>4</sup> cells/cm<sup>2</sup> for immunofluorescence analysis (Figure 3.1a).

For live cytometry, cells were changed from cardiac maintenance media to PBS with RI. CellTracker (Thermo Fisher Scientific) was spiked into samples and incubated at RT for 10 minutes. Samples were subsequently analyzed on a BD FACS Aria II and the resulting data was analyzed using FlowJo software (v.11).

For fixed cytometry, cells were fixed with 4% paraformaldehyde in microfuge tubes for 15-20 minutes at RT, then spun down at 400g x 3 minutes in a tabletop centrifuge, and subsequently washed 2x with PBS. Cells were transferred to 96 well v-bottom plates, and both groups were separated into 2 different wells for a negative control. Cardiac cells were stained with cardiac troponin-T (cTnT) (Table S2) overnight using FACS buffer (PBS, 5% BSA, 5mM EDTA, 0.25% triton-X). Subsequently, cells were washed and then Alexa Fluor 647 was added for 1-2 hours at RT. Samples were analyzed and sorted using the SHOX2:GFP reporter on a BD FACS Aria II and the sorted cells were analyzed using qPCR for gene expression of cardiac markers. Four groups (RBS+-Shox2<sup>-</sup>, RBS+-Shox2<sup>+</sup>, GiWi-unsorted, and RBS+-unsorted) were normalized to GiWi-Shox2<sup>-</sup> for analysis (Figure 3.1b-c).

In parallel, cells were plated, fixed with PFA for 15-20 minutes at RT, and stained with cTnT and Shox2. Alexa Fluor 555, Alexa Fluor 647, and Hoescht were subsequently added for 1-2 hours at RT. Endogenous *SHOX2*:GFP signal was assessed in comparison to immunofluorescence signal of Shox2. Stained cardiac cells were imaged on the Zeiss Axio Observer Z1 inverted microscope with a Hamamatsu ORCA-Flash 4.0 camera and qualitatively analyzed on Zen software and Fiji.

### **3.3. Results**

#### **3.3.1. Generation of reporter line**

*SHOX2* homology arms were cloned from genomic WTC11 DNA and ran on a 1.5% agarose gel to confirm ~800bp size. After the PCR cleanup and ligation of arms into the p05 backbone plasmids with GibsonAssembly, linearized plasmids were run on a gel to confirm the 8.4kbp plasmid (Figure 3.1a). Miniprepmed plasmids were sent out for genotyping to validate sequences and alignment. For best assessment, primers about 100bp upstream the junction or locus of interest were designed in-house and used from the company's free stock. For instance, the designed N-eGFP reverse primer and Quintara's M13 reverse primer were used in combination to validate the in-frame ligation of the homology arms. The sequences for all primers used for generating the donor plasmids are listed in Table S3.

Transfected cells were initially assessed based on numbers of mCherry<sup>+</sup> cells after 2 days. Cells were dissociated and sparsely replated in an attempt to expand a clonal population of *SHOX2*:GFP cells with the selection cassette. Following expansion, the 3' end of the *SHOX2* locus was amplified and assessed for insertion via electrophoresis by

running samples on a 1.5% gel in comparison to a WT non-transfected line and observing a 6kbp versus 2kbp band (Figure 3.1b). Green stars denote the best samples that were chosen to move forward. More testing was needed to critically assess the homogeneity of the P2A linked transgene, but based on relative amounts of mCherry<sup>+</sup> versus mCherry<sup>-</sup>, the brighter band is indicative of greater homogeneity compared to the lighter bands. Furthermore, the collected samples were from a polyclonal culture of cells, reflected by the double-band. Sequencing subsequently filtered samples and further confirmed the successful insertion and alignment of the cassette as well as the lack of mutagenesis from DNA repair.

After passing that checkpoint, the SHOX2:GFP chosen clone was re-transfected to cut-out the selection cassette as previously described. Following colony picking and expansion, mCherry<sup>-</sup> cells were collected for PCR amplification of the 3' end of the *SHOX2* locus, similar to before. When run on a gel, the amplicon size was now only 3kbp, verifying removal of the selection cassette and presence of the P2A-NLS-GFP cassette (Figure 3.1c). The chosen sample was picked based on band brightness and purity of single band denoting homozygous *SHOX2* alleles. The chosen samples were further confirmed with genotyping by assessing the *SHOX2-mEGFP* locus for mutations and frame shifts. The chosen clonal line was labeled #OG.

### **3.3.2. Karyotyping for abnormalities**

PCR-karyotyping or QF-PCR is an efficient and economical technique for detecting chromosomal abnormalities as a precursor to conventional karyotyping or fluorescence in-situ hybridization (FISH). PCR-karyotyping elucidated a putative

amplification in a minimal critical region of Chromosome 17q and a possible trisomy in Chromosome 20q (Figure 3.1d). These findings necessitated conventional karyotyping and FISH analysis on a culture of the reporter line.

Cell Line Genetics karyotyped eighteen cells in total and reported fifteen cells demonstrated an apparent normal male karyotype (Figure 3.1e). However, three cells demonstrated non-clonal chromosome aberrations, with two cells showing a very small duplication within band q11.2 of the long arm chromosome 20, which includes BCL2L1 (Figure 3.1e). As extra copies of this BCL2L1 region are associated with a proliferative growth advantage in hPSCs, it is important to note that this reporter line did proliferate slower than WT lines. As a follow-up, FISH was performed using 20q11.21/1q32.3 probe set in order to detect changes in Chromosomes 1 and BCL2L1 gene copy numbers. Trisomy 20q11.21 was detected in 28.5% of the cells, and the remaining cells demonstrated normal FISH signal pattern at a 99% confidence level based on cut-off values determined by CLG lab.

### **3.3.3. SHOX2:GFP signal is weak but detectable**

The reporter line was differentiated using both the GiWi and RBS+ protocol in parallel for up to D30 before being collected for analysis. GFP signal was not visible on EVOS nor inverted microscope using live imaging throughout the 30-day maintenance culture, but there were discernible beat rate differences between the two different treatment groups. Cells were collected for live and fixed cytometry to assess the SHOX2:GFP signal and reliability of GFP signal in fixed and live samples (Figure S3.1a). SHOX2:GFP signal was too low to segregate  $Shox2^+$  and  $Shox2^-$  clusters, but there was

sufficient signal for quantification and sorting. The GiWi differentiation yielded ~5.8% SHOX2:GFP<sup>+</sup> cells, while RBS<sup>+</sup> produced ~16.1% SHOX2:GFP<sup>+</sup> cells.

Differentiated cells were also replated and stained for Shox2 (red) to assess the immunofluorescence signal compared to that from endogenous SHOX2:GFP (green) expression (Figure 3.2b). SHOX2:GFP was visible but faint and had a lot of background noise. There is a significant increase in red and green cells in the RBS<sup>+</sup> group by D30 compared to GiWi. When merged, there are mostly yellow cells with some solo red cells from the low levels of SHOX2:GFP signal. This suggests that the quantity of SHOX2<sup>+</sup> cells may be underestimated by measurement of the GFP signal. Low SHOX2:GFP signal results in the presence of residual red cells and the lack of all yellow cells in the merged channel, and this is most likely causal to the low percentages of SHOX2<sup>+</sup> cells observed in cytometric analyses.

#### **3.3.4. SHOX2:GFP reporter supports RBS<sup>+</sup> differentiation as the most optimal**

To further assess the effectiveness of the SHOX2:GFP reporter line, cells were differentiated using GiWi and RBS<sup>+</sup>, as done previously, fixed, and sorted for subsequent qPCR analysis. Cells were stained for cTnT to assess overall cardiac differentiation efficiency with SHOX2:GFP expression for contextual sorting (Figure 3.2b). The respective gates were drawn conservatively into the positive populations to ensure confidence in cellular subtype. Nonetheless, this analysis supported previous findings that the GiWi protocol leads to efficient cardiomyocyte differentiation based on the high (74.2%) cTnT expression compared to lower levels (~61%) in the RBS<sup>+</sup> group. Notably, the GiWi group had distinct clusters of cTnT<sup>+</sup> and cTnT<sup>-</sup> populations, while RBS<sup>+</sup>

produced more overlapping clusters. This lack of separation is suggestive of transitioning cells or subsets of cells with mid-level expression of cTnT in the RBS+ group. Furthermore, the RBS+ protocol resulted in ~16% SHOX2:GFP<sup>+</sup> cells from the cardiac population, while GiWi had only 4%, similar to our live signal results.

From the two treatment groups, SHOX2:GFP<sup>+</sup> and SHOX2:GFP<sup>-</sup> cells were sorted from each group for analysis of cardiac marker gene expression (Figure 3.2c). To evaluate the specificity of sorting, unsorted samples of GiWi and RBS+ were also assessed; however, all samples were normalized to the GiWi-SHOX2<sup>-</sup> group. The RBS+-Shox2<sup>+</sup> group had lower *NKX2.5* expression than the GiWi-Shox2<sup>-</sup> group, as expected. Additionally, *HCN4*, *ISL1*, *TBX18*, and *TNNT2* were all upregulated by at least two-fold in RBS+-SHOX2<sup>+</sup> groups; *TBX3* was only slightly increased in this group. In general, all RBS+ groups behaved as predicted with increased levels of *HCN4*, *TBX18* and *TNNT2*. Interestingly, *NKX2.5* was slightly higher in RBS+-SHOX2<sup>-</sup> group than the GiWi-SHOX2<sup>-</sup> group. This is suggestive of the underlying causes for the upregulated *NKX2.5* levels that is observed in unsorted RBS+ groups. *TBX18* is a common epicardial marker in addition to being a marker of the SA node head region. Therefore, it was interesting to see such high expression of *TBX18* transcript in the RBS+-Shox2<sup>-</sup> group, whereas RBS+-Shox2<sup>+</sup> and unsorted RBS+ groups had similar levels of *TBX18* expression. Notably, GiWi unsorted unsorted cells displayed approximately zero-fold change for nearly all transcripts (except *TBX18* and *TNNT2*) in comparison to GiWi-Shox2<sup>-</sup> cells.

### **3.4. Discussion**

In conclusion, this SHOX2:GFP reporter line was created to identify SANLCs in heterogeneous cultures produced by the existing inefficient SAN differentiation protocols. At the time of this study, there were no reported SHOX2 reporter lines. We used CRISPR-Cas9 gene editing to incorporate a GFP cassette directly upstream the *SHOX2* stop codon. Due to the importance of *SHOX2*, a self-cleaving (P2A) sequence was chosen to link expression of GFP to the gene of interest, rather than generating a fusion protein. We chose to edit the C2A line in order to take advantage of a preexisting channelrhodopsin C2A line for future studies. Various quality checkpoints were used for the engineering of the plasmid and reporter cell line. The majority of engineered cells were karyotypically normal, but there was a small subset of cells that had a trisomy in Chromosome 20. These cells could be selected out in follow-up studies to prevent the overpopulation of these mutant cells.

After quality control, characterization was performed with the reporter line to assess its functionality. This study demonstrated that the GFP signal is low when the hiPSCs are differentiated using either ventricular or SAN differentiation protocols. *SHOX2* transcript levels and SHOX2<sup>+</sup> cells were increased in SAN differentiations (RBS+) compared to ventricular differentiations (GiWi), as indicated by both increased GFP signal and increased endogenous Shox2 signal. Although the GFP signal is dim in this reporter line, we demonstrated that it is sufficient to enable sorting by cytometry and subsequent qPCR analysis. With roughly a three-fold increase in SHOX2:GFP<sup>+</sup> cells in the RBS+ differentiation, there was also an upregulation of SAN markers in sorted SANLCs. This



study substantiates the use of this SHOX2:GFP line in future studies for the purification of SANLCs.

### 3.5. Figures

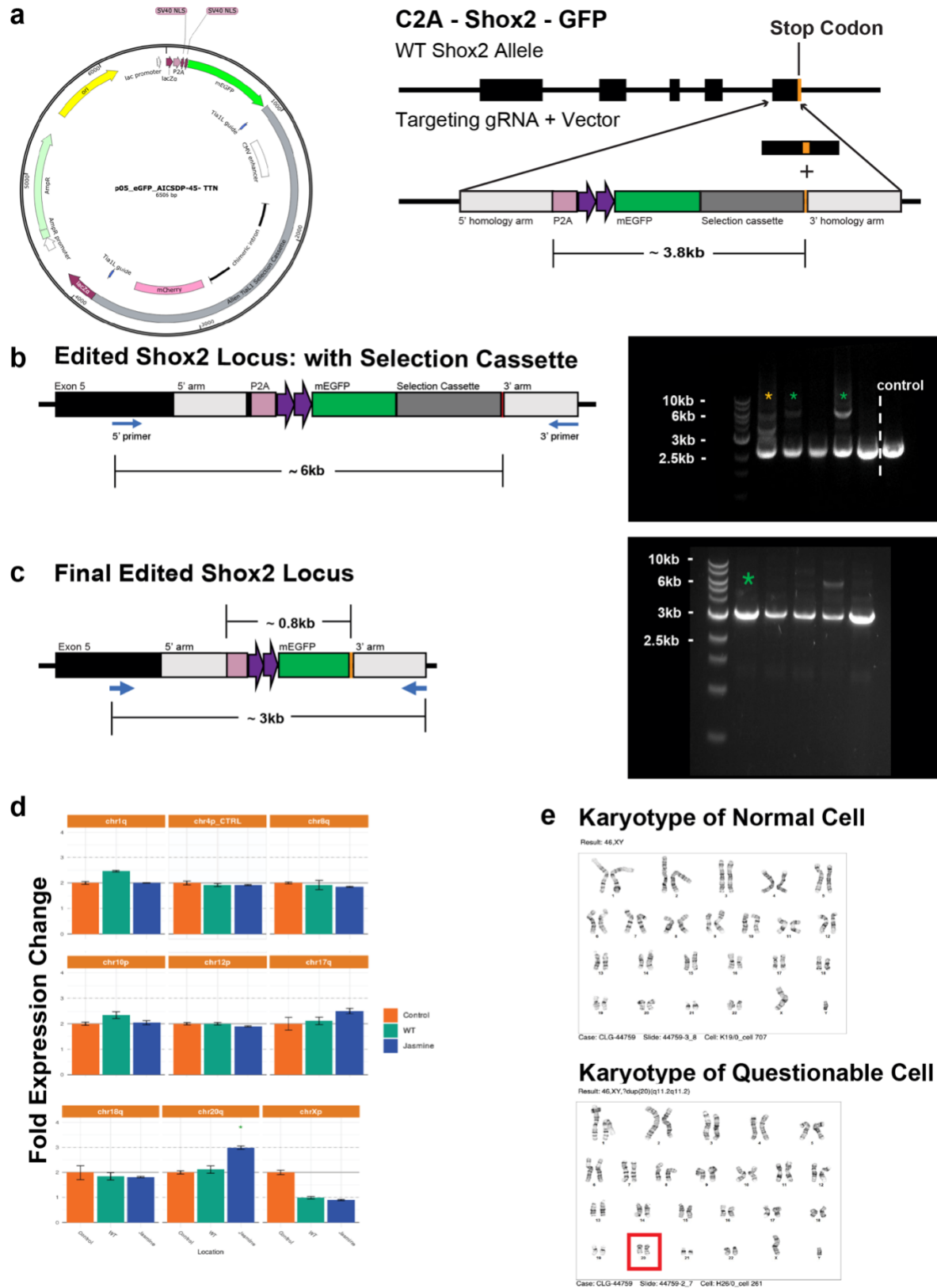
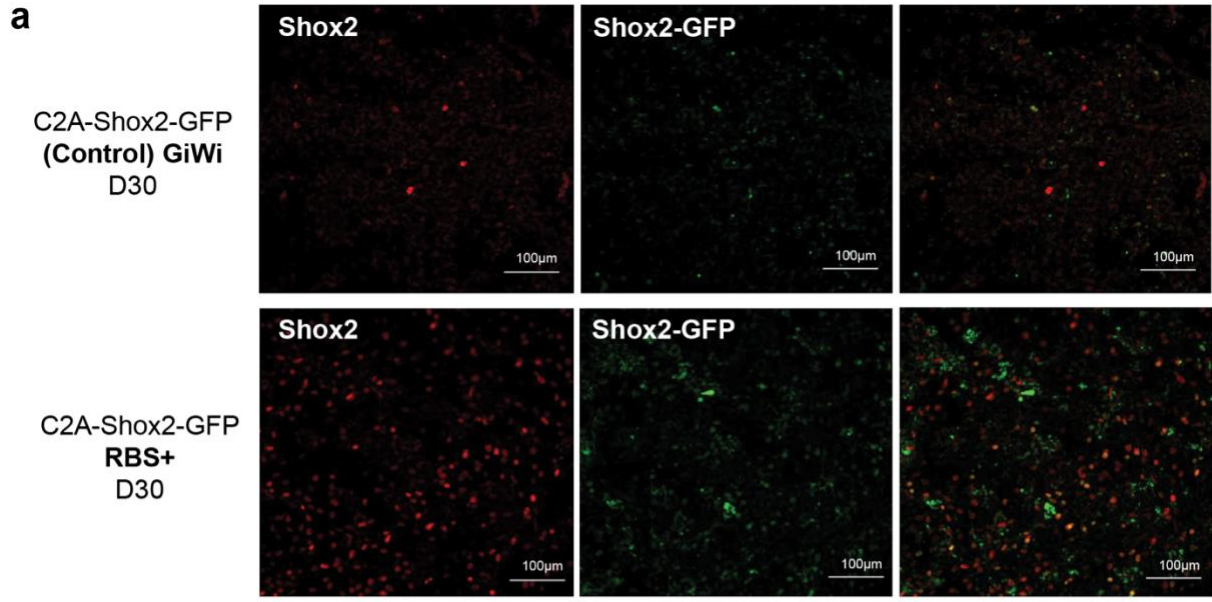
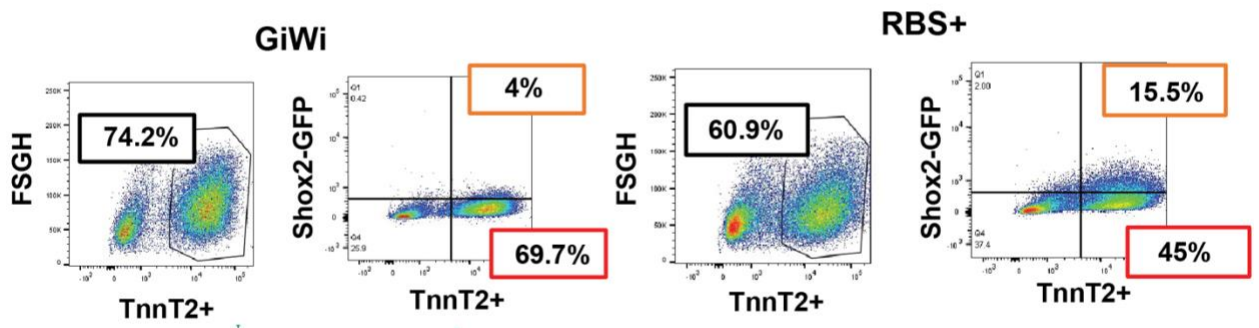


### Figure 3.1: Creating a SHOX2:GFP reporter line.

(a) A plasmid map and schematic of the donor construct that was used to link GFP directly upstream the *SHOX2* stop codon with a targeting gRNA using the CRISPR-Cas9 system. (b) A schematic of the edited *SHOX2* locus with insertion of the P2A-NLS-GFP and selection cassette with the corresponding agarose gel electrophoresis and respective bands (yellow star = potential clone; green star = selected clone). (c) A schematic of the final edited *SHOX2* locus after cutting out the selection cassette with CRISPR-Cas9 system and corresponding gel with the selected clone (green star = #OG = SHOX2:GFP line). (d) QF-PCR plot for detection of karyotypic abnormalities of #OG (blue) compared to internal control (orange) and WT C2A line (green). (e) Normal and questionable karyotype of the #OG line.



- b**
- Cardiac Cells (TnnT2+)
  - ▨ SANs (Shox2+/TnnT2+)
  - ▨ Cardiomyocytes (Shox2/TnnT2+)



**c** **Fold Change of Genes for Respective Groups**

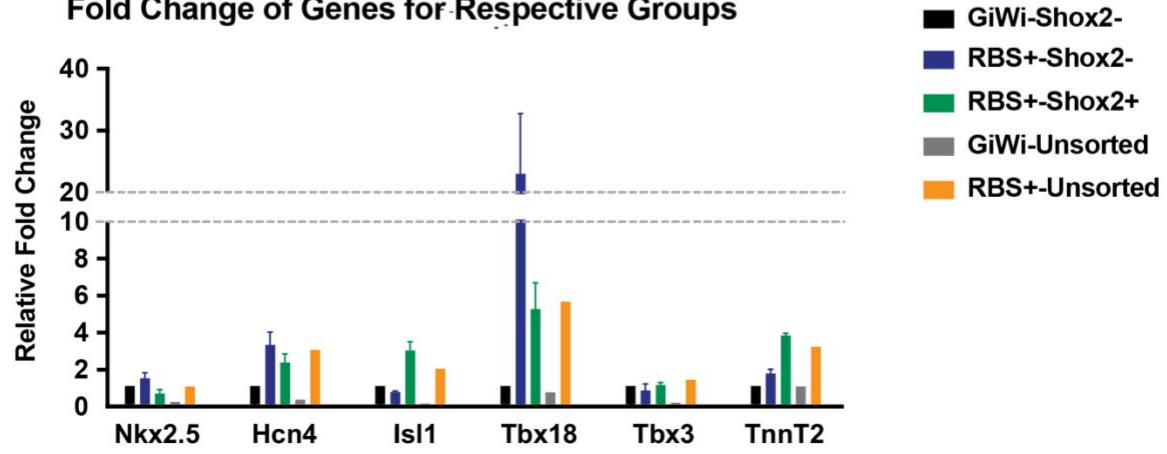


**Figure 3.2: SHOX2:GFP signal is weak but detectable.**

(a) Representative immunofluorescent images of stained SHOX2 (red) overlaid with endogenous SHOX2:GFP (green) signal to exhibit real signal from reporter line (yellow) in RBS+ compared to GiWi groups. (b) FACS plots of fixed GiWi and RBS+ samples stained with CTNT and gates used to sort using SHOX2:GFP signal. (c) Sorted and unsorted groups analyzed and compared to GiWi-SHOX2<sup>-</sup> via qPCR to assess the enrichment of SANLCs in RBS+-SHOX2<sup>+</sup> samples.

- Cardiac Subtypes (Shox2-)
- SANs (Shox2+)

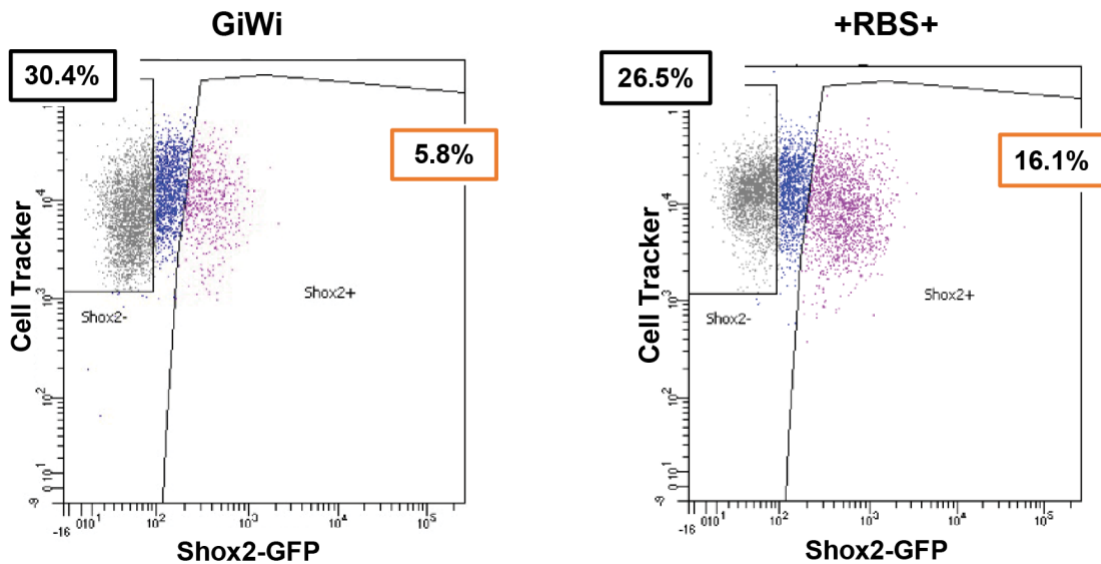


**Figure S3.1. Live SHOX2:GFP sorting is comparable to fixed sorting.**

Flow cytometric analysis of live SHOX2:GFP signal with Cell Tracker dye

## CHAPTER 4. FUNCTIONAL CHARACTERIZATION OF CARDIAC CELLS

### 4.1. Introduction

Cardiomyocytes (CMs) and sinoatrial nodal cells (SANs) are functionally different from each other and other cardiac cells as a result of differentially expressed ion channels<sup>7</sup>. CMs are the contractile cells responsible for heart contractions, and SANs are a subset of the conducting cells that generate and transmit electrical impulses throughout the heart<sup>15</sup>. This divergency gives rise to distinct functional properties like action potentials and calcium transients. Furthermore, the differentially expressed ion channels and consequently their respective functional properties are known to change throughout development<sup>7</sup>. Therefore, it is standard to functionally characterize cardiac cells to help elucidate their phenotype and developmental stage. For instance, *Hcn4* funny channels are known to be specific to the cardiac conduction system and are responsible for the spontaneous depolarization and lack of stable resting membrane potential in SANs. However, immature CMs also express *Hcn4* before it is restricted to the mature SA Node<sup>7,80</sup>. Additionally, expression of *Cacnb2*, a L-type Calcium channel, increases throughout development in SANs and contributes to an increased upstroke velocity in their action potential waveforms<sup>7,81</sup>. Most studies have functionally and phenotypically characterized CMs and SANs in murine models; however, van Eif et al. reported the genetic program of SANs in mice is conserved in humans. Nonetheless, it is important to note that mice have a significantly higher resting heart rate (roughly 10 times) compared to humans: 190-245 bpm in the fetal stage and 500-700bpm in the adult stage compared to 120-160bpm and 50-70bpm, respectively<sup>34,82,83</sup>.

Furthermore, calcium transients, action potentials, and molecular responsiveness have been characterized to assess the functional state of cardiac cells. Each assessment reveals something slightly different about function, but they all are dependent on molecular flux and are temporally related to one another. Various ions (i.e. sodium, calcium, potassium) and neurotransmitters (i.e. norepinephrine and acetylcholine) are endogenously produced in cardiac microenvironments. Cardiac cells respond to signaling molecules that are necessary for their different functions - i.e. contraction (CMs) vs conduction (SANs). Subsequently, a flux of ions rapidly changes the voltage across the membrane and thus causes an action potential. Various cardiac cellular subtypes have unique action potential waveforms based on differential expression of ion channels (i.e. *Hcn4<sup>+</sup>* vs *Hcn4*), and these parameters help identify the different cell types<sup>84</sup>. For this electrophysiological assessment, patch clamp is the gold standard; however, voltage sensitive dyes and microelectrode arrays (MEAs) have been used as substitutes for a higher throughput and more automated analysis. Fluorescence imaging (i.e. voltage sensitive dyes) is more user friendly and less labor-intensive, but it has its limitations with phototoxicity and photosensitivity<sup>68</sup>. Furthermore, calcium imaging can be used to determine the physiological state of CMs. Two of the primary calcium indicators are Calcium fluorescent dyes (Fluo-4 AM, green; Rhodamine-3 AM, red) or genetically encoded calcium sensor cell lines (GCaMP). Here, we used a multitude of techniques to assess the functional phenotype of SANLPCs and the need for pure cultures of SANLCs for future co-cultures.

Current directed differentiation protocols to generate hPSC-SANs and -CMs produce a heterogeneous mixture of ventricular-, atrial- and SAN-like cells<sup>52</sup>. At the time

of this study, the hPSC-SAN protocols had either low efficiency (~30%) or were dependent on sorting with a reporter line (~70% = NKX2.5<sup>-</sup>/CD90<sup>+</sup>) in comparison to a well-defined, efficient hPSC-CM protocol in which ~85% of the product are the desired cell type<sup>65,85,86</sup>. Due to electric-coupling, cardiac cultures functionally take on the phenotype of the enriched subtype in terms of beating frequencies, voltage and calcium-handling properties. However, it is unknown at what cellular ratios the functional phenotype shifts for respective cardiac subtypes. Therefore, we leveraged the power of GCaMP-hPSC-CMs cultured with hPSC-SANs from the Protze Lab (AKA SANLPCs) to understand the thresholding effect of heterogeneous cultures based on the change in calcium-handling properties of controlled cardiac microtissues. This approach was designed to also uncover the need or lack thereof for an enriched population of hPSC-SANs and a reporter line for future co-cultures with neurons (Chapter 5).

## **4.2. Materials & Methods**

### **4.2.1. Cardiac microtissue formation**

GCaMP-hPSC-CMs\* (D30 ±5; kindly donated by Will Flanigan) and SANLPCs (D30 ±5; kindly donated by Stephanie Prtoze) were dissociated with 0.25% Trypsin and then mixed together in proportions of 0%, 3%, 10%, and 30% of SANLPCs/CMs x 100 with a total of  $2 \times 10^6$  cells. Cell mixtures were seeded into 1000µm inverted pyramidal agarose microwells at a density of 2000 cells/well and aggregates allowed to self-assemble overnight in RPMI/B27+ with 10µM RI (Figure 4.1a)<sup>87</sup>. After 24 hours, the aggregated cardiac microtissues were removed from the wells and maintained in rotary



suspension culture at 1000 microtissues per 1 well of a 6-well plate for 7 days (Figure 1b-c).

\*GCaMP-hPSC-CMs were differentiated using the standard GiWi protocol, which also generates a small fraction of SANs ( $\sim 5\% \pm 2$ ).

#### **4.2.2. GCaMP analysis of cardiac microtissues to understand the impact of SANLPCs**

In this study, we analyze the calcium handling properties of heterogeneous cardiac microtissues. Spontaneous activity was recorded on a Zeiss Axio Observer Z1 inverted microscope while in a temperature/gas-controlled Oko chamber (Oko Labs). Paced activity was also recorded on the inverted microscope by placing electrodes in each respective well of the 6-well plate and applying electrical field stimulation at 1, 2, 3 and 4 Hz (MyoPacer, IonOptix). Video acquisition of calcium flux was obtained using Zen Professional software (v.2.0.0.0) with 10ms exposure and 100fps. One circular ROI (134 $\mu$ m or 525 $\mu$ m) was made at the center of each aggregate for data acquisition, and the mean fluorescent intensity values were plotted (Figure S4.1c). A custom lab R-script was used to further analyze the calcium transients and quantify the kinetics of each fluorescent intensity profile (i.e. amplitude, beat rate, velocity, time; Figure S4.1b).

#### **4.2.3. Voltage imaging**

Mature CMs have a stable membrane potential between action potentials unlike SANs which have a diastolic depolarization phase for their autonomic function<sup>84</sup>. SANs retain this autonomic phenotype throughout development due to the expression of funny

channels. Conversely, immature CMs develop from this immature fetal/neonatal state into a stable quiescent steady state postnatally in maturing rodents<sup>84,88,89</sup>. In comparison to adult CMs, the electrophysiology of newly differentiated hPSC-CMs is immature; this is consistent with PSC-SANs and other differentiated cell types<sup>42,90</sup>. The presence of diastolic depolarization makes the action potentials of hPSC-CMs and -SANs less discernible, but a slight plateau phase is still visible and indicative of a CM phenotype. However, quantifying waveform parameters like the action potential duration at 90s/50s (APD<sub>90/50</sub>) is the best metric to identify ventricular-like CMs (<1.4), nodal-like (1.4 - 1.7), and atrial-like CMs (>1.7). For simplicity, we used FluoVolt membrane potential dye to plot the waveforms and quantify APD<sub>90/50</sub> of dissociated single cells paced at 1Hz electrical field stimulation.

hPSC-cardiac cells from the GiWi and RBS+ (from Chapter 2) differentiations were plated on glass cover slips with plasma treatment and matrigel-coating. FluoVolt™ Membrane Potential Kit (Thermo Fisher) was used to measure action potentials of cardiac cells. Fresh FluoVolt Loading Solution was prepared by adding 100 µL of 100X PowerLoad concentrate (Component B) and 10 µL of FluoVolt dye, 1000X (Component A) to a 15-mL tube, then vortex to mix. 10mL of Tyrodes solution, consisting of: 140 mM NaCl, 5.4 mM KCl, 1 mM MgCl<sub>2</sub>, 1.8 mM CaCl<sub>2</sub>, 10 mM glucose and 10 mM HEPES at pH 7.4, was added and mixed by inverting the tube. Cardiac cells were then washed with Tyrodes solution before being loaded with 100µL Fluovolt loading solution for 15-30 minutes and incubated at room temperature before being imaged using Zeiss Axio Observer Z1 inverted microscope with a Hamamatsu ORCA-Flash 4.0 camera. 20 second videos were taken for each group to capture majority of the cells on the coverslip. ROIs

were drawn around about 50 cells, and videos were exported at 0.01s. Downstream video processing and analyses were performed by our electrophysiologist, Michael Lai, on pClamp Software (Molecular Devices). Individual action potentials were plotted and averaged using low-pass filters. Subsequently, each cell's APD<sub>90/50</sub> ratio was quantified and plotted for assessment of the differentiation efficiency.

#### **4.2.4. Chemical responsiveness assay of CMs and SANLPCs on MEAs**

SANLPCs were assessed for their adrenergic and cholinergic receptivity and responsiveness in comparison to hPSC-CMs (differentiated with GiWi and donated by Will Flanigan) using MEAs and treatment with norepinephrine (NE), acetylcholine (Ach), carbachol (Cch; cholinergic agonist; EMD Millipore), and isoproterenol (Iso;  $\beta$ -adrenergic agonist; Sigma Life Sciences). When cardiomyocytes are plated over a MEA, they couple and form a spontaneously beating syncytium. Each beat is characterized by a propagating electrical signal, measured as the field potential, that triggers a coordinated, mechanical contraction. To acquire and analyze data, Axion Integrated Studio (AxIS) Navigator (v.2.0) measures field potentials, contractility, action potentials, and propagation from CM networks. In order to run all these assays on the same samples, CytoView plates were used for the following assays as opposed to BioCircuit plates. These MEA plates can detect Local Extracellular Action Potentials (LEAP) by enhancing cell-electrode coupling and approximating the waveform of an intracellular action potential.

D30 hPSC-cardiac cells (50k/well) were replated on Maestro Edge 24-well plates (CytoView; Axion Biosystems) coated with matrigel\*. Cellular recovery was tracked over

12 days by measuring spontaneous basal activity after 3 days of plating. This is a consequence of optimal Na<sup>+</sup> spikes and T-wave amplitudes being achieved after 10-14 days in culture. The plate was loaded into the Maestro Edge machine and equilibrated for 10 minutes at 37°C and 5% CO<sub>2</sub> before recording for 15 minutes using AxIS Navigator Software (Axion Biosystems) and Cardiac Beat Detector Software to analyze samples with a detection threshold of 150µV. This was repeated the following days for chemical responsiveness assays (Figure 4.3a). A basal reading was taken prior to any addition of molecules. Subsequently, small molecules were diluted to 1mM and 4mM or 5mM in DMSO for experimental concentrations of 1µM, 2µM, 4µM or 5µM and 10µM. Each group was treated with either DMSO (n=3) or respective drug (n=3). Molecules were mixed into media at designated concentrations then (500µL) added to respective wells and incubated at 37°C for 10 minutes with each sample starting at 1µM for each drug. Thereafter, the Maestro plate was loaded into the Maestro Edge machine, equilibrated, and recorded like prior readings before repeating each step and adding higher concentrations sequentially to a final 10µM concentration. Changes in contractility and field potentials were used to assess beat amplitude, beat period, and excitation-contraction delay.

\*In a parallel experiment, a lab-mate was assessing the effects of different media compositions on the metabolism of hPSC-CMs. With the donated hPSC-CMs in RPMI/B27+, hPSC-CMs maintained in fatty acid and physiological media were also donated and used in this assay (Figure 4.3b).

#### **4.2.5. Statistics**

The mean +/- standard deviation was calculated from at least 3 biological replicates for all data unless otherwise noted. One-way analysis of variance (ANOVA) followed by Tukey's post hoc analysis was performed to compare three or more groups. For all comparisons, statistical significance was determined at  $p < 0.05$ . The range of statistical significance is shown by an asterisk within the figure panels: ns = not significant, \* =  $p < 0.05$ , \*\* =  $p < 0.01$ , \*\*\* =  $p < 0.001$ , \*\*\*\* =  $p < 0.0001$ . All statistical analysis was performed using GraphPad Prism 9.0 software

### **4.3. Results**

#### **4.3.1. Visible phenotypic differences of cardiac microtissues**

We generated cardiac microtissues of varying percentages of SANLPCs (from 0% to 30%) and CMs. Prior to functional analysis of cardiac microtissues, there were observable differences between different compositions of aggregates. 0% and 3% aggregates were visibly more compact with their solid appearance compared to 10% and 30% aggregates that had an inner core of cells with a halo of loosely connected cells (Figure 4.1c and S4.1a). CMs are known to be contractile cells compared to SANs with their differential expression of faster gap junctions (i.e. Cx43), and previous work in our [McDevitt] lab shows that an efficient (~70 - 90% TnnT+) but not an overly enriched (greater than 90% TnnT+) differentiation of CMs can promote better aggregate formation. The in-house sourced GCaMP differentiation was moderately efficient (~70% TnnT+), and the externally sourced SANLPC stock was highly enriched (~78% Nkx2.5-/TnnT+) as shown in Figure 2.3c. GFP was tagged to Nkx2.5, a CM transcription factor, in the HES3-

NKX2-5<sup>gfp/w</sup> line that was used to differentiate SANLPCs. In the sourced SANLPCs, ~20% of the cells were GFP+ CMs. Accordingly, we observed an increasing amount of constitutively-expressed GFP in aggregates from 3% to 30% (Figure 4.1c). From these observations, we hypothesized that there would be functional differences observed with 30% or greater SANLPCs in microtissues.

#### **4.3.2. 10% or higher composition of SANLPCs shift the calcium handling properties of cardiac microtissues**

Due to our interests in the impact of SANLPCs on the function of heterogeneous microtissues, aggregates were given 7 days of recovery to allow structural organization for proper function before calcium transients of individual aggregates were analyzed. After 7 days, 10% and 30% microtissues reorganized to resemble compact aggregates similar to 0% and 3% (Figure 4.1c and S4.1a). Spontaneous beat rate significantly increased with the addition of SANLPCs for all respective groups, but the beat rate was the highest in 10% and 30% groups compared to microtissues containing only GCaMP-CMs (Figure 4.1f). Moreover, the amplitude of calcium transients significantly decreased in only the 10% and 30% groups. This metric is inconclusive due to the fact that amplitude is relative to fluorescence, and peak height can also be proportional to the number of GCaMP-CMs that are present in 0% and 3% aggregates. On the other hand, hSANS are known to have a shorter calcium transient amplitude (~100nM) compared to hCMs (~500nM) as a consequence of their lower metabolic demand for calcium handling and thus contractility<sup>58,91,92</sup>. Additionally,  $V_{maxup}$  and  $V_{maxdown}$  were significantly decreased in the 10% and 30% groups which corresponded to a shift towards a more SAN-like phenotype

with a slower upstroke velocity and longer overall duration of the calcium transient (Figure 4.1f)<sup>91</sup>. However, there were no significant changes in  $t_{90}$  up and down between groups. The calcium handling properties of microtissues containing the least SANLPCs (0% and 3%) showed greater variability with increased standard deviations for  $V_{\max}$  up and  $V_{\max}$  down, and  $t_{90}$  down. This reflects inconsistent responses between microtissues within these groups and is either telling of the need for a certain ratio of SANs in cardiac tissues for proper function or the variability in aggregates at these small sizes. These results suggest that there is a thresholding effect with SANLPCs that is around 10% or greater to consequently shift the functional phenotype to a more SAN-like tissue. Furthermore, this supports the conclusion that calcium handling properties of engineered microtissues are regulated by heterotypic interactions of different cardiac subtypes.

Additionally, calcium handling properties were analyzed by subjecting microtissues to a series of increasing electrical field stimulation frequencies at 1Hz, 2Hz, 3Hz and 4Hz (Figure 4.1g-h). At day 7, all microtissue groups were able to keep pace with 1Hz, 2Hz, and 3Hz stimulation. At 3Hz, variability in keeping up with pacing was increased in all groups, but it was greater in the 0% and 3% groups. Beat rate was only able to be stimulated to 180 beats per minute (3Hz) for all groups (Figure 4.1h). Though pacing failed at 4Hz for all groups, the least amount of variability in beating frequency was observed in the 30% group.

### **4.3.3. RBS+ treatment shifts the bulk electrophysiology to a more SAN-like phenotype**

At the time of this study, we wanted to thoroughly assess the effectiveness of our best SAN differentiation protocol (RBS+; Section 2.2.4) according to qPCR data showing upregulation of SAN genes. Action potentials were analyzed of single cells in the SAN and GiWi protocols (Figure 4.2). GiWi at baseline is a ventricular differentiation protocol that produces populations of over 70% ventricular-like cells based on 20/28 cells having an APD<sub>90/50</sub> ratio of 1.4 or less (Figure 4.2 d-e). Nonetheless, GiWi still produces a fraction (~18%) of nodal cells, as a consequence of 5/28 cells having an APD<sub>90/50</sub> ratio of 1.4 - 1.7. With the addition of RA, Bmp4, SB, and FGF<sub>i</sub>, the culture shifted to a more SAN-like phenotype with ~31% nodal cells being detected. These numbers are comparable to what has been reported<sup>85</sup>.

\*At the time of this study, in-house differentiations were less efficient than normal based on cTnT+ percentage via flow cytometry.

### **4.3.4. SANLPCs are responsive to adrenergic and cholinergic stimulants**

Signaling molecules are critical for proper heart function. The autonomic nervous system innervates the heart and secretes neurotransmitters that systemically regulate heart rate. Norepinephrine is primarily secreted by sympathetic neurons to increase heart rate, and acetylcholine is primarily secreted by parasympathetic neurons to slow down heart rate<sup>93</sup>. In the heart, norepinephrine primarily binds to  $\beta$ -adrenergic receptors while acetylcholine primarily binds to muscarinic receptors<sup>94</sup>.



In preparation for future co-cultures, MEAs were used to assess the electrical activity of SANLPCs at baseline and in response to adrenergic and cholinergic stimulants in comparison to CMs. SANLPCs and CMs were monitored over a 12-day recovery period due to optimal activity being achieved after 10-14 days in culture (Figure 4.3e). Analyses were not started until D4 to allow the restoration of functional components after dissociation. In the earlier timepoints (D4-D7), cells had a lower field potential amplitude compared to time points later in the recovery period. However, electrical activity and detection improves with time in culture, and this is evident in the field potentials and higher activity on the activity map from AxIS Navigator (Figure 4.3c). On D12, only 2 SANLPC wells were detected on the MEA prior to starting the drug screen, and they had an average beat rate of ~98bpm. Conversely, all CM wells were detected except for 3 wells of CMs in physiological media. CMs in RPMI/B27+ had an average beat rate of 59bpm; CMs in fatty acid media had an average beat rate of ~72bpm; and CMs in physiological media had an average beat rate ~52bpm. 1 $\mu$ M carbachol was initially added to each well; the addition of the cholinergic agonist engendered detectable activity in 3 additional SANLPC wells (Figure 4.3h). However, SANLPCs didn't have the expected drug response of a significant decrease in beat rate to 1 $\mu$ M carbachol; instead, the 2 SANLPC wells only decreased an average of ~5bpm. Conversely, CMs in RPMI/B27+ had an average drop-in beat rate of ~10bpm; CMs in fatty acid media had an average drop-in beat rate of ~20bpm; and CMs in physiological media had an average beat rate ~5bpm (Figure 4.3i and S4.2a). Subsequently, additional 1mM doses were sequentially added for final concentrations of 2 $\mu$ M, 4 $\mu$ M, and 10 $\mu$ M to test the cells dosing response. None of the groups had a proper dose response to carbachol with a continuous gradual decrease in

beat rate (Figure S4.2a). Individual beat rates of wells display the variability in SANLPCs compared to CMs (Figure 4.3f-g).

On D13, baseline beat rates of SANLPCs were an average of ~78bpm in 3 wells (Figure 4.3h). CMs had beat rates of ~56bpm, ~74bpm, and ~53bpm for RPMI/B27+, fatty acid, and physiological groups, respectively (Figure 4.3i and S4.2b). Treatment with 1 $\mu$ M norepinephrine elicited a significant increase in beat rate of ~60bpm for only 1 well of SANLPCs. The other 2 wells had little to no increase in beat rate, but the other 2 wells became detectable. On the other hand, CMs had an average increase in beat rate of ~32bpm, ~50bpm, and ~38bpm, respectively. Again, there were no concentration-dependent changes in beat rate for any of the groups (Figure S4.2b).

On D14, 5 wells of SANLPCs had an average rate of ~123bpm (Figure 4.3h). Interestingly, when treated with acetylcholine, only 3 wells had an average significant decrease in beat rate of ~49bpm; contrarily, 2 wells had a significant average increase in rate of ~24bpm. CMs had an average decrease in beat rate of ~16bpm, ~22bpm and ~9bpm, respectively (Figure 4.3i, S4.2c). Furthermore, there were no dosing effects with increasing concentrations of acetylcholine (Figure S4.2c).

On D16, baseline readings of SANLPCs were ~114bpm for 4 wells. Meanwhile, CMs had average beat rates of ~57bpm, ~77bpm, and ~40bpm, respectively, after a full day of recovery post-acetylcholine treatment. Subsequently, treatment with 1 $\mu$ M isoproterenol (adrenergic agonist) increased the beat rate at an average rate of ~80bpm, ~29bpm, ~47bpm, and ~35bpm, for SANLPCs, CMs in RPMI/B27+, fatty acid, and physiological media, respectively (Figure 4.3h-i and S4.2d). Moreover, there were no concentration-dependent responses to isoproterenol for SANLPCs and all CMs except

for the physiological group (Figure S4.2d). CMs in physiological media when dosed with 2 $\mu$ M isoproterenol increased ~10bpm from the beat rate at 1 $\mu$ M.

LEAP detection was tested on this Cytoview plate after isoproterenol treatment. CMs cultured in R/B+ had a ventricular-like APD 90/50 ratio of 1.29 while SANLPCs also had a ventricular-like APD<sub>90/50</sub> of 1.31. This low APD ratio could be a consequence of poor electrode coupling or inadequate media composition for the stability of phenotype in the SANLPC condition. More analyses are needed to determine the basis of this misrepresentative value.

#### **4.4. Discussion**

The unique functional phenotype of SANs compared to contractile (CMs) and other conducting (pacemaker) cells is the basis of the SAN's critical role as the primary pacemaker. The SAN only consists of about 10,000 cells, which is a specialized fraction of pacemaker cells in the cardiac conduction system that make up only 1% of the total cardiac muscle cells compared to the 2-3 billion CMs (99% of cells) in the myocardium<sup>14,18,95</sup>. The small percentage of SANs with their positioning at the head of the cardiac conduction system in the right atrium is sufficient for driving the electrical impulse of the heart.

Cardiac differentiations are heterogeneous due to the generation of all various residual myocardial cells. The infamous GiWi protocol is primarily a ventricular protocol that produces a small fraction of SANs. Furthermore, protocols are not efficient in producing an enriched population of SANs without a reporter line; therefore, we wanted to understand the level of enrichment of SANs needed in a culture to achieve an SAN

phenotype. The functional difference between SANs and CMs (conducting vs contractile, respectively) leads to different calcium demands for excitation-contraction coupling and thus different calcium handling properties. We tested varying percentages of SANLPCs in cardiac microtissues and discovered that microtissues demonstrated SAN-like kinetics of calcium handling properties with the addition of SANLPCs. ~10% SANs in microtissues are needed to shift the beat rate, amplitude of calcium handling, and upward/downward max velocity of calcium handling.

Despite less mature calcium transient profiles as a consequence of lower amplitude and upstroke velocity, the highest composition of SANLPCs (30%) most consistently paced up to 3Hz, and even though it was unable to be paced at 4Hz, there was less failure compared to other groups. This is important to note because previous data (Matthys) shows that more mature CMs are able to be paced up to 4Hz; therefore, the improved pacing in microtissues containing SANLPCs indicates that higher numbers of SANs may be able to compensate for immature CMs in rhythmicity. Additionally, although a percentage of ~10% SANLPCs was detected as the fraction needed for a shift in calcium handling properties, the thresholding for this study is potentially dependent on the small number of total cells ( $2 \times 10^3$ ) compared to the true total number of myocardial cells ( $\sim 2-3 \times 10^9$ ).

Fluorescent dyes are a relatively new method for assessing the electrophysiology of cardiac cells compared to patch clamp that has been the gold standard for decades. SANLPCs were previously characterized with patch clamp to confirm their SAN-like functional phenotype. Here, we assessed the electrophysiology of the RBS+ protocol with Fluovolt and discovered that RBS+ slightly shifts the functional phenotype of cardiac

differentiations from ~18% to ~31% SANs. An interesting future study would be a direct comparison of a culture of SANLPCs to a culture of the RBS+ protocol due to patch clamp being an assessment of single cells compared to Fluovolt being a bulk analysis.

Moreover, we wanted to assess the electrophysiology and functional competency of SANLPCs by using MEAs and treating cells with adrenergic and cholinergic stimulants in comparison to CMs. Foremost, there is more variability in beat rate between replicates of SANLPCs compared to CMs early in the recovery period. This variability aligns with studies that have demonstrated that individual pacemaker cells have varying rates of activity, rhythmicity, and current densities<sup>96,97</sup>. This physiological phenomenon could be driving this irregularity. Alternatively, this variability could be a consequence of the reorganization of SANLPCs and thus affecting their positioning on electrodes. SANs naturally are poorly electrically coupled in comparison to CMs as a result of their differential expression of Connexin 45 (small conductance gap junction) versus Connexin 43 and 40 (large conductance gap junctions). These differentially expressed transmembrane proteins are most likely correlated to the poor attachment of SANs. This poor attachment is observed in the activity map on AxIS Navigator and changes throughout the recovery period; activity becomes higher later in the recovery period. This supports the technical recommendations to run analyses D10-14 for optimal electrical activity. In the earlier timepoints (D4-D7), the low amplitude and wide spike of the field potential is likely reflective of immature cells, possibly in combination with poor attachment or low density. This is very characteristic of any iPSC-CM culture at this early timepoint.

Nonetheless, CMs exhibited a functional competency for co-cultures with autonomic neurons by their consistent responsiveness to adrenergic and cholinergic stimulants. However, SANLPCs were more inconsistent with their electrical activity and responsiveness to stimulants. This is suggestive of the heterogeneity that exists in SANLPCs. This heterogeneity is important for their function and insulation of electrical activity in the SAN for proper cardiac output<sup>19</sup>. Furthermore, LEAP analysis exhibited a ventricular-like profile with an APD<sub>90/50</sub> ratio of less than 1.4 for SANLPCs and CMs; when patch clamp previously confirmed the SAN-like profile of SANLPCs as a consequence of the action potential waveform<sup>42</sup>. This discrepancy between electrophysiology profiles is likely a consequence of the lower efficiency of LEAP induction due to the geometry and material of the electrodes in the Cytoview plate and the affinity of some cell types.

Additionally, we assessed the differential electrical activity of CMs cultured in different metabolic media, and we observed an increased maturation in CMs cultured with high fatty acid content based on their overall electrical activity and response to stimulants. Furthermore, a longitudinal study illustrated some maturation of CMs and SANLPCs with time after treatment with adrenergic and cholinergic stimulants (Figure S4.2 g-j). This study supports the importance of media composition for proper function of cardiac cell types and suggests there is a correlation between adrenergic/cholinergic stimulation and maturation.

## 4.5. Figures

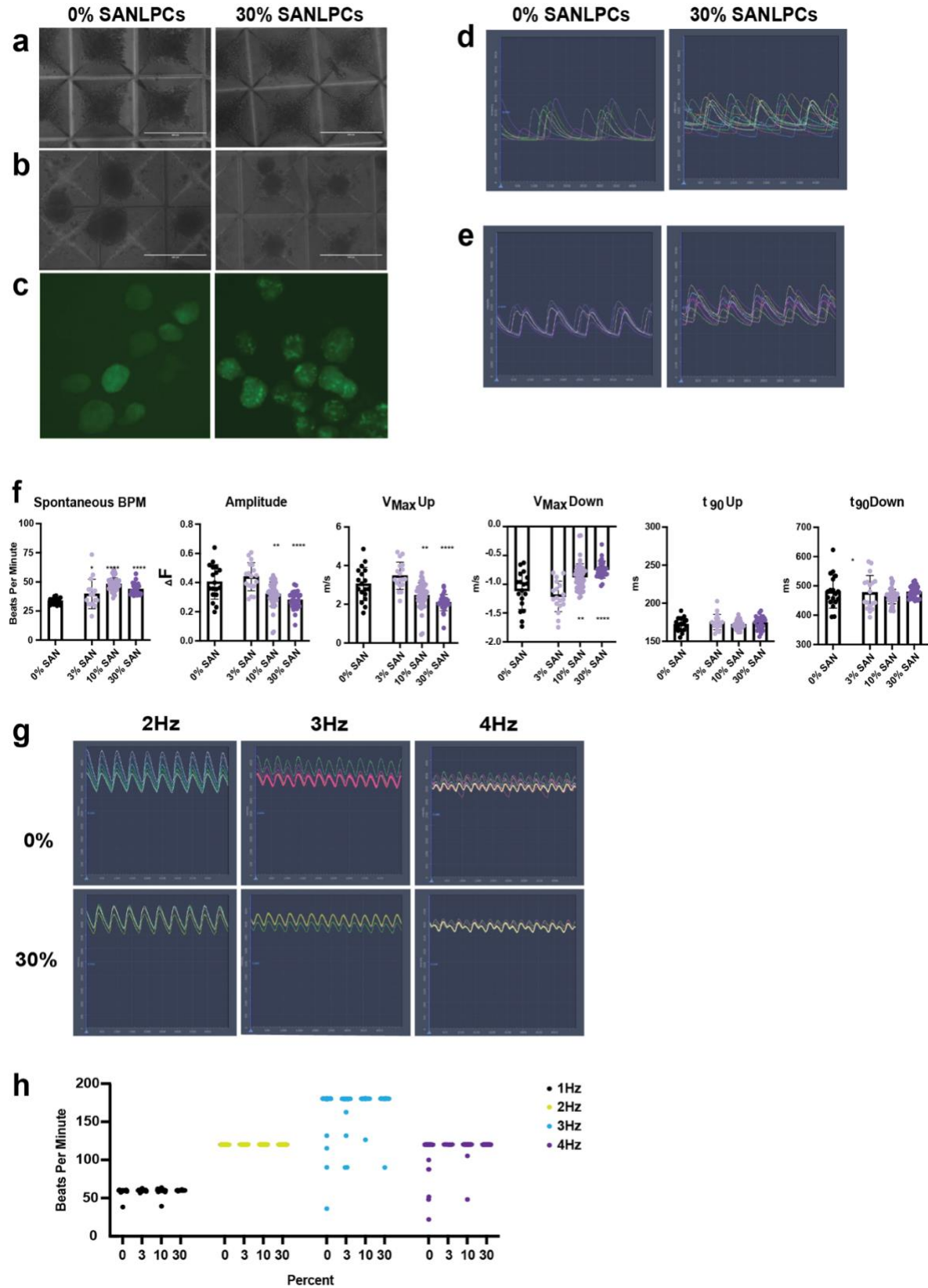
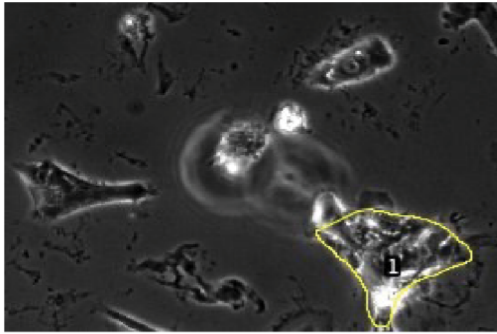


**Figure 4.1: 10% or great SANLPCs are needed to shift the calcium handling properties of cardiac microtissues.**

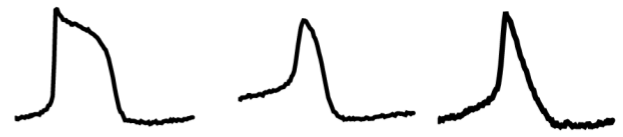
(a) Cardiac microtissue formation of GCaMP-CMs and SANLPCs mixed and seeded in various ratios at 2000 cells per microwell on D0. Scale bar = 400 $\mu$ m. (b) Self-assembled aggregates of heterotypic cell mixtures 1 day post-seeding (c) Stable microtissues after 7 days in culture exhibiting GFP signal of flashing GCaMP signal and increasing NKX2-5:GFP cells with increasing SANLPC ratios. (d) Representative spontaneous calcium transients for 0% and 30% SANLPC microtissues (e) Representative calcium transients for 0% and 30% SANLPC microtissues paced at 1Hz (f) Spontaneous beat rates of cardiac microtissues were quantified, and they were subsequently paced at 1Hz to analyze and quantify calcium transient amplitude, upstroke velocities, and time to 90% of peak and resting potential. (g) Representative calcium transients for 0% and 30% groups when subjected to 2Hz, 3Hz, and 4Hz electrical field stimulation. (h) Quantification of respective beat rates when each group of microtissues is paced at 2Hz, 3Hz, and 4Hz.



**a**

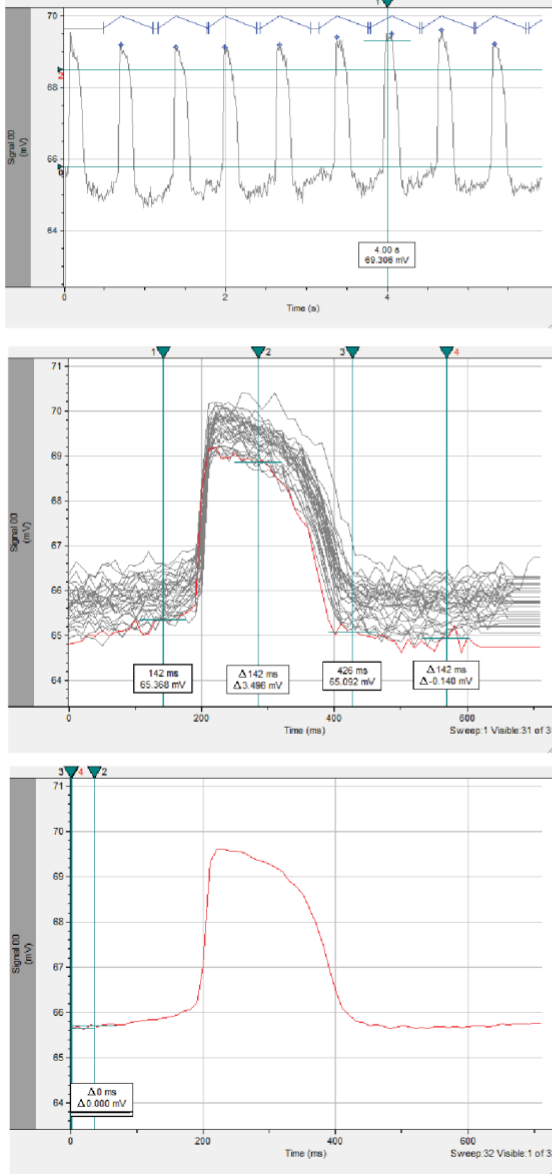


**b**

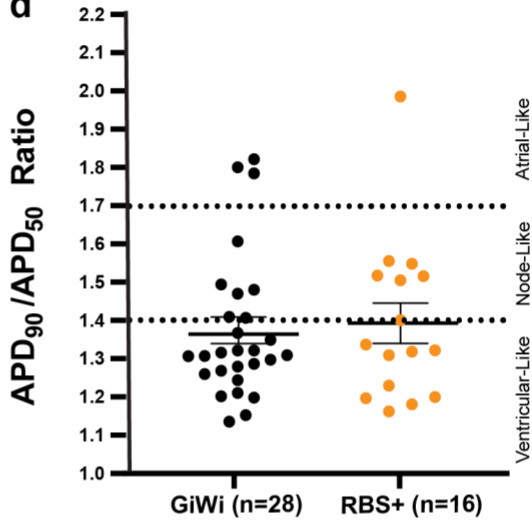


Ventricular - Like  $APD_{90}/APD_{50} < 1.4$     Nodal - Like  $1.4 < APD_{90}/APD_{50} < 1.7$     Atrial-Like  $APD_{90}/APD_{50} > 1.7$

**c**



**d**



**e**

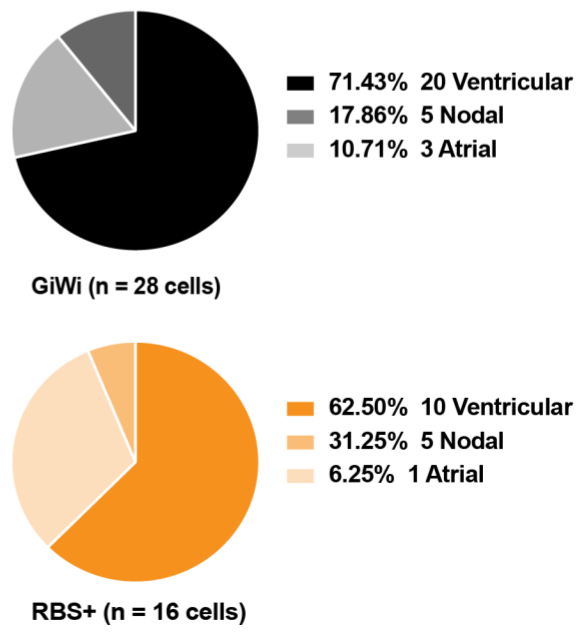


**Figure 4.2: Electrophysiological analysis demonstrates an enrichment of SANLCs in RBS+ differentiations.**

(a) Representative brightfield image of sparsely plated cells with drawn ROI for signal detection. (b) Representative ventricular-like, atrial-like, and SA node-like action potential waveforms with respective APD<sub>90/50</sub> ratios. (c) Analysis of raw signal (top) by averaging action potential waveforms (middle) and passing through low-pass filters to get final representative waveform (bottom). (d) Quantification of APD<sub>90/50</sub> ratios for GiWi and RBS+ groups in respect to the values that identify different cardiac cell types. (e) Pie graph of the proportions of cardiac cell types in GiWi and RBS+.

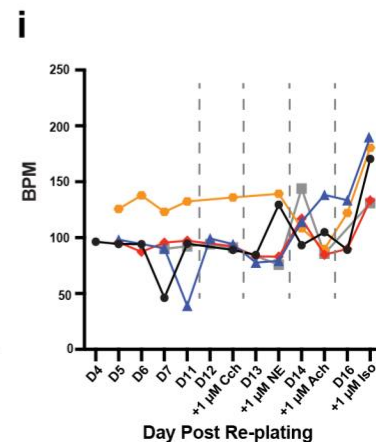
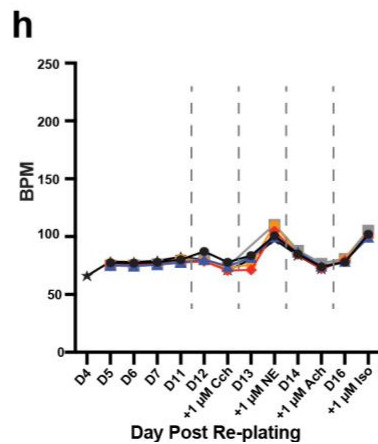
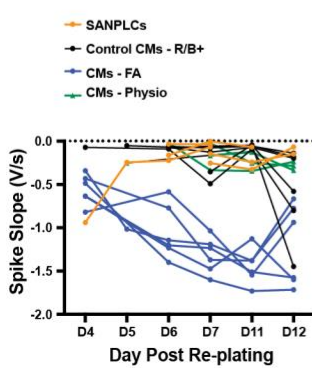
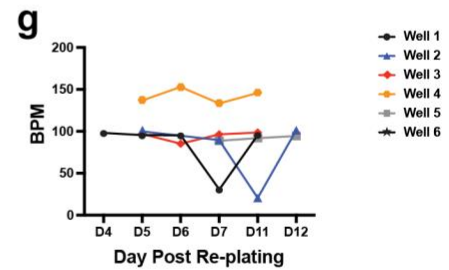
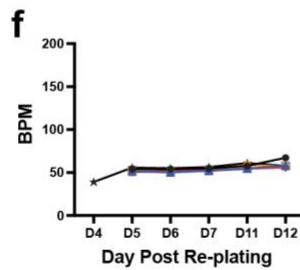
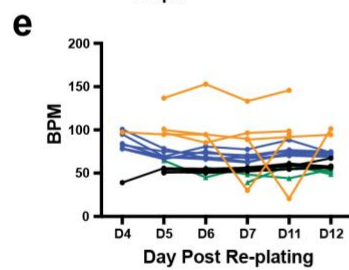
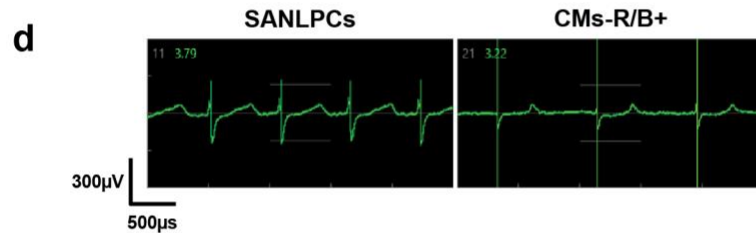
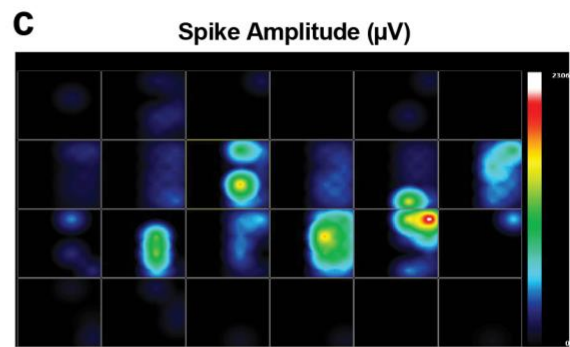
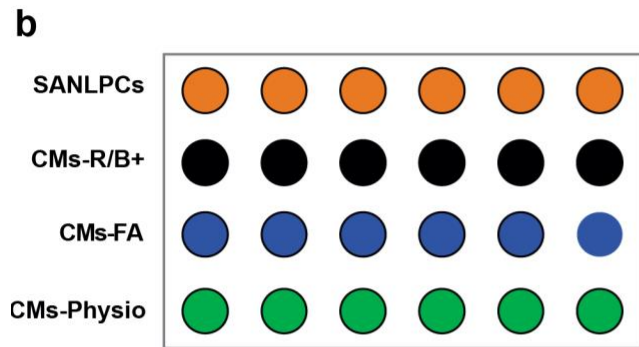
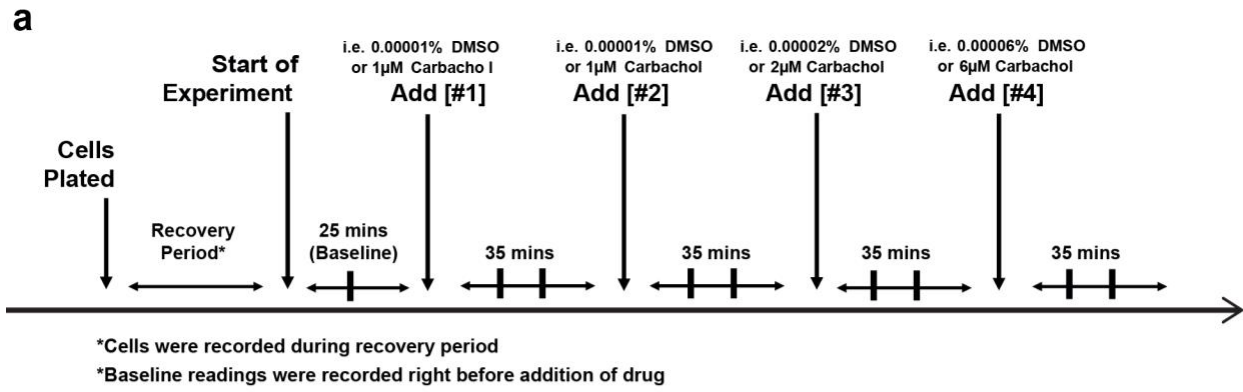


**Figure 4.3: MEAs elucidate heterogeneity in SANLPCs and responsiveness of cardiac cell types to cholinergic and adrenergic stimulants.**

(a) A schematic representation of the experimental protocol to assess the responsiveness of cardiac cell types to cholinergic and adrenergic stimulants. (b) Axion's MEA Cytoview Plate Layout with respective cardiac cell types: SANLPCs, CMs - R/B+ (CMs cultured in R/B+ media), CMs - FA (CMs cultured in fatty acid media), and CMs – Physio (CMs cultured in physiologically-based media). (c) Representative MEA Activity Plate Map in AxIS Navigator. (d) Representative MEA field potentials of SANLPCs and CMs cultured in R/B+ with a max detection threshold of  $300\mu\text{V}$  over  $500\mu\text{s}$ . (e) Assessment of averaged spontaneous beat rates and spike slopes throughout the 12-day recovery period for all 4 cardiac cell types. (f) Individually plotted spontaneous beat rates of CMs - R/B+ for all 6 wells (g) Individually plotted spontaneous beat rates of detected SANLPCs for all 6 wells. (h) Averaged spontaneous beat rates of CMs - R/B+ and (I) SANLPCs during recovery and experimental period in response to Carbachol (Cch), Norepinephrine (NE), Acetylcholine (ACh), and Isoproterenol (Iso).

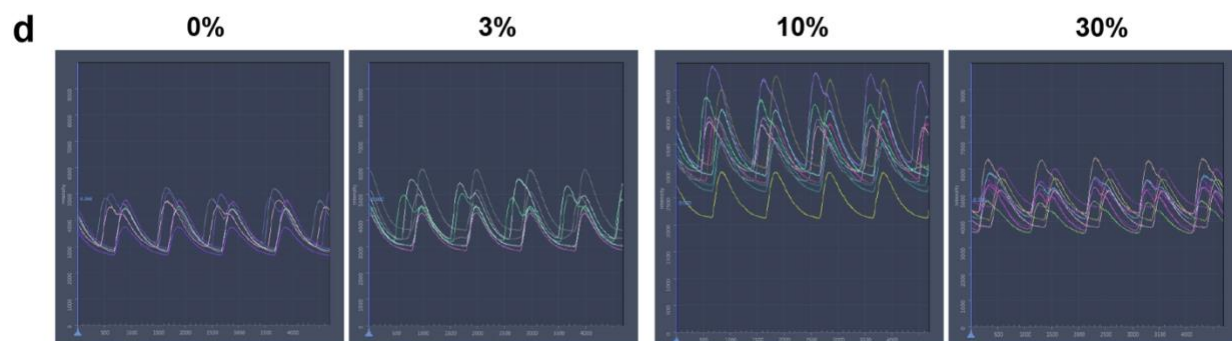
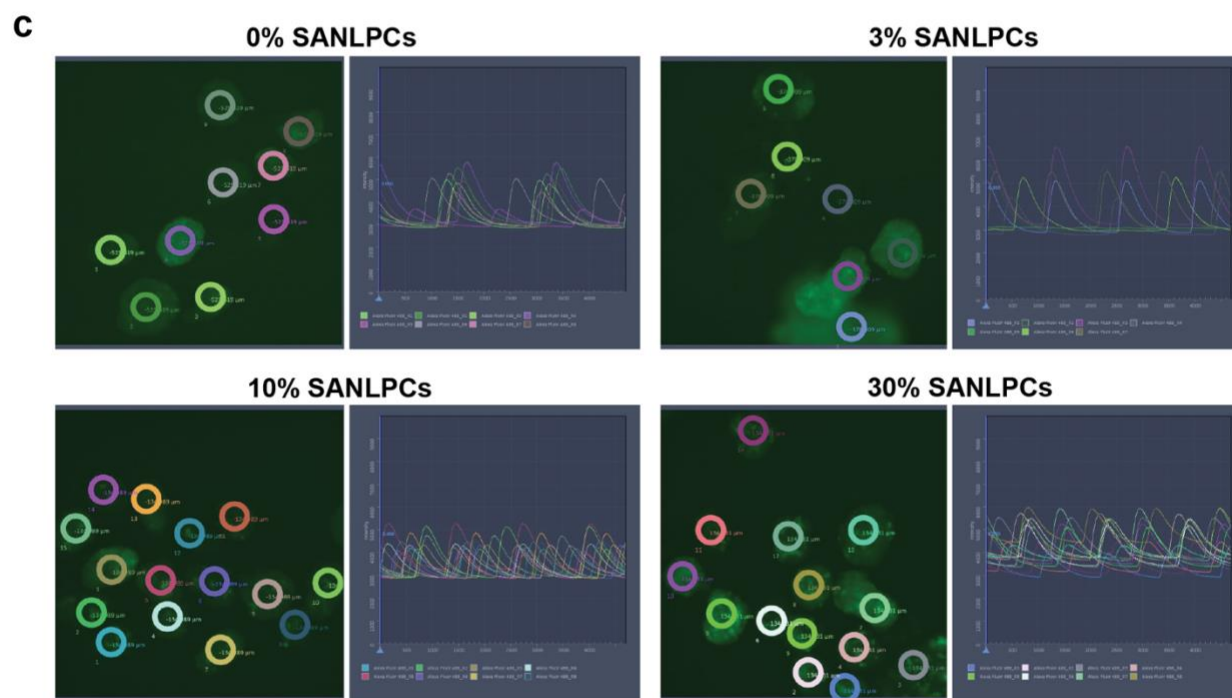
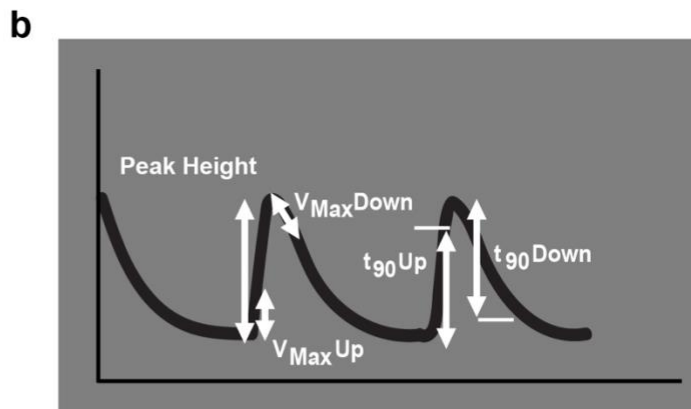
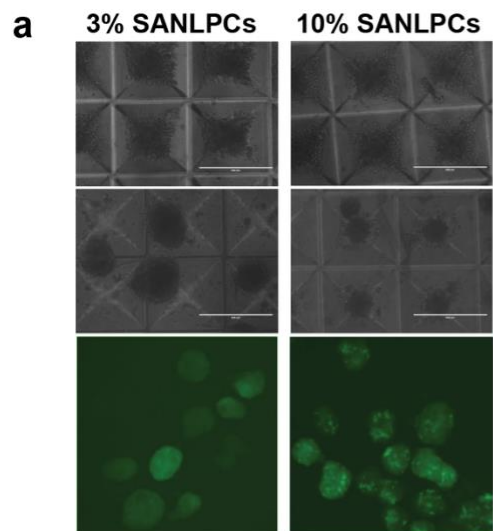


**Figure S4.1. GCaMP analysis of heterotypic microtissues.**

(a) Cardiac microtissue formation (top), aggregation (middle), and GFP signal (bottom) for 3% and 10% SANLPC groups. (b) Quantitative metrics of calcium handling transients. (c) ROIs were selected at the center of each spontaneously beating tissue ( $n > 10$ ) and Zen software exported respective calcium transients for each group. (d) Stimulation of increasing biphasic calcium transient waveforms with increasing numbers of SANLPCs when microtissues are paced at 1Hz.

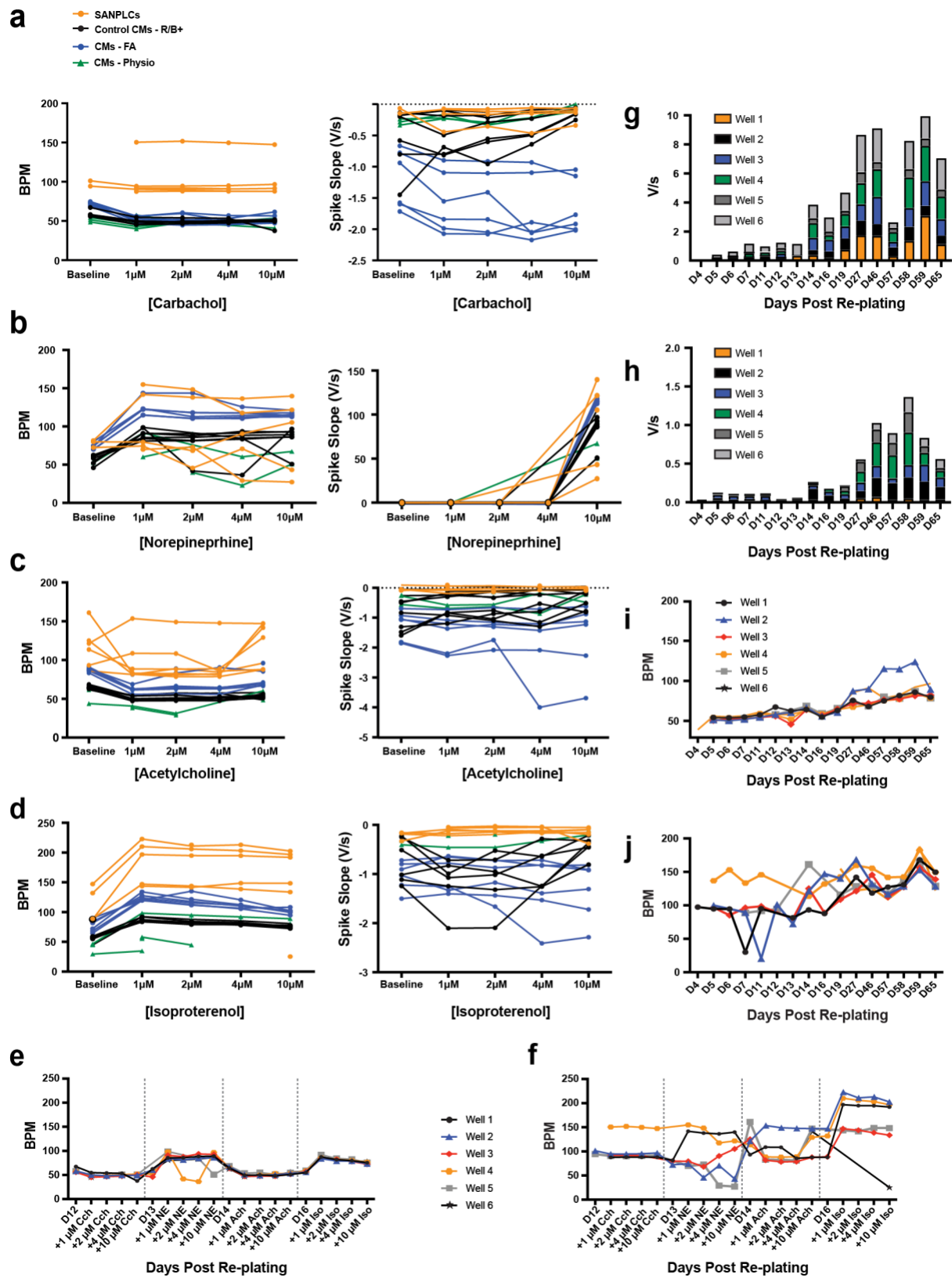


**Figure S4.2. MEAs additionally elucidate a poor dose-response of cardiac cell types to drugs, a fatty acid-induced maturation of cardiomyocytes, and a regression of maturation in SANLPCs and CMs with a lapse in cholinergic and adrenergic stimulation.**

(a) Spontaneous beat rate and spike slope of different cardiac cell types with increasing concentrations of Carbachol, (b) Norepinephrine, (c) Acetylcholine, and (d) Isoproterenol. (e) Cumulative assessment of spontaneous beat rates of CMs - R/B+ and (f) SANLPCs in response to increasing concentrations of cholinergic and adrenergic stimulants. (g) Analysis of spike amplitude throughout time (65 days) for CMs - R/B+ and (h) SANLPCs. (i) Analysis of spontaneous beat rate throughout time (65 days) for CMs - R/B+ and (j) SANLPCs



## CHAPTER 5. *IN VITRO* INNERVATED CARDIAC SYSTEM

### 5.1. Introduction

The heart is the first organ to develop in the fetus, and the pacemaking activity of the SA node is the first element to function in the cardiac conduction system<sup>4</sup>. Therefore, there are both ethical complications and practical challenges associated with studying SA node development in humans. Nonetheless, there are notable studies that have captured the timing of cardiac innervation in the venous pole as early as E10.5-11.5 in mice and the fifth week of human development<sup>93,94</sup>.

Due to its primary pacemaking function, the SA node is highly innervated compared to other tissues in the heart<sup>1,2,59,94,98</sup>. Innervation is first dominated by the excitatory sympathetic nervous system in infancy, which explains the fast fetal heart rate before the gradual increase of parasympathetic neurons for a co-dominant system in adulthood and a slower heart rate<sup>8</sup>. Though murine systems are widely used due to scalability and usability, cardiac innervation and overall cardiac output in murine animals is notably different from humans to support their rapid basal heart rate. Furthermore, murine and other animal systems are inefficient in predicting drug effects in humans because of species differences. Therefore, development of *in vitro* hPSC-assays to investigate the SA node is a potent strategy for the advancement of basic scientific knowledge about its function and potentially the development of therapeutics to modify it in disease.

In published hPSC-derived co-culture systems, sympathetic neurons (SNs) have been the primary neuronal type used in studies with cardiomyocytes (CMs)<sup>47,55,99,100</sup>. To my knowledge, there has been only one study that has co-cultured hPSC-SA nodal cells

(hPSC-SANs) with autonomic neurons, but that study was assessing the connectivity of hPSC-autonomic neurons due to the poor connectivity of hPSC-CMs with them<sup>78</sup>. Ghazizadeh et al. reported the maturation of hPSC-autonomic neurons similar to published co-culture studies with primary CMs<sup>99,101</sup>. The following study assesses the phenotypic maturation of hPSC-SANs after co-culture with specifically hPSC-SNs. We hypothesized that structural changes will be observed in hPSC-SANs upon co-culture, such as upregulation of ion channels and shifts in levels and organization of contractile proteins (i.e. TnnT2) due to the known functional connectivity of hPSC-SANs with hPSC-autonomic neurons and known functional changes in maturing SANs<sup>102</sup>. To test this hypothesis, hPSC-SANs, hPSC-CMs, and SANLPCs were co-cultured with hPSC-SNs in microfluidic devices and compared to monocultures and co-cultures with hPSC-CMs.

Over the past two decades, co-culture systems, like organ-on-a-chip, have leveraged the power of microfluidic devices for the compartmentalized analysis of different cell types. Other applications for these novel devices include the control of factors like the degree of innervation and directionality of signals as well as the nature of heterotypic interactions (i.e. juxtacrine, paracrine)<sup>99,101</sup>. Innervation in open co-culture systems can be very random in regards to the outgrowth of axons between different populations of CMs and SNs. Microfluidic devices add a level of control to limit the number of axons that reach hPSC-SANs and CMs with the presence of 100-micron long microchannels that separate the central and outer channels. Additionally, the devices provide depth to allow the assessment of changes in hPSC-SANs in different proximity to hPSC-SNs. To our knowledge, this is the first study to compare the differential innervation phenotype between hiPSC-SANs and hiPSC-CMs.

## **5.2. Materials & Methods**

### **5.2.1. Pluripotent stem cell culture**

The C2A-SHOX2:GFP reporter line from Chapter 3 was cultured on matrigel-coated (80/μg/mL; Corning) plates in mTeSR medium (Stem Cell Technologies). Cells were grown to 70% confluence, passaged using Accutase (Innovative Cell Technologies), and seeded in mTeSR medium with 10μM Rock Inhibitor (RI, Y27632, SelleckChem) for the first 24 hours at a density of  $1.3 \times 10^4$  cells/cm<sup>2</sup> in a T25 flask (Corning) and  $3.9 \times 10^4$  cells/cm<sup>2</sup> in a 12-well plate (Corning), roughly every 3 days. Media was refreshed daily with mTeSR.

### **5.2.2. Cardiomyocyte differentiation**

Differentiation of CMs and SANs from hiPSCs was achieved by using the GiWi and RBS+ protocols from Chapter 2<sup>42,61</sup>. Shox2-C2A:GFP hiPSCs were grown to 80-90% confluency for 3 days in mTeSR. On day 0 (D0) of differentiation, the cultures were fed with RPMI 1640 medium (Thermo Fisher) and B27 supplement minus insulin (RPMI/B27-; Life Technologies) supplemented with 12μM CHIR99021 (SelleckChem). The mesodermal induction medium was completely removed after 24 hours and exchanged with RPMI/B27- medium. On D3 of differentiation, the medium was changed to RPMI/B27- supplemented with only 5μM IWP2 (Tocris) for GiWi. and RBS+ group was additionally supplemented with 3ng/mL Bmp4, 0.5μM SB-431542, 0.25μM retinoic acid, and 100nM PD173074 48 hours before being replaced with RPMI/B27-. On D7 of differentiation, the medium was changed to RPMI 1640 medium and B27 supplement plus

insulin (RPMI/B27+) and subsequently refreshed every 3 days thereafter for maintenance.

### **5.2.3. Derivation of stem cells into sympathetic neurons**

SNs were differentiated from a hPSC optogenetic line in the Fattahi Lab using an optimized unpublished protocol that was modified from the Tchieu et al. paper to differentiate all major ectodermal lineages<sup>46</sup>. Differentiated autonomic neurospheres were cultured in suspension of neurobasal media that was supplemented with N2, B27, CHIR, FGF2, GDNF, and ascorbic acid to specify SNs. Similar to the protocol to differentiate SANs, SNs we specified using small molecule treatment at specific times throughout the differentiation. SN phenotype was validated and characterized using qPCR, immunofluorescence and flow cytometry. A detailed protocol layout and characterization data is not included because they are currently unpublished.

### **5.2.4. Fabrication & preparation of microfluidic devices**

The design of microfluidic devices was made in AutoCad with proper dimensions to be etched into silicon wafers to make the negative mold (Figure 5.1A). Wafers were made using photolithography and subsequently replica molding was used to generate Polydimethylsiloxane (PDMS) gaskets for increased durability in the repetitive fabrication of devices. PDMS (Sylgard 184; Dow-Corning) was mixed at 10:1 (base:curing agent), placed in a desiccator for 30 minutes to remove bubbles, and cured overnight in plastic mold at 60 °C. The PDMS was cut from the master mold, trimmed, and perforated with 5mm and 3mm dermal punches for in and out ports of all three chambers. Two different

types of devices were created for proximal neurosphere loading (Figure 5.1a-c). 3mm punches were also used to create a port in the middle of the top chamber for controlled neurosphere loading in close proximity to the middle chamber of CMs or SANs. Subsequently, devices and glass coverslips (25mm x 25mm) were surface activated by plasma treatment for 30 seconds before devices were bonded to glass coverslips and incubated at 100°C for 10 minutes to strengthen the bond. Devices were then washed overnight in a bath of 70% ethanol to remove any unpolymerized PDMS and sterilize devices.

For each experiment, three replicate devices were placed in a 10cm dish for each group of CMs, SANs, and SANLPCs with and without neurosphere port for a total of 18 devices per group. On the day of seeding, devices were plasma treated, sterilized in a UV chamber for 5 minutes, and treated with 0.01% poly-L-lysine for 2 hours at 37°C. Laminin was diluted 1:60 in PBS solution to a final concentration. Devices were washed three times with PBS before laminin solution was loaded into chambers and incubated at 37°C for 30 minutes to coat the surface of the top (neurosphere) and middle (cardiac) chambers.

#### **5.2.5. Loading of microfluidic devices**

CMs, SANLCs, and SANLPCs (D20+) were harvested with 0.25% trypsin for 30-45 minutes and quenched with cardiac quenching media (RPMI/B27+ containing 15% FBS + 10mM RI) and centrifuged at 84g for 5 minutes. The pellet was resuspended in 40 - 60µL of cardiac quenching media with an average cell count of 4 - 8 x 10<sup>6</sup> cells/mL. The central chamber was washed with media. 10µL of cell suspension was introduced into

the inlet port of the central channel at 5 $\mu$ L increments to allow cells to flow and adhere to the central chamber. Chambers were checked for cellular content before being incubated for 30 min. Subsequently, inlet and outlet ports were filled with cardiac quenching media and maintained at 37°C.

The next day, all chambers were aspirated and filled with RPMI/B27+ media in cardiac alone devices (Figure 5.1a), while only middle and bottom channels were aspirated and filled with RPMI/B27+. Subsequently, the top channel was replaced with neural media, and neurospheres were loaded into the neurosphere port. Culture medium was topped up every 2-3 days to prevent evaporation. Devices were monitored by brightfield imaging and were assayed between 7 and 10 days of co-culture.

#### **5.2.6. Immunocytochemistry**

Devices were fixed with 4% paraformaldehyde for 20 minutes at 37°C, washed 3x with PBS, and stained with cTnT,  $\beta$ 3-tubulin, synapsin, Cav3.1, and Cav1.3 overnight at 4°C. Secondary antibodies and Hoescht were added for 1-2 hrs at RT (Table S2 for antibody information and concentrations).

#### **5.2.7. Image acquisition & phenotypic assessment**

A minimum of 50 stained cells per device were imaged for each cell type group (CM alone, SANLC alone, SANLPC alone, CM + SN, SANLC + SN, and SANLPC + SN) on a custom-modified spinning disk confocal head (CSU-10, Yokogawa, Spectral Applied Research) with high power solid-state lasers, a scientific grade CCD camera (Clara, Andor), and an inverted microscope stand with integrated optical focus feedback

(TE2000-PFS, Nikon). Z-stack images were analyzed in Fiji (v.2.3.0). The proportionality and directionality of axiogenesis were assessed among co-culture groups (CM + SN vs. SANLC + SN vs. SANLPC + SN), and sarcomeric alignment in addition to ion channel expression were assessed among co-culture groups and between respective negative control (i.e. SANLPC + SN vs SANLPC alone).

### **5.3. Results**

#### **5.3.1. Microfluidics model innervated cardiac tissue**

SNs are the excitatory stimulus of the autonomic nervous system. Previous studies have shown that SNs induce both hypertrophic growth and cell cycle arrest in CMs to promote maturation<sup>36,37</sup>. Sympathetic axons primarily extend from the intrinsic cardiac nervous system and intrathoracic sympathetic ganglia. The microfluidic devices used in this study possess an outer chamber with an engineered neuroport for the loading of neurospheres near the central chamber (Figure 5.1c). This chamber replicates the ganglia where proximal and distal SNs reside for cardiac innervation. Microchannels support controlled axiogenesis by which SNs respond to secreted cardiac factors (aka neurotrophins) and extend axons through them and into the central channel (Figure 5.1e). Staining with  $\beta$ 3-tubulin and cTnT enabled visualization of the sympathetic innervation of CM and SANLPC tissue (Figure 5.1a & b).

#### **5.3.2. More abundant axiogenesis in SANLPC devices**

Innervation of cardiac chambers was observed in both devices containing CMs differentiated using the GiWi protocol and SANLPCs shipped from the Protze lab (Figure 5.2a & b). However, there was a distinct difference in the amount of neurite sprouting and

outgrowth between SANLPCs and CMs. On average, devices containing SANLPCs and SNs had significantly more axiogenesis and neurite outgrowth into central SANLPC channels than devices containing CMs (Figure 5.2 c & d). Neurites extended throughout the central cardiac chamber for both cardiac subtypes but at different densities. In contrast, SANLCs differentiated in-house with the RBS+ protocol had minimal to no innervation observed in the devices (Figure S5.1b).

### **5.3.3. More cytosolic L-type calcium channel in cardiac cells with sympathetic innervation**

The unique electrophysiology of each cardiac cell type is dependent on the expression and temporal function of differential ion channels. The L-type calcium channel Cav1.3 is specifically important in the upstroke velocity in pacemaker cells and is considered to be required for normal pacemaking activity<sup>7,103</sup>. In CMs, the predominant L-type calcium channel is Cav1.2, and its expression is correlated to the duration of the plateau phase of the CM action potential<sup>104</sup>. Transcriptomics in mouse SANs revealed the expression of CACNA1D (Cav1.3) before and after innervation<sup>7</sup>. However, to my knowledge, the localization of Cav1.3 has not been temporally pinpointed. In cardiac-only devices, Cav1.3 was mainly nuclear in CM and SANLPC controls (Figure f & h). However, after 5 days of innervation, there was a transition from nuclear to cytosolic Cav1.3 (Figure g & i). Additionally, there seemed to be an upregulation of Cav1.3 in CMs and SANLPCs that were either touching or proximal to neurites. This transition is suggestive of a neuronal impact on the maturation of cardiac cells.



#### **5.4. Discussion**

Though the SA node develops in parallel with the myocardium, its innervation is distinct, and the differences are speculated to be important for development<sup>8,102</sup>. Furthermore, the SA node is more densely innervated compared to the working myocardium<sup>32,102</sup>. Similar to what is observed *in vivo*, we found that SANLPC devices had a higher density of neurites extending into the cardiac tissue. This is suggestive of differential neurotrophins being secreted by SANLPCs compared to CMs. Future studies will assess this differential innervation phenotype.

Calcium handling is critical for proper cardiac function, and furthermore, L-type calcium channels (i.e. Cav1.3) are the main calcium influx pathway that mediates excitation–contraction coupling in cardiac muscle. Cav1.3 is responsible for over 50% of the calcium current in SANs<sup>103</sup>. Previous studies have shown that hPSC-SANs express Cav1.3, but it is primarily nuclear when visualized via immunofluorescence, even in long-term (60 day) cultures<sup>78</sup>. However, in our innervated cardiac model we observed a shift of nuclear Cav1.3 to a more cytosolic-functional state after sympathetic innervation. To my knowledge, this is the first study that assesses the expression of Cav1.3 before and after innervation. We are continuing the quantification of Cav1.3 fluorescence to conclusively derive a correlation between innervation and cardiac function and maturation.

#### **5.5. Future Directions**

There are many potential directions for follow-up studies with not only this innervated cardiac model but also with the acquired data. There was a clear difference in the amount of beating cells and overall syncytium beating in all three cardiac cell groups co-cultured

with SNs compared to those cultured alone. A functional correlation study will be performed by quantifying beat rate for a head-to-head comparison between co-culture and control groups. Furthermore, devices were numbered so the innervation and cardiac phenotype (i.e. degree of innervation and expression of ion channels) can be compared to the functional phenotype (i.e. beat rate and degree of beating). If there is a significant difference in the functional phenotype of cardiac cells in this innervated model, follow-up studies will assess the signaling mechanism underlying this difference (i.e. paracrine vs juxtacrine signaling). Those studies will compare cardiac cells similarly co-cultured with SNs versus those cultured alone but with conditioned media replacing SNs that will be collected from a separate SN culture.

With the known importance of developmental timing, future studies will consider the role of innervation timing in co-cultures. Those studies have the potential to assess the functional and innervation phenotype by varying the timing of innervation with younger versus older cardiac cells or with younger versus older SNs. Additional future studies will further assess the functional maturation of cardiac cells in terms of their responsiveness to agonists and antagonists. Winbo et al. reported a change in the responsiveness of hPSC-CMs to nicotine in co-culture with SNs versus monoculture<sup>100</sup>. Similar studies will be performed to assess the responsiveness of cardiac cells to compounds like nicotine as well as the cholinergic and adrenergic stimulants from Chapter 4 after co-culture with SNs. Chapter 4's MEA study demonstrated a lack of a dose response in cardiac cells to cholinergic and adrenergic stimulants. Therefore, these studies will help elucidate the importance of SNs in cardiac maturation.

In addition to SNs, parasympathetic neurons (PSNs) are another main component in autonomous cardiac function. PSNs are not only the first neural cell type to colonize the heart, but they are also more abundant than SNs in the human and porcine SA node<sup>3,93</sup>. Throughout development, there are shifts in the dominating nervous system and the density of neurons control normal cardiac function as well as contribute to physiologic alterations like changes in heart rate that are well established in humans<sup>7</sup>. Therefore, studies assessing the differential effects of sympathetic and parasympathetic innervation on cardiac (CM and SAN) maturation will be powerful for the field due to the technical and systemic limitations of similar *in vivo* studies. To support this study, our collaborator as well as other labs are in the process of optimizing protocols for the specification of hPSC-PSNs. Ultimately, the power of microfluidics to dissect mechanisms will fully be leveraged in future studies to assess the role of innervation in cardiac maturation, specifically that of SANs.

## 5.6. Figures

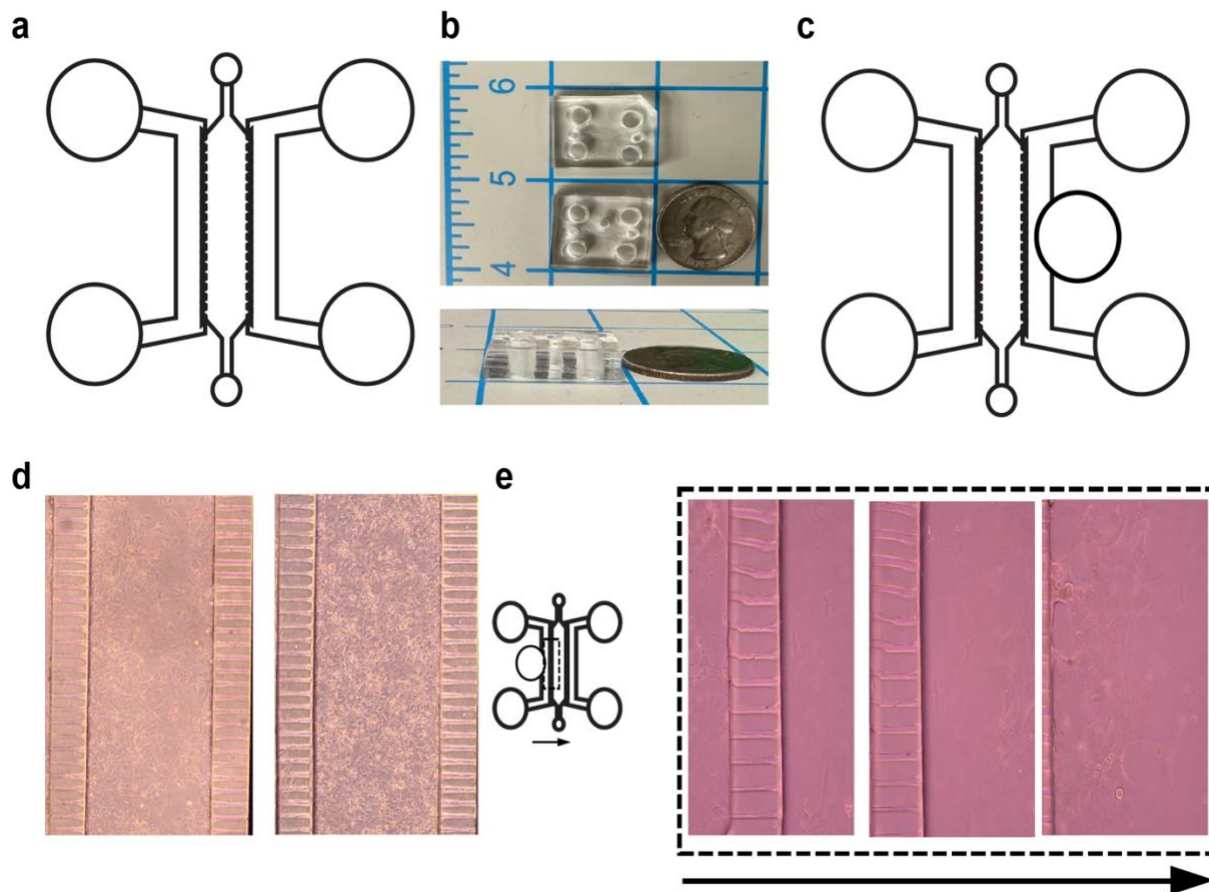


**Figure 5.1. An innervated cardiac platform models the myocardium and SA node.**

(A) Layout of microfluidic device for CMs or SANs only cultures. (B) Top and side view of microfluidic devices with respective sizing. (C) Layout of microfluidic device for the co-culture of CMs or SANs with SNs. (D) Brightfield images of CM only (left) and SAN only (right) devices 1 day after seeding. (E) Brightfield images of representative SAN + SN device in correlation with chamber positioning. Scale bar = 100 $\mu$ m

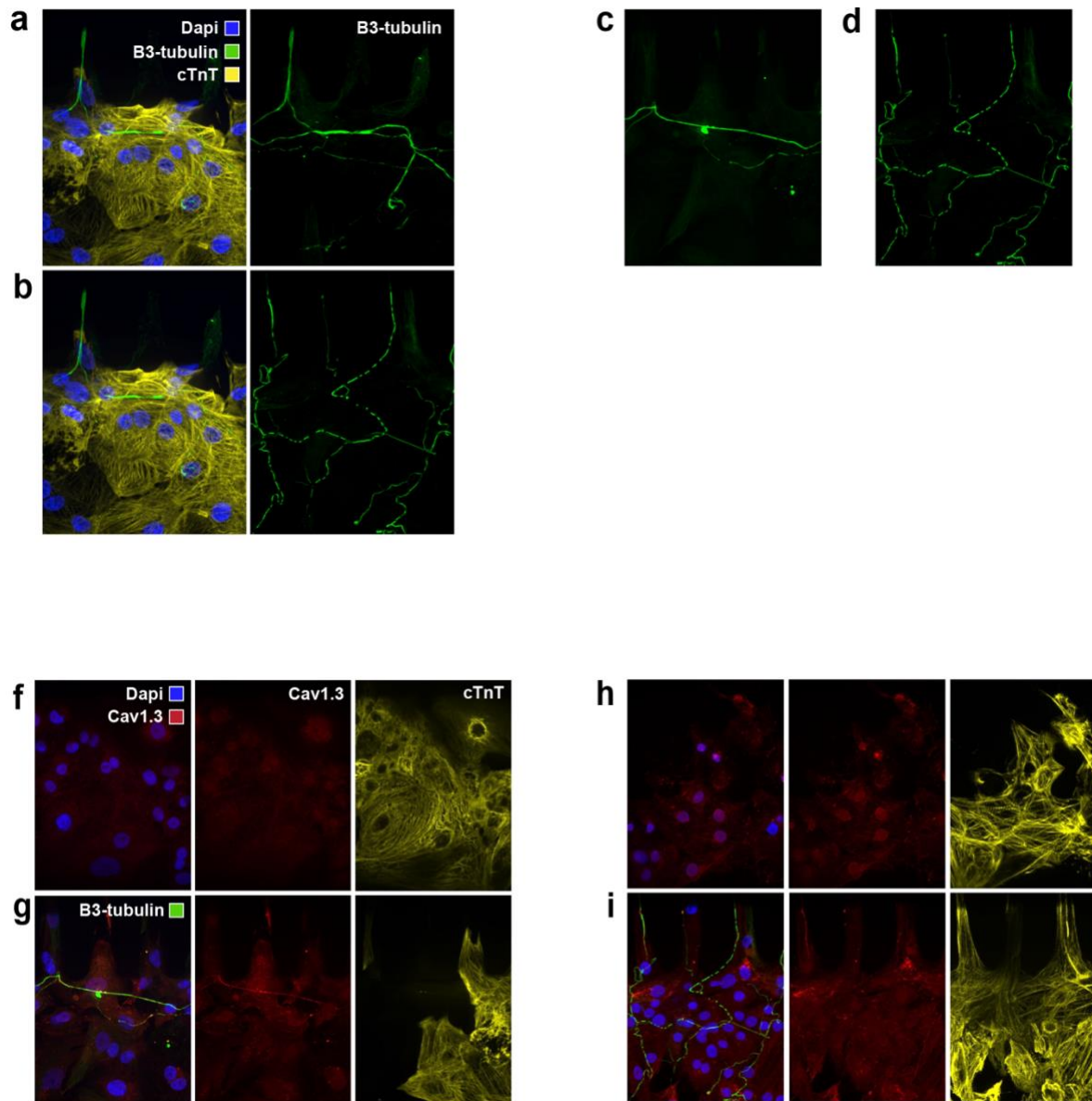


**Figure 5.2. Differential innervation and functional phenotypes in SANLPCs and CMs cultured with SNs.**

(a) Immunofluorescent co-staining of nuclei (DAPI), neuronal ( $\beta$ 3-tubulin), and cardiac (cTnT) marker illustrating innervation in devices with CMs and (b) SANLPCs. (c) Representative  $\beta$ 3-tubulin staining depicting the differential neurite outgrowth in devices with CMs compared to (d) SANLPCs. (f) Representative panel of immunofluorescent

images of CMs stained for nuclei (DAPI), a L-type ion channel (Cav1.3), and cardiac marker (cTnT) after being cultured in devices without and (g) with SNs. (h) Representative panel of immunofluorescent images of SANLPCs stained for nuclei (DAPI), a L-type ion channel (Cav1.3), and a cardiac marker (cTnT) after being cultured in devices without and (g) with SNs. Scale bar = 100 $\mu$ m

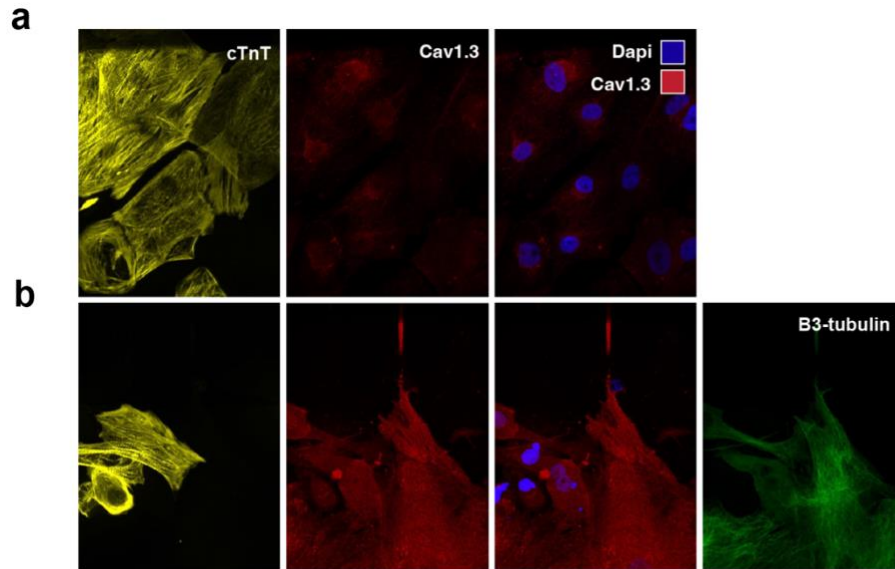


**Figure S5.1. SANLCs differentiated with RBS+ protocol demonstrate less axiogenesis.**

(a) Representative panel of immunofluorescent images of SANLCs stained for a cardiac marker (cTnT), nuclei (DAPI), a L-type ion channel (Cav1.3), and a neuronal marker ( $\beta$ 3-tubulin) after being cultured in devices without and (b) with SNs. Scale bar = 100 $\mu$ m

## REFERENCES

1. Boyett, M. & Lundby, A. *A New Window onto the Pacemaker of the Heart, the Sinus Node, Provided by Quantitative Proteomics and Single-Nucleus Transcriptomics*.
2. Pauza, D. H. *et al.* Neuroanatomy of the murine cardiac conduction system. A combined stereomicroscopic and fluorescence immunohistochemical study. *Auton Neurosci* **176**, 32–47 (2013).
3. Hanna, P. *et al.* Innervation and Neuronal Control of the Mammalian Sinoatrial Node a Comprehensive Atlas. *Circ Res* **128**, 1279–1296 (2021).
4. Boullin, J. & Morgan, J. M. The development of cardiac rhythm. in *Heart* vol. 91 874–875 (2005).
5. Marvin, W. J., Hermsmeyer, K., McDonald, R. I., Roskoski, L. M. & Roskoski, R. *Ontogenesis of Cholinergic Innervation in the Rat Heart*. *Circ Res* vol. 46 <http://circres.ahajournals.org/> (1980).
6. Kreipke, R. E. & Birren, S. J. Innervating sympathetic neurons regulate heart size and the timing of cardiomyocyte cell cycle withdrawal. *J Physiol* **593**, 5057–5073 (2015).
7. van Eif, V. W. W. *et al.* Transcriptome analysis of mouse and human sinoatrial node cells reveals a conserved genetic program. *Development (Cambridge)* **146**, (2019).
8. Chow, L. T. C., Chow, S. S. M., Anderson, R. H. & Gosling, J. A. Autonomic innervation of the human cardiac conduction system: Changes from infancy to

- senility - An immunohistochemical and histochemical analysis. *Anatomical Record* **264**, 169–182 (2001).
9. Hage, F. G. & Iskandrian, A. E. Cardiac autonomic denervation in diabetes mellitus. *Circulation: Cardiovascular Imaging* vol. 4 79–81 Preprint at <https://doi.org/10.1161/CIRCIMAGING.111.963967> (2011).
  10. Chua, S. K. K., Saffari, S. E., Lee, S. J. Y. & Tan, E. K. Association Between Parkinson's Disease and Coronary Artery Disease: A Systematic Review and Meta-Analysis. *Journal of Parkinson's Disease* vol. 12 1737–1748 Preprint at <https://doi.org/10.3233/JPD-223291> (2022).
  11. Hookway, T. A. *et al.* Bi-directional Impacts of Heterotypic Interactions in Engineered 3D Human Cardiac Microtissues Revealed by Single-Cell RNA-Sequencing and Functional Analysis. *bioRxiv* (2020) doi:10.1101/2020.07.06.190504.
  12. Iseoka, H. *et al.* Pivotal Role of Non-cardiomyocytes in Electromechanical and Therapeutic Potential of Induced Pluripotent Stem Cell-Derived Engineered Cardiac Tissue. *Tissue Eng Part A* **24**, 287–300 (2018).
  13. Hookway, T. A. *et al.* Phenotypic Variation between Stromal Cells Differentially Impacts Engineered Cardiac Tissue Function. *Tissue Eng Part A* **25**, 773–785 (2019).
  14. Zhou, P. & Pu, W. T. Recounting cardiac cellular composition. *Circulation Research* vol. 118 368–370 Preprint at <https://doi.org/10.1161/CIRCRESAHA.116.308139> (2016).



15. Cristy, I. Pacemaker Surgery and Epicardial Pacing. *Journal of Universal Surgery* **10**, (2022).
16. Boyett, M. R., Honjo, H. & Kodama, I. *The sinoatrial node, a heterogeneous pacemaker structure. Cardiovascular Research* vol. 47  
[www.elsevier.com/locate/cardiores](http://www.elsevier.com/locate/cardiores)[www.elsevier.nl/locate/cardiores](http://www.elsevier.nl/locate/cardiores) (2000).
17. Unudurthi, S. D., Wolf, R. M. & Hund, T. J. Role of sinoatrial node architecture in maintaining a balanced source-sink relationship and synchronous cardiac pacemaking. *Frontiers in Physiology* vol. 5 Preprint at <https://doi.org/10.3389/fphys.2014.00446> (2014).
18. Vedantham, V. New Approaches to Biological Pacemakers: Links to Sinoatrial Node Development. *Trends in Molecular Medicine* vol. 21 749–761 Preprint at <https://doi.org/10.1016/j.molmed.2015.10.002> (2015).
19. Easterling, M., Rossi, S., Mazzella, A. J. & Bressan, M. Assembly of the cardiac pacemaking complex: Electrogenic principles of sinoatrial node morphogenesis. *Journal of Cardiovascular Development and Disease* vol. 8 Preprint at <https://doi.org/10.3390/jcdd8040040> (2021).
20. Boyett, M. R. *et al.* *Connexins in the Sinoatrial and Atrioventricular Nodes. Adv Cardiol* vol. 42 (2006).
21. Christoffels, V. M., Smits, G. J., Kispert, A. & Moorman, A. F. M. Development of the pacemaker tissues of the heart. *Circulation Research* vol. 106 240–254  
Preprint at <https://doi.org/10.1161/CIRCRESAHA.109.205419> (2010).

22. Wiese, C. *et al.* Formation of the sinus node head and differentiation of sinus node myocardium are independently regulated by Tbx18 and Tbx3. *Circ Res* **104**, 388–397 (2009).
23. Ye, W. *et al.* A common Shox2–nkx2-5 antagonistic mechanism primes the pacemaker cell fate in the pulmonary vein myocardium and sinoatrial node. *Development (Cambridge)* **142**, 2521–2532 (2015).
24. Li, H. *et al.* Nkx2-5 defines a subpopulation of pacemaker cells and is essential for the physiological function of the sinoatrial node in mice. *Development (Cambridge)* **146**, (2019).
25. Espinoza-Lewis, R. A. *et al.* Shox2 is essential for the differentiation of cardiac pacemaker cells by repressing Nkx2-5. *Dev Biol* **327**, 376–385 (2009).
26. van Mierop, L. H. S. *Location of pacemaker in chick embryo heart at the time of initiation of heartbeat.* [www.physiology.org/journal/ajplegacy](http://www.physiology.org/journal/ajplegacy) (1967).
27. Christoffels, V. M., Smits, G. J., Kispert, A. & Moorman, A. F. M. Development of the pacemaker tissues of the heart. *Circulation Research* vol. 106 240–254 Preprint at <https://doi.org/10.1161/CIRCRESAHA.109.205419> (2010).
28. Vedantham, V., Galang, G., Evangelista, M., Deo, R. C. & Srivastava, D. RNA sequencing of mouse sinoatrial node reveals an upstream regulatory role for Islet-1 in cardiac pacemaker cells. *Circ Res* **116**, 797–803 (2015).
29. Monfredi, O., Dobrzynski, H., Mondal, T., Boyett, M. R. & Morris, G. M. The anatomy and physiology of the sinoatrial node-A contemporary review. *PACE - Pacing and Clinical Electrophysiology* vol. 33 1392–1406 Preprint at <https://doi.org/10.1111/j.1540-8159.2010.02838.x> (2010).

30. Chandler, N. J. *et al.* Molecular architecture of the human sinus node insights into the function of the cardiac pacemaker. *Circulation* **119**, 1562–1575 (2009).
31. Unudurthi, S. D., Wolf, R. M. & Hund, T. J. Role of sinoatrial node architecture in maintaining a balanced source-sink relationship and synchronous cardiac pacemaking. *Frontiers in Physiology* vol. 5 Preprint at <https://doi.org/10.3389/fphys.2014.00446> (2014).
32. Kimura, K., Ieda, M. & Fukuda, K. Development, maturation, and transdifferentiation of cardiac sympathetic nerves. *Circulation Research* vol. 110 325–336 Preprint at <https://doi.org/10.1161/CIRCRESAHA.111.257253> (2012).
33. Hasan, W. Autonomic cardiac innervation. *Organogenesis* (2013) doi:10.4161/org.24892.
34. Männer, J. When Does the Human Embryonic Heart Start Beating? A Review of Contemporary and Historical Sources of Knowledge about the Onset of Blood Circulation in Man. *Journal of Cardiovascular Development and Disease* vol. 9 Preprint at <https://doi.org/10.3390/jcdd9060187> (2022).
35. Nishii, K. & Shibata, Y. Mode and determination of the initial contraction stage in the mouse embryo heart. *Anat Embryol (Berl)* **211**, 95–100 (2006).
36. Kowalski, W. J. *et al.* Sympathetic Neurons Regulate Cardiomyocyte Maturation in Culture. *Front Cell Dev Biol* **10**, (2022).
37. Kreipke, R. E. & Birren, S. J. Innervating sympathetic neurons regulate heart size and the timing of cardiomyocyte cell cycle withdrawal. *Journal of Physiology* **593**, 5057–5073 (2015).

38. Passier, R., van Laake, L. W. & Mummery, C. L. Stem-cell-based therapy and lessons from the heart. *Nature* vol. 453 322–329 Preprint at <https://doi.org/10.1038/nature07040> (2008).
39. Takahashi, K. & Yamanaka, S. Induction of Pluripotent Stem Cells from Mouse Embryonic and Adult Fibroblast Cultures by Defined Factors. *Cell* **126**, 663–676 (2006).
40. Lian, X. *et al.* Robust cardiomyocyte differentiation from human pluripotent stem cells via temporal modulation of canonical Wnt signaling. *Proceedings of the National Academy of Sciences* **109**, E1848-1857 (2012).
41. Zhang, Q. *et al.* Direct differentiation of atrial and ventricular myocytes from human embryonic stem cells by alternating retinoid signals. *Cell Res* **21**, 579–587 (2011).
42. Protze, S. I. *et al.* Sinoatrial node cardiomyocytes derived from human pluripotent cells function as a biological pacemaker. *Nat Biotechnol* **35**, 56–68 (2017).
43. Fattahi, F. *et al.* Deriving human ENS lineages for cell therapy and drug discovery in Hirschsprung disease. *Nature* **531**, 105–109 (2016).
44. Matthys, O. B., Hookway, T. A. & McDevitt, T. C. Design Principles for Engineering of Tissues from Human Pluripotent Stem Cells. *Current Stem Cell Reports* vol. 2 43–51 Preprint at <https://doi.org/10.1007/s40778-016-0030-z> (2016).
45. Hou, X. *et al.* Chemically defined and small molecules-based generation of sinoatrial node-like cells. *Stem Cell Res Ther* **13**, (2022).

46. Tchieu, J. *et al.* A Modular Platform for Differentiation of Human PSCs into All Major Ectodermal Lineages. *Cell Stem Cell* **21**, 399-410.e7 (2017).
47. Takayama, Y. *et al.* Selective Induction of Human Autonomic Neurons Enables Precise Control of Cardiomyocyte Beating. *Sci Rep* **10**, (2020).
48. Gorabi, A. M. *et al.* TBX18 transcription factor overexpression in human-induced pluripotent stem cells increases their differentiation into pacemaker-like cells. *J Cell Physiol* **234**, 1534–1546 (2019).
49. Takeuchi, J. K. & Bruneau, B. G. Directed transdifferentiation of mouse mesoderm to heart tissue by defined factors. *Nature* **459**, 708–711 (2009).
50. Qian, L. & Srivastava, D. Direct cardiac reprogramming: From developmental biology to cardiac regeneration. *Circulation Research* vol. 113 915–921 Preprint at <https://doi.org/10.1161/CIRCRESAHA.112.300625> (2013).
51. el Wazan, L., Urrutia-Cabrera, D. & Wong, R. C. B. Using transcription factors for direct reprogramming of neurons in vitro. *World Journal of Stem Cells* vol. 11 431–444 Preprint at <https://doi.org/10.4252/wjsc.v11.i7.431> (2019).
52. Liu, F. *et al.* Enrichment differentiation of human induced pluripotent stem cells into sinoatrial node-like cells by combined modulation of BMP, FGF, and RA signaling pathways. *Stem Cell Res Ther* **11**, (2020).
53. Wu, H. F. & Zeltner, N. Overview of Methods to Differentiate Sympathetic Neurons from Human Pluripotent Stem Cells. *Curr Protoc Stem Cell Biol* **50**, (2019).

54. Perez-Bermejo, J. A. *et al.* SARS-CoV-2 infection of human iPSC-derived cardiac cells reflects cytopathic features in hearts of patients with COVID-19. *Sci. Transl. Med* vol. 13 <http://stm.sciencemag.org/> (2021).
55. IEEE Engineering in Medicine and Biology Society, Annual International Conference of the IEEE Engineering in Medicine and Biology Society 35 2013.07.03-07 Osaka, EMBC 35 2013.07.03-07 Osaka & EMBS Annual Conference 35 2013.07.03-07 Osaka. *Microfabricated device for co-culture of sympathetic neuron and iPS-derived cardiomyocytes.*
56. Marx, U. *et al.* Biology-inspired microphysiological system approaches to solve the prediction dilemma of substance testing. *ALTEX* **33**, 272–321 (2016).
57. Kutys, M. L. *et al.* Uncovering mutation-specific morphogenic phenotypes and paracrine-mediated vessel dysfunction in a biomimetic vascularized mammary duct platform. *Nat Commun* **11**, (2020).
58. Psaras, Y. *et al.* CalTrack: High-Throughput Automated Calcium Transient Analysis in Cardiomyocytes. *Circ Res* **129**, 326–341 (2021).
59. Linscheid, N. *et al.* Quantitative proteomics and single-nucleus transcriptomics of the sinus node elucidates the foundation of cardiac pacemaking. *Nat Commun* **10**, (2019).
60. Junhee Seok *et al.* Genomic responses in mouse models poorly mimic human inflammatory diseases. *Proc Natl Acad Sci U S A* **110**, 3507–3512 (2013).
61. Lian, X. *et al.* Directed cardiomyocyte differentiation from human pluripotent stem cells by modulating Wnt/ $\beta$ -catenin signaling under fully defined conditions. *Nat Protoc* **8**, 162–175 (2013).

62. Burridge, P. W. *et al.* Chemically defined generation of human cardiomyocytes. *Nat Methods* (2014) doi:10.1038/nMeth.2999.
63. Kleinsorge, M. & Cyganek, L. Subtype-Directed Differentiation of Human iPSCs into Atrial and Ventricular Cardiomyocytes. *STAR Protoc* **1**, (2020).
64. Yechikov, S. *et al.* NODAL inhibition promotes differentiation of pacemaker-like cardiomyocytes from human induced pluripotent stem cells. *Stem Cell Res* **49**, (2020).
65. Ren, J. *et al.* Canonical Wnt5b Signaling Directs Outlying Nkx2.5+ Mesoderm into Pacemaker Cardiomyocytes. *Dev Cell* **50**, 729-743.e5 (2019).
66. Monfredi, O., Dobrzynski, H., Mondal, T., Boyett, M. R. & Morris, G. M. The anatomy and physiology of the sinoatrial node-A contemporary review. *PACE - Pacing and Clinical Electrophysiology* **33**, 1392–1406 (2010).
67. Harris, K. *et al.* Comparison of electrophysiological data from human-induced pluripotent stem cell-derived cardiomyocytes to functional preclinical safety assays. *Toxicological Sciences* **134**, 412–426 (2013).
68. Maddah, M. *et al.* A non-invasive platform for functional characterization of stem-cell-derived cardiomyocytes with applications in cardiotoxicity testing. *Stem Cell Reports* **4**, 621–631 (2015).
69. Takaki, T. *et al.* Optical recording of action potentials in human induced pluripotent stem cell-derived cardiac single cells and monolayers generated from long QT syndrome type 1 patients. *Stem Cells Int* **2019**, (2019).
70. Si-Tayeb, K. *et al.* Highly efficient generation of human hepatocyte-like cells from induced pluripotent stem cells. *Hepatology* **51**, 297–305 (2010).

71. Zhao, M., Tang, Y., Zhou, Y. & Zhang, J. Deciphering Role of Wnt Signalling in Cardiac Mesoderm and Cardiomyocyte Differentiation from Human iPSCs: Four-dimensional control of Wnt pathway for hiPSC-CMs differentiation. *Sci Rep* **9**, (2019).
72. Bruneau, B. G. *et al.* Chamber-Specific Cardiac Expression of *Tbx5* and Heart Defects in Holt-Oram Syndrome. <http://www.idealibrary.com> (1999).
73. Martin, K. E. & Waxman, J. S. Atrial and sinoatrial node development in the zebrafish heart. *Journal of Cardiovascular Development and Disease* vol. 8 1–17 Preprint at <https://doi.org/10.3390/JCDD8020015> (2021).
74. Moses, K. A., Demayo, F., Braun, R. M., Reecy, J. L. & Schwartz, R. J. Embryonic expression of an *Nkx2-5/Cre* gene using ROSA26 reporter mice. *Genesis (United States)* **31**, 176–180 (2001).
75. Mohan, R. A., Boukens, B. J. & Christoffels, V. M. Developmental Origin of the Cardiac Conduction System: Insight from Lineage Tracing. *Pediatric Cardiology* vol. 39 1107–1114 Preprint at <https://doi.org/10.1007/s00246-018-1906-8> (2018).
76. Liang, X. *et al.* HCN4 dynamically marks the first heart field and conduction system precursors. *Circ Res* **113**, 399–407 (2013).
77. Bakker, M. L. *et al.* Transcription factor *Tbx3* is required for the specification of the atrioventricular conduction system. *Circ Res* **102**, 1340–1349 (2008).
78. Ghazizadeh, Z. *et al.* A dual SHOX2:GFP; MYH6:mCherry knockin hESC reporter line for derivation of human SAN-like cells. *iScience* **25**, (2022).
79. Kraus, F., Haenig, Â. & Kispert, A. Cloning and expression analysis of the mouse *T-box* gene *Tbx18*. [www.elsevier.com/locate/modo](http://www.elsevier.com/locate/modo) (2001).



80. Sartiani, L., Cerbai, E. & Mugelli, A. The Funny Current in Cardiac Non-Pacemaker Cells: Functional Role and Pharmacological Modulation. in *Modern Pacemakers - Present and Future* (2012). doi:10.5772/13086.
81. Lyashkov, A. E. *et al.* Calcium cycling protein density and functional importance to automaticity of isolated sinoatrial nodal cells are independent of cell size. *Circ Res* **100**, 1723–1731 (2007).
82. Janssen, P. M. L., Biesiadecki, B. J., Ziolo, M. T. & Davis, J. P. The need for speed: Mice, men, and myocardial kinetic reserve. *Circ Res* **119**, 418–421 (2016).
83. Yu, Q., Leatherbury, L., Tian, X. & Lo, C. W. Cardiovascular Assessment of Fetal Mice by In Utero Echocardiography. *Ultrasound Med Biol* **34**, 741–752 (2008).
84. Sartiani, L., Cerbai, E. & Mugelli, A. *The Funny Current in Cardiac Non-Pacemaker Cells: Functional Role and Pharmacological Modulation*.  
www.intechopen.com.
85. Lee, J. H., Protze, S. I., Laksman, Z., Backx, P. H. & Keller, G. M. Human Pluripotent Stem Cell-Derived Atrial and Ventricular Cardiomyocytes Develop from Distinct Mesoderm Populations. *Cell Stem Cell* **21**, 179-194.e4 (2017).
86. Lian, X. *et al.* Robust cardiomyocyte differentiation from human pluripotent stem cells via temporal modulation of canonical Wnt signaling. *Proc Natl Acad Sci U S A* **109**, (2012).
87. Hookway, T. A., Butts, J. C., Lee, E., Tang, H. & McDevitt, T. C. Aggregate formation and suspension culture of human pluripotent stem cells and differentiated progeny. *Methods* **101**, 11–20 (2016).

88. Cerbai, E., Pino, R., Sartiani, L. & Mugelli, A. *Influence of postnatal-development on I occurrence and properties in f neonatal rat ventricular myocytes. Cardiovascular Research* vol. 42  
<https://academic.oup.com/cardiovasres/article/42/2/416/278290> (1999).
89. Robinson, R. B., Yu, H. & Chang, F. Developmental change in the voltage-dependence of the pacemaker current,  $I_f$ , in rat ventricle cells. *Pflügers Arch – Eur J Physiol* **433**, (1997).
90. Besser, R. R. *et al.* Engineered microenvironments for maturation of stem cell derived cardiac myocytes. *Theranostics* **8**, 124–140 (2018).
91. Verkerk, A. O., van Borren, M. M. G. J. & Wilders, R. Calcium transient and sodium-calcium exchange current in human versus rabbit sinoatrial node pacemaker cells. *The Scientific World Journal* **2013**, (2013).
92. Gu, J. mo *et al.* Induced cardiac pacemaker cells survive metabolic stress owing to their low metabolic demand. *Exp Mol Med* **51**, (2019).
93. Hildreth, V., Anderson, R. H. & Henderson, D. J. Autonomic innervation of the developing heart: Origins and function. *Clinical Anatomy* **22**, 36–46 (2009).
94. Fedele, L. & Brand, T. The intrinsic cardiac nervous system and its role in cardiac pacemaking and conduction. *Journal of Cardiovascular Development and Disease* vol. 7 1–33 Preprint at <https://doi.org/10.3390/jcdd7040054> (2020).
95. Tirziu, D., Giordano, F. J. & Simons, M. Cell communications in the heart. *Circulation* vol. 122 928–937 Preprint at <https://doi.org/10.1161/CIRCULATIONAHA.108.847731> (2010).


96. Kim, M. S. *et al.* Heterogeneity of calcium clock functions in dormant, dysrhythmically and rhythmically firing single pacemaker cells isolated from SA node. *Cell Calcium* **74**, 168–179 (2018).
97. Wilders, R. & Jongsma, H. J. *Beating Irregularity of Single Pacemaker Cells Isolated from the Rabbit Sinoatrial Node*. *Biophysical Journal* vol. 65 (1993).
98. Rysevaite, K. *et al.* Immunohistochemical characterization of the intrinsic cardiac neural plexus in whole-mount mouse heart preparations. *Heart Rhythm* **8**, 731–738 (2011).
99. Sakai, K. *et al.* Functional innervation of human induced pluripotent stem cell-derived cardiomyocytes by co-culture with sympathetic neurons developed using a microtunnel technique. *Biochem Biophys Res Commun* (2017) doi:10.1016/j.bbrc.2017.10.065.
100. Winbo, A. *et al.* Functional coculture of sympathetic neurons and cardiomyocytes derived from human-induced pluripotent stem cells. *Am J Physiol Heart Circ Physiol* **319**, 927–937 (2020).
101. Dong, X. *et al.* Functional Coupling with Cardiac Muscle Promotes Maturation of hPSC-Derived Sympathetic Neurons. *Cell Stem Cell* (2016) doi:10.1016/j.stem.2016.05.002.
102. van Eif, V. *et al.* Transcriptome analysis of mouse and human sinoatrial node cells reveals a conserved genetic program. *Development* **146**, dev.173161 (2019).
103. Striessnig, J., Pinggera, A., Kaur, G., Bock, G. & Tuluc, P. L-type Ca<sup>2+</sup> channels in heart and brain. *Wiley Interdiscip Rev Membr Transp Signal* **3**, 15–38 (2014).

104. Morales, D., Hermosilla, T. & Varela, D. Calcium-dependent inactivation controls cardiac L-type Ca<sup>2+</sup> currents under  $\beta$ -adrenergic stimulation. *Journal of General Physiology* **151**, 786–797 (2018).

## Publishing Agreement

It is the policy of the University to encourage open access and broad distribution of all theses, dissertations, and manuscripts. The Graduate Division will facilitate the distribution of UCSF theses, dissertations, and manuscripts to the UCSF Library for open access and distribution. UCSF will make such theses, dissertations, and manuscripts accessible to the public and will take reasonable steps to preserve these works in perpetuity.

I hereby grant the non-exclusive, perpetual right to The Regents of the University of California to reproduce, publicly display, distribute, preserve, and publish copies of my thesis, dissertation, or manuscript in any form or media, now existing or later derived, including access online for teaching, research, and public service purposes.

DocuSigned by:  
  
1885707A04B84F7... Author Signature

3/21/2023  
Date